USGS
science for a changing world

Topographic Change Detection at Select Archeological Sites in Grand Canyon National Park, Arizona, 2007–2010

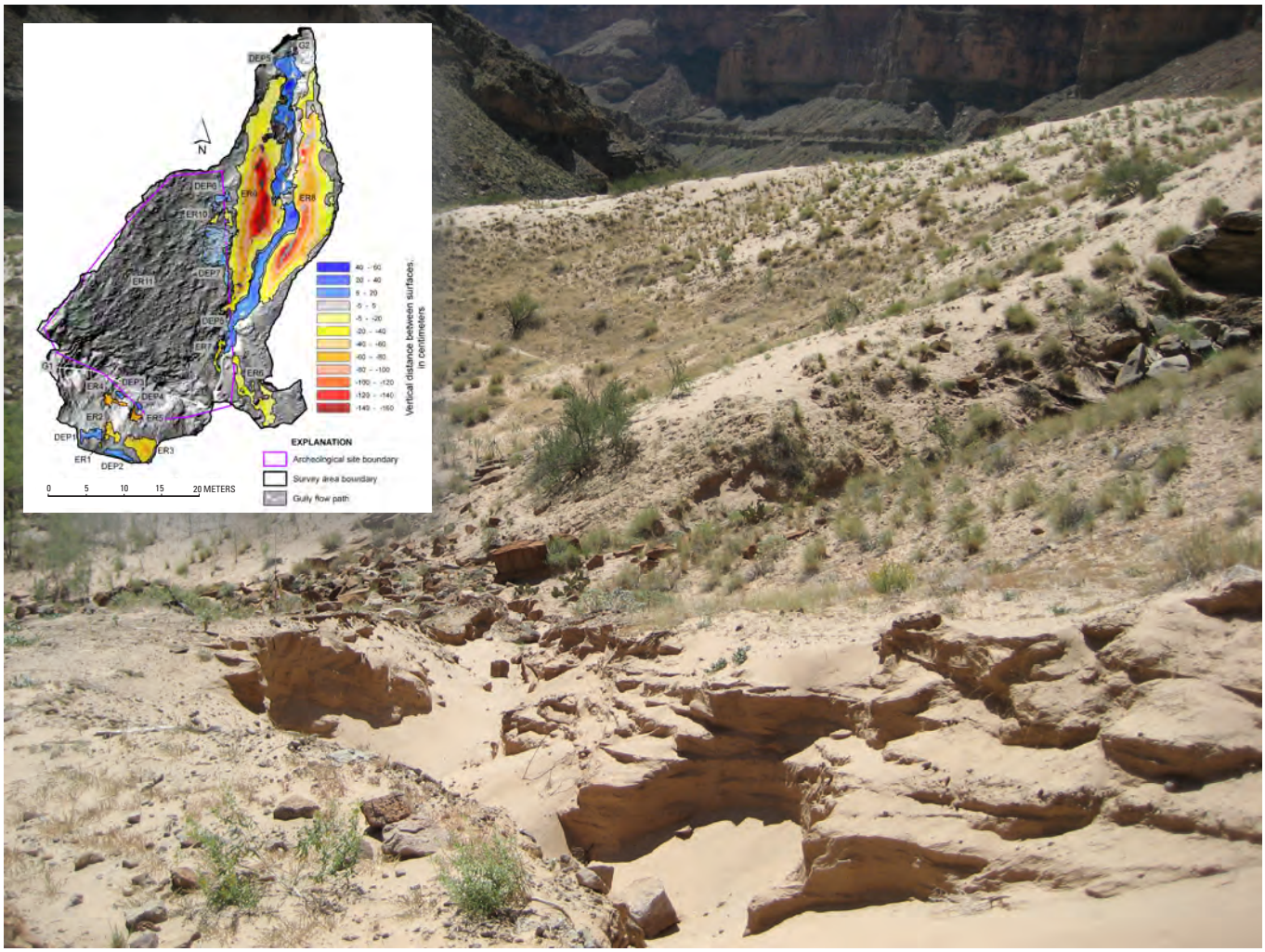

Scientific Investigations Report 2012–5133

U.S. Department of the Interior
U.S. Geological Survey

COVER

Photograph of one of the archeological sites in Grand Canyon National Park where topographic change was investigated. This site (AZ:B:10:0225) has both sand dunes and (in foreground) gully erosion. Inset is the resultant 5-cm gridded output map of topographic change for this site, showing erosion (warm colors) and deposition (cool colors).

Topographic Change Detection at Select Archeological Sites in Grand Canyon National Park, Arizona, 2007–2010

Brian D. Collins, Skye C. Corbett, Helen C. Fairley, Diane Minasian, Robert Kayen, Timothy P. Dealy, and David R. Bedford

Scientific Investigations Report 2012–5133

U.S. Department of the Interior
U.S. Geological Survey

U.S. Department of the Interior
KEN SALAZAR, Secretary

U.S. Geological Survey
Marcia K. McNutt, Director

U.S. Geological Survey, Reston, Virginia: 2012

This report and any updates to it are available online at:
http://pubs.usgs.gov/sir/2012/5133/

For more information on the USGS—the Federal source for science about the Earth, its natural and living resources, natural hazards, and the environment—visit http://www.usgs.gov or call 1–888–ASK–USGS

For an overview of USGS information products, including maps, imagery, and publications, visit http://www.usgs.gov/pubprod

To order this and other USGS information products, visit http://store.usgs.gov

Suggested citation:
Collins, B.D., Corbett, S.C., Fairley, H.C., Minasian, D., Kayen, R., Dealy, T.P., and Bedford, D.R., 2012, Topographic change detection at select archeological sites in Grand Canyon National Park, Arizona, 2007–2010: U.S. Geological Survey Scientific Investigations Report 2012–5133, 77 p.

Contents

Figures

Tables

Datum Information

Horizontal coordinate information was collected referenced to the North American Datum of 1983 (NAD83) and projected to Arizona Central Zone 0202 State Plane coordinates expressed in meters. For the purpose of protecting the sensitive nature of the archeological sites, all coordinates have been translated to a fictitious origin, still expressed in meters.

Vertical coordinate information is referenced to the North American Datum of 1983 (NAD83) ellipsoid height, expressed in meters.

Elevation, as used in this report, refers to distance above the vertical datum.

This page intentionally left blank.

Topographic Change Detection at Select Archeological Sites in Grand Canyon National Park, Arizona, 2007–2010

By Brian D. Collins, Skye C. Corbett, Helen C. Fairley, Diane Minasian, Robert Kayen, Timothy P. Dealy, and David R. Bedford

Abstract

Human occupation in Grand Canyon, Arizona, dates from at least 11,000 years before present to the modern era. For most of this period, the only evidence of human occupation in this iconic landscape is provided by archeological sites. Because of the dynamic nature of this environment, many archeological sites are subject to relatively rapid topographic change. Quantifying the extent, magnitude, and cause of such change is important for monitoring and managing these archeological sites. Such quantification is necessary to help inform the continuing debate on whether and how controlled releases from Glen Canyon Dam, located immediately upstream of Grand Canyon National Park, are affecting site erosion rates, artifact transport, and archeological resource preservation along the Colorado River in Grand Canyon. Although long-term topographic change resulting from a variety of natural processes is inherent in the Grand Canyon region, continued erosion of archeological sites threatens both the archeological resources and our future ability to study evidence of past cultural habitation. Thus, this subject is of considerable interest to National Park Service managers and other stakeholders in the Glen Canyon Dam Adaptive Management Program.

Understanding the causes and effects of archeological site erosion requires a knowledge of several factors, including the location, timing, and magnitude of the changes occurring in relation to archeological resources, the rates of change, and the relative contribution of potential causes. These potential causes include sediment depletion associated with managed flows from Glen Canyon Dam, site-specific weather and overland flow patterns, visitor impacts, and long-term regional climate change. To obtain this information, highly accurate, spatially specific data are needed from sites undergoing change. Using terrestrial lidar techniques, and building upon three previous surveys of archeological sites performed in 2006 and 2007, we collected two new datasets in April and September 2010 and processed and improved upon existing methods to generate high-accuracy (3 to 5 cm vertical change threshold) topographic change-detection maps for 10 survey areas encompassing 9 archeological sites along the Colorado River corridor. We also used terrestrial lidar techniques to investigate several other metrics for studying archeological site stability, including monitoring cultural structures and artifacts and remotely measuring cryptobiotic soil crust areas.

Our topographic change results indicate that 9 of 10 survey areas showed signs of either erosion, deposition, or both during the 2007–2010 time interval and that these changes can be linked to a variety of geomorphic processes, primarily overland flow gullying and aeolian sand transport. In several cases, large (>50 cm) vertical change occurred, and in one case, more than 100 m^3 of sediment was eroded. Further, for all sites monitored throughout the river corridor during this time period, the overall signal was related to erosion rather than deposition. These results highlight the potential for rapid archeological site change in Grand Canyon. Whereas the topographic change results presented herein provide the highest level of change detection yet performed on entire archeological sites in Grand Canyon, additional work in combining these results with site-specific weather, hydrology, and geomorphology data is needed to provide a more thorough understanding of the causes of the documented topographic changes. Linking lidar-derived measurements of topographic changes with these other data sources should provide land managers with a scientific basis for making management decisions regarding archeological resources in Grand Canyon National Park and assist in answering open questions regarding the influence that sediment-depleted flows from Glen Canyon Dam have on archeological site stability.

Introduction

Human occupation in Grand Canyon, Arizona, dates from at least 11,000 years before present to the modern era (Fairley, 2005). For most of this period, the only evidence of human occupation in this iconic landscape is provided by archeological sites. Because these sites contain valuable information about the past and serve as tangible evidence of Native Americans' prehistoric use of this area, topographic

change and potential degradation of archeological sites within the Colorado River corridor of Grand Canyon National Park (GCNP) (fig. 1), located below Glen Canyon Dam, is a subject of considerable interest and concern to park managers, Native Americans, scientists, and other members of the American public who value these historic places. In 1997, the United States Secretary of the Interior established the Glen Canyon Dam Adaptive Management Program (GCDAMP) to research and mitigate potential negative impacts of Glen Canyon Dam on downstream resources, including archeological sites, fish, wildlife, recreational values, and power-generation interests (see, for example, Gloss and others, 2005). One aspect of this management program aims to determine whether controlled releases from Glen Canyon Dam are affecting rates of archeological site erosion and the preservation of archeological resources (for example, Yeatts, 1996). Many archeological sites are located within or adjacent to the historical river flood zone. Because the dam prevents sediment from moving downstream and only 15 percent of the pre-dam sediment supply is contributed by tributaries below Glen Canyon Dam, and additionally because the dam severely restricts the magnitude and duration of flood flows (Topping and others 2003), pre-dam flood zones are no longer scoured or replenished by sediment-enriched floods. This has resulted in a reduction in the size, volume, and distributions of sand bars that might contribute sand to nearby archeological sites through aeolian transport. It has been hypothesized that a reduction in open sand area in river sand bars has resulted in a reduction in aeolian sand cover at archeological sites and that this has resulted in an increase in surface runoff and a consequent increase in the rate of site erosion via precipitation-induced surface water gullying (Hereford and others, 1991, 1993; Thompson and Potochnik, 2000; Draut and Rubin, 2008; fig. 2). Although long-term topographic change resulting from a variety of natural processes is typical in high-relief, semiarid landscapes such as the Grand Canyon region, continued erosion of archeological sites threatens both the archeological resources and our future ability to study evidence of past human habitation (fig. 3). Thus, determining the rates of topographic change and the potential causes contributing to site degradation continues to be a priority for the GCDAMP and the National Park Service (Leap and others, 1996, 1997, 2000).

The monitoring of topographic change at archeological sites in Grand Canyon has undergone considerable advances during the past 20 years. Beginning with qualitative repeat oblique photography and quantitative total station surveys (Leap and others, 2000) and through to modern use of digital photogrammetry (Pederson and others, 2006) and lidar techniques (Collins and others, 2008, 2009), topographic surveys have become more accurate and applicable to larger areas. Currently, terrestrial lidar techniques are at the forefront of high-accuracy surveys, and their applicability and utility have been clearly demonstrated by previous survey efforts in Grand Canyon (for example, Collins and others, 2009), as well as encouraged by an independent review panel (Kintigh and others, 2007). High-resolution, highly accurate (centimeter-level) surveys have been found to be necessary to track small-scale topographic changes that can act as indicators of future response because these are often the scales at which existing geomorphological processes occur (for example, aeolian sand transport, overland flow, and gullying). Further, the ability to collect data over a wide area (as opposed to more focused surveys such as total station thalweg surveys) makes it possible to put overall processes into context and ensures that important changes are not missed during data collection. For example, previous results (Collins and others, 2008, 2009) have shown that, whereas focused thalweg surveys can correctly identify the approximate magnitude of change, they cannot always confirm the overall cause of the change, which might, for example, be from areas outside the thalweg line where lidar surveys also collect data. As a result of these studies and clear contributions to understanding archeological site change, the Sociocultural Program of the U.S. Geological Survey's Grand Canyon Monitoring and Research Center (GCMRC) has pursued evaluating the applicability of terrestrial lidar for monitoring entire archeological site areas for topographic change in order to address the stated concerns of the GCDAMP (see, for example, Fairley and others, 2007). A series of reports have been published, detailing first the applicability of using terrestrial lidar in GCNP for monitoring a variety of resources (Collins and Kayen, 2006) and then specifically using terrestrial lidar for archeological site monitoring (Collins and others, 2008, 2009).

In Collins and others (2009), results using what was then a state-of-the-art terrestrial-lidar laser scanning device were presented. Since then, new advances in technology have resulted in laser scanning devices with much greater accuracy and more sophisticated software, with an improved potential to measure small-scale (centimeter-level) topographic change. This report presents the results of topographic surveys performed in GCNP between 2007 and 2010, using first a combination of the "old" and "new" technology, followed by surveys using only the newest technology. It follows much the same format as an earlier report (Collins and others, 2009) and builds upon the results reported therein.

In all cases, the focus of this report is on change detection, with the goal of detecting topographic and archeological site change at the highest resolution possible. In addition to monitoring the sites described in previous reports, we include four new sites, each with a different topographic and archeological signature (for example, a site with artifacts scattered over an active dune slope and a habitation site with masonry walls). We also present several analyses aimed at pushing the latest technology forward so that its use for monitoring both archeology and geomorphology can reach its highest potential. These include using terrestrial lidar for monitoring change to cultural structures, for delineating cryptobiotic crust areas,

and for establishing point density guidelines for various forms of change detection (that is, overall topographic site change versus smaller scale geomorphologic change).

As with the previously referenced reports (Collins and others, 2008, 2009), we present a detailed description of terrestrial lidar methods and associated error analyses, because the technology is still somewhat new and few error analyses for terrestrial lidar exist in the literature. We also provide detailed descriptions of each of the survey areas for which data are presented. Finally, whereas high-resolution data and geomorphologic signatures are presented for a variety of sites that show both erosion and deposition during the monitoring period (2007–2010), in this report we do not attempt to link these changes to operations of Glen Canyon Dam. Instead, as in previous reports, we present high-quality topographic change detection data, with the intention that these data will be used for future dam- and river-process related and predictive modeling studies.

Methods

Field Logistics

Building upon three existing datasets (Collins and others, 2009) covering the topographic change detected between 2006 and 2007 at a total of 9 archeological sites (10 separate survey areas; table 1, fig. 1), we conducted two additional data collection efforts in Grand Canyon National Park in 2010. The current research effort uses the last 2007 survey (September 2007) as the initial baseline survey, which is compared to the two datasets collected in 2010 (April 2010 and September 2010). For simplicity, we refer to the efforts whose results are presented herein as the September 2007, April 2010, and September 2010 surveys. In April 2010, only sites in the upper half of Grand Canyon (above Phantom Ranch) were surveyed,

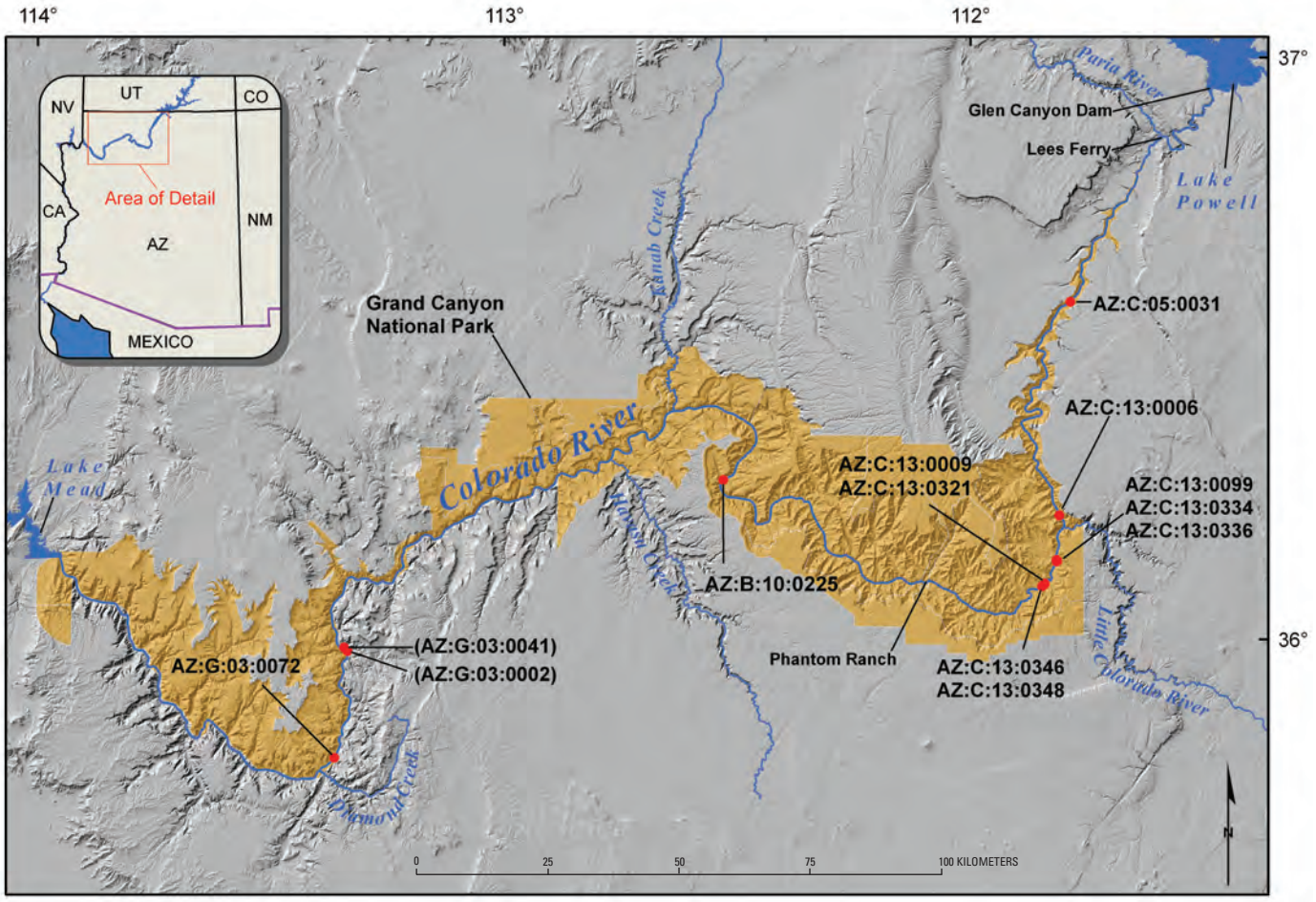

Figure 1. Site map of Grand Canyon National Park showing general location of sites referenced in this investigation and identified by archeological site number. Results for sites in parentheses are included in Collins and others (2009) and are not presented here. Exact locations are not shown to protect the archeological resources.

Figure 2. Gullying at an archeological site in Grand Canyon National Park. This area contains cultural artifacts buried by aeolian sediments and subject to precipitation-induced erosion.

Figure 3. Excavation of an archeological site in Grand Canyon National Park. This site was previously buried by aeolian and alluvial sediments and emerged as precipitation runoff and wind deflation exposed habitation features.

whereas in September 2010 sites both above and below Phantom Ranch were surveyed. The 2010 field efforts included data collection at 8 of the 10 areas previously surveyed in 2006–2007, including one site previously surveyed in 2007 but with no previous change detection analysis performed. In addition, we collected data at three new sites not previously surveyed (table 1). Two sites originally surveyed in 2006 and 2007 (AZ:G:03:0041 and AZ:G:03:0002) were not surveyed in 2010 because of logistical constraints on the surveying effort.

The sites selected for surveying encompassed a variety of archeological site types. These include some where erosion has been previously identified as having an impact on site resources and others where relatively little previous erosion has been documented. To protect the sensitive nature of the sites, specific site location information is omitted from this report, and the GCNP archeological site identification number is used for reference (table 1). At each site, data collection was focused on the terrain surrounding one or more gully systems; these gully systems are referred to in this report as G1, G2, and so on, and numbered sequentially moving from upstream to downstream along the river corridor or the adjacent side drainage.

Each survey effort was supported by two GCMRC motor rafts carrying all personnel and equipment for trips lasting from 10 to 18 days. Equipment consisted of camping gear and food supplies, a battery charging system for all electronics, and survey equipment, including a terrestrial lidar laser scanner, a total station unit, a pair of survey-grade differential GPS receivers, and associated control point reflectors and tripods. Personnel consisted of researchers from the U.S. Geological Survey (USGS) in Menlo Park, California, and researchers and staff from the GCMRC in Flagstaff, Arizona. In April 2010, a contract surveyor (Brian Fisher of Geodetic Analysis, LLC, Phoenix, Arizona) accompanied the trip to perform survey coordinate data collection. Raft pilots (boatmen) contracted through Humphrey Summit Support Inc., supervised the travel and camp logistics for each trip.

Lidar Data Collection

High-resolution topographic data from each archeological site were collected using the newest generation of terrestrial (ground-based) lidar surveying laser scanners. Terrestrial lidar sends and receives laser pulses along exactly known trajectories to build a point file of three-dimensional

Table 1. Dates of lidar data collection at archeological sites in the Colorado River corridor of Grand Canyon National Park.

[Survey area codes are National Park Service archeological site identifiers; n/a, no data collection]

Survey area	May 2006	May 2007	September 2007	April 2010	September 2010
AZ:C:05:0031	n/a	n/a	n/a	4/11/2010	9/16/2010
AZ:C:13:0006	5/6/2006	4/28/2007	9/15/2007	4/13/2010	9/17/2010
AZ:C:13:0336	5/7/2006	4/29/2007	9/16/2007	4/14/2010	9/19/2010
AZ:C:13:0099	5/8/2006	4/29/2007	9/16/2007	4/15/2010	9/20/2010
AZ:C:13:0099 playa area	5/7/2006	4/29/2007	9/16/2007	4/14/2010	9/19/2010
AZ:C:13:0321	n/a	n/a	n/a	4/15/2010	9/21/2010
AZ:C:13:0009	n/a	n/a	n/a	4/16/2010	9/21/2010
AZ:C:13:0346 and AZ:C:13:0348	5/8/2006	4/30/2007	9/17/2007	n/a	9/22/2010
AZ:B:10:0225	n/a	n/a	9/20/2007	n/a	9/27/2010
AZ:G:03:0041	5/14/2006	5/7/2007	9/24/2007	n/a	n/a
AZ:G:03:0002	5/15/2006	5/8/2007	9/25/2007	n/a	n/a
AZ:G:03:0072 US (upstream area)	5/17/2006	5/9/2007	9/26/2007	n/a	10/1/2010
AZ:G:03:0072 DS (downstream area)	5/16/2006	5/10/2007	9/26/2007	n/a	9/30/2010

(3-D) coordinates of virtually any reflecting surface. The points are then viewed in 3-D software so that data filtering, surface building, and change detection can be performed. The technology is relatively new (10+ years) and continues to evolve rapidly. Whereas a Riegl Z210 laser scanner was used in previous studies (Collins and others, 2009), including for the change detection analysis of the 2007 dataset presented herein, the present study (2010 datasets) used a Riegl Z420i laser scanner as a tripod-mounted survey instrument (fig. 4). We present detailed error analyses in a later section of this report to account for differences in the hardware and software used between these surveys. The Riegl Z420i uses a Class 1 (eye safe under normal operating conditions), near-infrared, pulsed laser diode with a beam divergence of 0.014° (approximately 25 mm at 100-m range). Typical maximum range for natural targets with 10 percent and 80 percent reflectivity is 350 m and 1,000 m, respectively, with 10-mm accuracy at 50-m range. Using 12-volt, sealed, gel-cell, lead-acid batteries, the laser system consumes relatively low power (typically 78 W).

Most laser scanners operate using some combination of precisely aligned rotating polygonal mirrors and extremely small stepping motors to guide the laser paths over the area of interest. With the Riegl Z420i, laser pulses are reflected from a triangular mirror rotating around the horizontal axis (with minimum angle step width of 0.004°), while the entire head of the scanner pans around the vertical axis of the laser diode origin (also with minimum angle step width of 0.004°). The technology, specifically developed for rapid topographic surveys, allows data to be collected at rates of thousands of points per second, generating a "point cloud" of 3-D coordinates. Acquisition of sufficiently dense point clouds (that is, point-to-point spacing on the order of 5 cm or less) can, in most cases, fully describe site topography. The point files from data collection are transformed into 3-D surfaces for cross-section and volumetric analyses.

We followed an essentially identical set of surveying protocols as in previous field efforts. At each survey location, we used an elevated tripod (up to 2.6 m tall) to position the laser above each site to capture a wide range and more direct line of sight to the area topography (fig. 4). We collected multiple scans from different locations during each survey to fill in "shadow zones" of areas not directly in the line of sight of the laser and to expand the range and density of the point data. Data with the Riegl Z420i were collected at a rate of 8,000 points per second using a single, last return for each point. Each scan typically collected data over a 360° range in the horizontal direction (aimed at the

region of interest) and over a range of ±40° (measured from the horizontal) in the vertical direction. This provided approximately 4,000,000 to 8,000,000 points for each scan, although only a portion (about 50 percent) of those were located within the site area of interest. One additional survey protocol implemented in 2010 was the attempt to locate the laser instrument outside of the archeological site boundaries as much as possible. This was done to minimize additional site disturbance, but also resulted in lower point density in some cases, in particular for narrow gullies located at oblique angles to the laser instrument locations. When this occurred and affected the development of a robust surface model, it is further discussed within the context of each site's results.

Combining point-cloud data from multiple scan locations into a single georeferenced model continues to be the most challenging and error-producing component of terrestrial lidar scanning. Although many methods exist, the most accurate methods rely on the collection of georeferenced survey points on either the laser itself, a network of visible reflectors within the scans, or both. At each site, we collected high-accuracy survey control on all scanner origins and a network of six control targets visible to the laser during data collection using either or both of a Topcon total station survey device and a pair of survey-grade, real-time kinematic differential Topcon Hiper+ GPS receivers. Coordinates were determined by locating the instrument over known survey benchmarks or by collecting total station or Global Positioning System (GPS) positions on the laser and target locations. Nearly all laser and control point locations represent transient locations between temporally consecutive datasets. Permanent monuments for each of these points (with the exception of total station and GPS base station locations) could not be constructed because of the sensitive and wilderness environment of these sites, and instead we rely on the high-accuracy survey data for georeferencing the point clouds. Processed coordinates were provided by survey personnel following each trip and their quality assessed within the scan-alignment registration procedures outlined in the following sections. Overall accuracy, measured relative to fixed benchmarks at each site and averaged for both survey techniques, was 1.2 cm horizontal and 2.5 cm vertical at the 95-percent confidence level (see the "Error Analysis" section for additional details). We note that the root mean square (RMS) survey control error represents a relative level of horizontal and vertical control in georeferenced space, because the control-point benchmarks used in the survey are only known to a three-dimensional accuracy of 5 cm to 8 cm (Grand Canyon Monitoring and Research Center, 2008). However, because identical benchmarks were used throughout the study (that is, total station and GPS base stations were always set up on the identical fixed points during repeat surveys), this component of error is not included in the subsequently outlined error analysis.

Data Processing

We processed the lidar data through an integrated suite of registration, georeferencing, filtering, and surface-model-generation techniques specific to terrestrial lidar data. Our methodology follows much the same framework as previously reported in Collins and others (2009), but it has been updated to reflect advances in data collection, processing, and change detection analysis. These advances include more rigorous and accurate registration techniques using Riegl RiScan Pro v.1.4.3 software (http://www.riegl.com/products/software-packages/riscan-pro/), surface modeling based on point-density proxies in I-SiTE Studio v. 3.4 software (http://www.maptek.com/products/i-site/i-site_studio.html), and more accurate change detection thresholding using ArcGIS v. 9 (http://www.esri.com/software/arcgis/).

The processing methodology for data collected in 2010 consists of an integrated workflow that ensures data quality and accuracy, particularly with respect to change detection. This workflow is described here with the appropriate software package shown in brackets. Note that the workflow for processing the September 2007 datasets as outlined in Collins and others (2009) is slightly different but is not repeated here.

1. Raw Data Archiving—The data are archived in raw field format to preserve a backup copy. [Riegl RiScan Pro]

2. Survey Data Processing—The survey data provided by total station or GPS are processed to determine accurate coordinates for the scanner and reflector center heights and to eliminate common field errors such as miscalculated tripod or antenna heights.

3. Registration—Data from individual scan locations are combined together within a local coordinate system based on the best-fit alignment of control points scanned in the field. This is preliminarily performed in the field and then recalculated in the office to ensure data consistency and accuracy. [Riegl RiScan Pro]

4. Georeferencing—Local coordinate locations of control points and laser setup locations are aligned with their respective geographic coordinates from Step 2 using a best-fit error minimization algorithm. The target accuracy is typically better than 1.5 cm. [Riegl RiScan Pro]

5. Quality Control Check—Registered, georeferenced point clouds are first visually checked for data misfits within each site's point clouds and then checked for overall close alignment with previous datasets using histogram cumulative frequency analysis. [I-SiTE Studio]

6. Preliminary Scan Filtering—Extraneous points that define such items as people, equipment, dust, or birds are removed from the raw scan files using both manual filtering and maximum point separation distances (that is, all points more than 50 cm from all other points are removed). Distant points outside the overall study area are also removed using a polygon filter. [I-SiTE Studio]

Figure 4. Terrestrial lidar data collection in Grand Canyon National Park. The extendable tripod allows a larger area of data collection and less oblique laser returns from areas of flat topography. Total station prism (shown) or differential global positioning system (GPS) unit with fixed radio-linked base station are used to georeference the instrument location, along with temporary reflector control points shown in mid-ground.

7. Topographic Filtering—Points representing anything other than the ground surface are removed from each scan using a sequence of topographic filtering steps. Following a rough, manual removal of tall vegetation points, the lowest point within each 50-cm-square grid cell is identified and a surface (triangulated irregular network, TIN) is constructed from these points. All points vertically within 10 cm of this surface are then identified. Finally, the lowest point within each 5-cm-square grid cell of these 10-cm surface proximity points is selected. These steps generally achieve a well-refined, high-resolution ground point data file, although additional manual manipulation of the data is always required for particularly small and large vegetation. [I-SiTE Studio]

8. TIN Surface Model Generation—The final surface model is created using a new TIN created from the point set that results from Step 7. Minor filtering of the TIN is sometimes needed to remove obvious remaining extraneous high points from tall vegetation. In some cases, difficulties in the manual filtering of larger vegetation may lead to inconsistencies in the final surface models—for example, when a large boulder is mistaken as a similar-sized bush or tree. [I-SiTE Studio]

9. Grid Digital Elevation Model Generation—Although TINs are generally preferred for high-resolution surface modeling of complex topography and especially for areas with steep or overhanging geometry, digital elevation model (DEM) raster grids offer several advantages with respect to change detection analysis and plotting. Therefore our processing includes grid creation with a 5-cm cell size, using the natural neighbor TIN to raster method. [ArcGIS]

Surface Model Comparison

For each site, three surface models were created where applicable—one each for the September 2007, April 2010, and September 2010 field efforts. We methodically analyzed the surface models by comparing temporally sequential datasets with one another (for example, September 2007 to April 2010, April 2010 to September 2010, and so forth), thereby allowing site changes to be compared over time. Given the relatively long period of time for some comparisons (as much as three years, from September 2007 to September 2010, in the case of sites AZ:B:10:0225 and AZ:G:03:0072), it is possible that cycles of erosion and deposition may have occurred that

cannot be identified from the data. Regardless, the comparisons still provide definitive results for the time period in which monitoring occurred.

Two types of surface change maps were used to detect vertical change—a three-dimensional TIN surface change map and a two-dimensional grid of the surface change. The three-dimensional surface change map was constructed by differencing the more recent surface with the previous TIN surface, thereby producing an elevation change map. In the results, we report the number of points used in the construction of each TIN surface as an indication of the relative model point density—the actual number of points collected is typically an order of magnitude greater and indicates that the majority of the points are generally removed during vegetation filtering and surface creation, as previously described. We used these results only as a preliminary map for detecting change because the TIN-generation process typically fills in areas where little to no data existed (connecting areas of low point density with large facets than cannot adequately model the fine-scale site topography). Thus, these results can only be used accurately where change can be positively identified on the basis of sufficient point density.

To perform surface-model change detection using a uniform point density representative of the true topographic surface, we applied a point-density-based masking algorithm to each surface model DEM. The ArcGIS-based suite of algorithms (fig. 5) applied a filtering mask to the point data such that grid cells with insufficient point density for performing realistic change detection (here, selected as less than 6 points per 25 cm by 25 cm grid cell or equivalent to 96 points per m^2) were removed from the surface. Vertical change on the remaining grid cells was then analyzed and the resulting change detection DEM was displayed with warm colors (reds, oranges, yellows) representing surface lowering (erosion) and cool colors (blues, greens) representing surface heightening (deposition). Vertical change detection thresholds used to create the color maps were based on error analyses performed on each dataset and are described in subsequent sections of this report (see "Error Analysis"). For each survey area, we use the resulting colored grid maps as the representation of the change that occurred during each monitoring period.

For presentation purposes, the change maps are overlaid on a DEM hillshade map (colored with shades of gray—see "Results" section) constructed of the initial bare-ground model for each site. In some cases, these maps may include areas where no change detection was performed because of insufficient point density (that is, less than 96 points per m^2). These areas are generally small (<1 m^2) and represent isolated pockets of vegetation and shadows behind objects such as shrubs or boulders. In some cases, these areas can be identified in the hillshade DEMs by "smooth" areas of the DEM, but they should not be confused with areas outside the survey boundaries where the point density was much too low (< 10 points per m^2) to attempt detailed topographic surface construction.

When change was detected, we performed quantitative geometric and qualitative process assessments to determine the extent and likely causes of the change. If no change was detected, no additional analysis was performed. To describe detected changes, we use the generalized terms "erosion" and "deposition" to indicate surface lowering and surface rising, respectively. Thus, these may, at times, capture processes, such as visitor-induced surface compaction, that are technically neither erosional nor depositional processes. When a more specific geomorphic process could potentially be related, such as soil creep, we identified this within the results for each site. We used a combination of DEM color change maps, TIN surfaces, cross-sections, and photographs to derive the two-dimensional areal extent of the change, the overall change statistics (means, standard deviations, and maximums), and the volumes of sediment mobilized either into or out of the site. In all cases, we verified changes using either prechange and postchange photographs or additional detailed analysis of the point cloud alignment; when change could not be verified using either or both of these methods, the change was not reported.

Error Analysis

Terrestrial lidar data, similarly to any other survey data, are subject to errors originating from both the data collection and postprocessing methodologies. We include a detailed analysis of the errors associated with the data to allow the objective presentation of limitations in detecting topographic change. Because the datasets presented here (April 2010 and September 2010) were collected differently from those used for comparing and calculating change detection results (September 2007), we present a summary of error analyses for both datasets, as well as the resulting change detection analysis error for comparisons between the datasets.

Two types of analysis are presented: deterministic and empirical. These are then combined into a hybrid error analysis used to define the error bounds of the results. Deterministic error analysis was performed for all datasets previously presented (May 2006, May 2007, September 2007; Collins and other, 2009) and is generally more conservative (that is, overestimates actual errors). It is calculated by assuming that the average or maximum possible errors occurred (for example, that the average or maximum laser instrument error is inherent in every data point) and that each component of error is independent from all others (that is, errors are only additive). Empirical error analysis is not generally conservative, but it is typically more accurate. Here, empirical errors are determined by comparison of selected subsections of data with their known locations. The errors determined from this comparison are then assumed to represent the error inherent in the entire dataset. As long as a spatially valid subset of data is used in the empirical determination, the resulting error analysis is generally valid throughout the dataset. Although either of the error analysis methods can be used depending

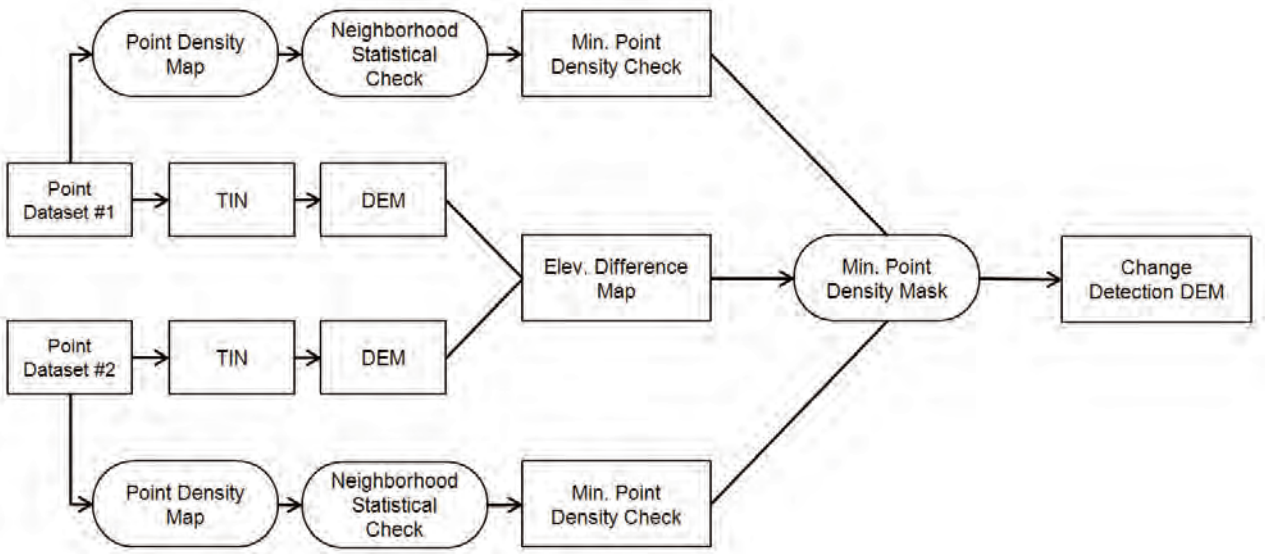

Figure 5. Schematic flow chart showing digital elevation model (DEM) processing steps for point density masking and DEM comparison. Point datasets are initially converted to triangulated irregular networks (TINs) and then DEMs through filtering and surface building routines. Subroutines check that minimum point density thresholds are met and the final change detection DEM is performed on only those areas that meet the minimum point density specification.

on the desired degree of conservatism, we adopt a hybrid approach that uses the results of both analyses, coupled with the inclusion of a surface-building-and-gridding error term that provides a final indication of the confidence in the change detected and reported in the results.

Deterministic Error Analysis

Because the 2007 and 2010 datasets used different laser instruments and consequently different registration procedures, two descriptions of deterministic error analysis are presented. The September 2007 deterministic error analysis follows that presented in Collins and others (2009) and is summarized here. Errors for this dataset originated from three sources: (1) positioning and georeferencing the laser scanner and control points (E_{survey}), (2) the laser instrument (E_{laser}), and (3) the local coordinate registration process (E_{reg}). Because two registration procedures were used to constrain all six degrees of freedom (DOF) for these datasets (three translation DOFs constrained by fixed scanner locations which do not require registration, a single registration for two rotation DOFs constrained by simultaneous rotation between two scan positions, and the final registration by an additional rotation DOF constrained by simultaneous rotation of a third scan position with the previous two—see Collins and others, 2009), E_{reg} was included twice in the overall error analysis. The resulting four error terms are assumed to be independent of one another such that the total error (E_{total}) is:

$$E_{total\ (2007)} = \sqrt{E_{survey}^{\ 2} + E_{laser}^{\ 2} + E_{reg1}^{\ 2} + E_{reg2}^{\ 2}} \qquad (1)$$

Note that each of these error terms is presented only for the vertical component, consistent with how topographic change detection maps are typically presented. The result of equation 1 for the September 2007 data was determined to be 41.8 mm, or approximately 4 cm (Collins and others, 2009). We note that no absolute georeferencing error relative to real-world coordinates is included in this or any other error estimate because the same, identical survey reference benchmarks were used for all surveys (including those performed in 2010). Therefore, in calculating differences between the datasets, any additional benchmark-related error (typically between 5 cm and 8 cm positional accuracy; Grand Canyon Monitoring and Research Center, 2008) can be ignored as long as maximum benchmark stability and minimal differential tectonic movement between benchmarks and site areas can be assumed. Similarly to previous research (Collins and others, 2009), we judge that these are both valid for short-duration surveys in Grand Canyon.

Following a similar methodology as equation 1, we computed the vertical error from the 2010 datasets. We determined the mean georeferencing error (E_{survey}) by averaging the 95-percent confidence level error bound for 113 vertical measurements in which we recorded duplicate (redundant) survey coordinates (that is, completely independent total station and (or) GPS measurements). These included laser instrument locations, control point locations, and survey benchmarks at each site. The result was a mean vertical georeferencing error (E_{survey}) of 24.7 mm. We judge this to be a conservative estimate because two standard deviations (2σ = 95-percent confidence interval assuming normally distributed data) make up the error

bounds and multiple technologies (GPS and total station) were sometimes used to obtain redundant observations.

For calculating the vertical component of error in the laser beam for the instrument used in this study (Riegl Z420i), we use the average results of an absolute accuracy calculation (11.2 mm) calculated at 50-m range by Lichti and Jamtsho (2006), which accounts for both laser beam divergence and angular resolution, and a fixed object calibration test (1.7 mm) conducted at between 15-m and 60-m range on precisely translated objects by Boehler and others (2003). The average result for E_{laser} is 6.5 mm.

We calculated registration errors by averaging the control point and laser location RMS error for each site in April 2010 and September 2010. The algorithm determines the best three-dimensional orientation of the datasets based on a comparison of finely scanned control points visible in adjacent scans. Approximately 10 surveyed points were collected at each of the 11 sites, yielding a total of 186 surveyed points and resulting in an overall average three-dimensional error (3–D error) of 13 mm for each site. Calculating the vertical component of registration error requires an assumption that the error is evenly distributed between the x, y, and z directions (that is, the 3–D error/√3; a valid assumption for this dataset), such that the average vertical registration error (E_{reg}) is 7.5 mm.

Following the methodology presented for the 2007 dataset in equation 1, and noting that only one measure of registration error is needed for the 2010 data because of the different registration procedure (control point registration versus multiple scan rotation registration—see "Data Processing" section and Collins and others, 2009), the resulting equation is:

$$E_{total\ (2010)} = \sqrt{E_{survey}{}^2 + E_{laser}{}^2 + E_{reg}{}^2} \qquad (2)$$

Using the presented values for the data collected in 2010 yields a total vertical error of 26.6 mm, or approximately 3 cm. Assuming that errors generated by either the 2007 or 2010 datasets are independent of one another (a conservative assumption because some errors such as those from the laser are likely not independent between datasets), the absolute errors between surface data can be computed by summing each component (whether from 2007 or 2010). Thus, for comparison of September 2007 data to either April 2010 or September 2010 data, the absolute vertical error is 7 cm (4 cm from 2007 and 3 cm from 2010). Similarly, for comparison of April 2010 data to September 2010 data, the absolute vertical error is 6 cm (3 cm each from each of the two 2010 datasets).

Empirical Error Analysis

Our empirical error analysis uses direct point-to-point comparisons of objects at each survey area that are "fixed" (that is, immobile) and visible within the point cloud data. We compare their absolute positions between temporally consecutive scan datasets using all point clouds from each dataset. Rocks between 25 cm and 2 m in diameter (for example, R1 through R10—see fig. 6) were the primary objects judged to be immobile for the purposes of this analysis, although large tree-trunks were used in some cases where rocks were not plentiful. Analysis consisted of isolating the points that describe a particular rock feature from each temporally different dataset and computing two sets of distance metrics to compare the relative errors between the point objects. The first distance metric compares the three-dimensional closest vectors between all points for each dataset (that is, each vector describing the distance between two points—one in each temporally different dataset). The second metric uses an iterative closest point (ICP) algorithm to solve for the preregistration and postregistration best fit of the points between datasets and again calculates the vector difference between the two sets of points. Using this algorithm, the preregistration solution provides an indication of the relative distances between the points with respect to the initial configuration of the points (but only uses the "best" fitting points rather than all points, as the first distance metric describes). Here, the postregistration results are not used because they are not representative of the registration process between the full datasets.

The calculated error statistics (tables 2 and 3) could technically be deconvoluted from a three-dimensional value to x, y, and z directions as previously shown and performed. However, because the objects and points selected (that is, the upper surfaces of rocks in most cases) are predominantly aligned with the z (up) direction, we use the statistics as direct estimates of the error associated with the vertical direction of change. We chose to compare only a single metric for determination of the change detection error thresholds and used the mean vector distance between points (first metric) rather than the mean pre-ICP point metric (second metric). This is a slightly conservative, but also more representative metric because it computes distances between all points in each analysis.

The results indicate that the mean error and standard deviation were 2.2 cm and 1.2 cm, respectively, for the comparison of the September 2007 and April 2010 datasets and 1.5 cm and 0.6 cm, respectively, for the comparison of the April 2010 and September 2010 datasets (tables 2 and 3). Assuming normally distributed errors (a valid assumption for these data—see fig. 6 with errors centered about the mean difference), the maximum empirical errors at two standard deviations (95-percent confidence interval) are 4.6 cm and 2.7 cm for the September 2007-April 2010 and April 2010-September 2010 datasets, respectively. Note that these error thresholds represent the vertical error between datasets directly, such that doubling the errors is not necessary for obtaining a change detection threshold estimate. The results are somewhat less than the deterministic and more conservative error analysis, which is expected. They represent the best analytical estimate of errors between consecutively scanned datasets.

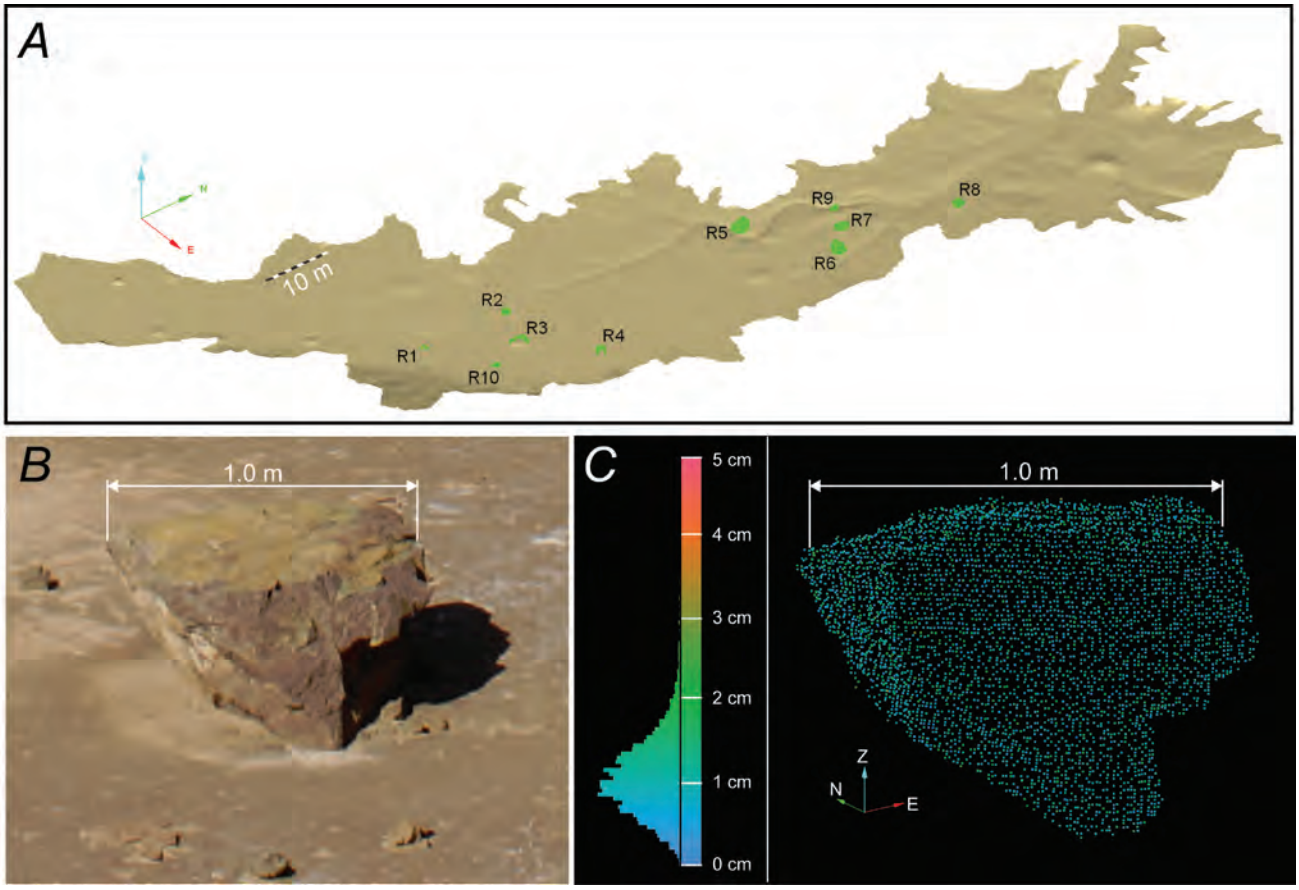

Figure 6. Empirical error analysis using fixed objects to determine mean point cloud registration differences. *A,* Oblique map view. *B,* Photo. *C,* Point cloud. The point cloud in *C* is colored according to the adjacent histogram which shows the distribution of differences between point clouds collected in April 2010 and September 2010 for one rock (R2) of the 10 shown in *A*. In most cases, only the upper surface of the objects could be described and compared, thereby providing a direct estimate of the vertical error.

Table 2. Empirical error analysis results for September 2007 to April 2010 change detection.

[Survey area codes are National Park Service archeological site identifiers; ICP refers to the iterative closest point algorithm; std.dev., standard deviation]

Survey Area	Number of independent objects	Mean vector distance between points (cm)	Std. dev. of vector distance between points (cm)	Mean pre-ICP best-fit-based distance (cm)	Std. dev. of pre-ICP best-fit-based distance (cm)
AZ:C:13:0006	5	3.0	1.5	2.0	0.7
AZ:C:13:0336	3	2.3	1.3	1.8	0.7
AZ:C:13:0099	4	2.0	0.9	1.6	0.6
AZ:C:13:0099 playa	10	2.3	1.5	1.4	0.5
AZ:C:13:0346 and AZ:C:13:0348	3	2.6	1.6	1.8	0.6
AZ:B:10:0225	8	1.5	0.7	1.2	0.4
AZ:G:03:0072 US	3	1.9	1.0	1.5	0.6
AZ:G:03:0072 DS	3	1.9	1.2	1.4	0.5
Total no. or average dist.	39	2.2	1.2	1.6	0.6

Table 3. Empirical error analysis results for April 2010 to September 2010 change detection.

[Survey area codes are National Park Service archeological site identifiers; ICP refers to the iterative closest point algorithm; std.dev., standard deviation]

Survey Area	Number of independent objects	Mean vector distance between points (cm)	Std. dev. of vector distance between points (cm)	Mean pre-ICP best-fit-based distance (cm)	Std. dev. of pre-ICP best-fit-based distance (cm)
AZ:C:05:0031	10	1.7	0.2	1.6	0.2
AZ:C:13:0006	5	1.8	0.9	1.3	0.5
AZ:C:13:0336	3	1.1	0.5	1.0	0.4
AZ:C:13:0099	4	1.6	0.7	1.3	0.5
AZ:C:13:0099 playa	10	1.2	0.5	1.1	0.4
AZ:C:13:0321	3	1.3	0.9	0.9	0.3
Total no. or average. dist.	35	1.5	0.6	1.2	0.4

Final Hybrid Error Analysis

Although both error analyses (deterministic and empirical) can be used to bracket the degree of change detection possible for the datasets, a final error analysis was performed by integrating the two analyses and coupling these with an additional error term to take into account the error associated with model building and grid calculation. Calculation of surface models can technically introduce additional error through interpolation of the point cloud to build the continuous surface required for performing large-scale change detection. This error is primarily dependent on the data density (point spacing) used in surface generation and the relative change in slope (actual surface roughness) between data points. In addition, it can be influenced by artifacts in the point cloud data (for example, small-scale vegetation such as grasses) that may not have been removed during filtering. The effect of these features is an abnormally rough surface that is not necessarily representative of the true ground conditions, such that the small-scale surface features dominate the apparent change. To account for these errors, we used the empirical error analyses previously described and visually adjusted them in the direction of the deterministic analysis results until the selected error threshold included the majority of the small-scale perturbations (that is, all small-scale perturbations could be positively identified with vegetation or TIN surface roughness rather than actual change, as determined by close comparison between point clouds, TIN models, and site photos). Essentially, this hybrid approach provides a more tractable change detection analysis result when comparing time series surfaces from the datasets.

Whereas the hybrid error analysis results varied between survey areas depending on the modeled surface perturbations (for example, resulting from variations in low-level vegetation at each survey area), for the sake of simplicity we adopted a single conservative change detection error threshold for each temporal set of datasets. The final hybrid error change detection thresholds were determined to be 5 cm and 3 cm for comparisons between September 2007 and April 2010, and April 2010 and September 2010 datasets, respectively. The surface perturbations discussed previously are therefore below this threshold. These thresholds are nearly identical to the 95-percent confidence level results using the empirical error analysis results and are used for all survey area change detection results presented in this report. They indicate what portion of the data realistically changed with respect to all known and potential errors—changes smaller than these limits are assumed to be unreliable with respect to determining topographic change. Whereas real topographic changes below these thresholds may have occurred, they are below the level of error detection and are therefore not reported.

Results

The results for 10 of the 11 survey areas are presented here. The additional site (AZ:C:13:0009) was monitored only for changes to structural walls rather than topography; results are reported in the "Monitoring Archeological Structure Stability" section. In the following subsections, brief descriptions of the topography, geomorphology, hydrology, archeology, and general vegetation ecology for each of the 10 topographically monitored areas are provided. Pederson and others (2003), Draut and others (2005), and Collins and others (2009) provide additional details about some of these areas. Base maps for site presentation were developed from the USGS GCMRC Internet Map Server (U.S. Geological Survey, 2008). However, to protect the sites, the maps do not contain georeferenced identifiable features. Change detection results highlight areas of significant erosion and deposition measured between the three surface models of the 2007–2010 datasets. As a reference, table 4 provides a summary of the number of scan locations and measured areas where data were collected, along with the area and number of points used in the creation of each surface model for the presented results. The collected and modeled surface areas are different in size because of the lack of overlap between some of the datasets and the difficulty with accurately analyzing change at the boundaries of the site area or in areas of dense vegetation.

Table 4. Summary of 2010 data collection and surface modeling at each survey area.

[Survey area codes are National Park Service archeological site identifiers]

Survey area	Number of scan locations	Approximate surface area of data collection (m^2)	Approximate number of points used in each surface model	Approximate surface area modeled for change detection (m^2)
AZ:C:05:0031	6	8,530	1,230,000	2,510
AZ:C:13:0006	7	7,150	330,000	1,280
AZ:C:13:0336	4	3,940	390,000	1,440
AZ:C:13:0099	2	860	200,000	640
AZ:C:13:0099 playa	6	10,300	1,000,000	3,400
AZ:C:13:0321	2	1,200	50,000	140
AZ:C:13:0009[1]	4	6,600	10,000	20
AZ:C:13:0346 and AZ:C:13:0348	8	6,910	670,000	3,040
AZ:B:10:0225	4	1,680	370,000	1,170
AZ:G:03:0072 US	9	2,280	567,000	1,210
AZ:G:03:0072 DS	7	2,000	170,000	590

[1] This site was monitored only for changes to structural walls within the site; results are reported in a separate section.

Site AZ:C:05:0031

Site AZ:C:05:0031 was not investigated by previous lidar surveys; the current surveys (April and September 2010) present the first opportunity for detailed change detection analysis. The site is archeologically important as an ancestral Puebloan camp site dating to the 11th or early 12th century and contains evidence of roasting features, pottery sherds, stone tool-making debris, and low stacked-stone walls (Fairley and others, 1994). The site is located immediately below a steep outcrop of Redwall Limestone. Aeolian dune sands ramp from the Colorado River up to the base of the outcrop, and the site itself is primarily located on these dune sands. A prominent gully (G1) bounds the site and the majority of the dune field to the south. The site is covered mostly by sand, but large (1 to 2 m diameter) boulders and isolated vegetation cover portions of the site. Vegetation includes clusters of prickly pear cactus (*Opuntia* sp. including beavertail cactus, *Opuntia basilaris*), ephedra (*Ephedra* sp.), dropseed grass (*Sporobolus* sp.), Indian rice grass (*Achnatherum hymenoides*), asters (Asteraceae family), dicoria (*Dicoria canescens*), and nonnative Russian thistle (*Salsola tragus*) (Draut, 2011). O'Brien and Pederson (2009a) identified gullying, aeolian transport, piping, and creep as the geomorphic processes affecting this site and noted that whereas aeolian transport and recent revegetation efforts have stabilized some parts of the site, some archeological resources continue to be affected by creep processes. Additional site details are included in O'Brien and Pederson (2009a).

We performed change detection in the area of the archeological site below the Redwall outcrop and in six areas of dune sand located between the outcrop and the Colorado River (figs. 7 and 8). The purpose of the dune-sand change detection was to identify areas potentially subject to aeolian aggradation in response to the building of a sand bar immediately upwind of the dune area during a March 2008 high flow experiment (Hazel and others, 2010). This is important to study because it has been suggested that the creation of new sand bars during sediment-enriched high flows could potentially increase the amount of

Table 5. Summary of detailed topographic change at Site AZ:C:05:0031.

Area number	Time period (m/yyyy)	Area (m^2)	Average depth (cm)	Volume (m^3)
AZ:C:05:0031 – ER1	4/2010-9/2010	4.7	4	-0.20
AZ:C:05:0031 – ER2	4/2010-9/2010	5.5	4	-0.24
AZ:C:05:0031 – ER3	4/2010-9/2010	15.7	5	-0.70
AZ:C:05:0031 – ER4	4/2010-9/2010	21.9	4	-0.92
AZ:C:05:0031 – ER5	4/2010-9/2010	36.8	4	-1.57
AZ:C:05:0031 – ER6	4/2010-9/2010	2.1	3	-0.07
AZ:C:05:0031 – ER7	4/2010-9/2010	2.1	3	-0.08
AZ:C:05:0031 – ER8	4/2010-9/2010	46.1	4	-1.91

aeolian sand transported towards archeological sites, thereby helping to protect the archeological sites from further degradation (Draut and others, 2010a).

Surface comparison between the April 2010 and September 2010 datasets indicates that four areas (ER1 through ER4) underwent erosion within or near the archeological site and four areas (ER5 through ER8) underwent erosion in the adjacent dune-sand areas during this time period (fig. 9, table 5). Aeolian processes were the likely primary cause for these changes, as evidenced by the sand ripples observed at the site and the generally small depths and widespread areas in which change occurred. No areas of deposition were identified, suggesting that the sand was transported out of the general vicinity of the archeological site, most likely either towards the river or northward to another area of active dunes.

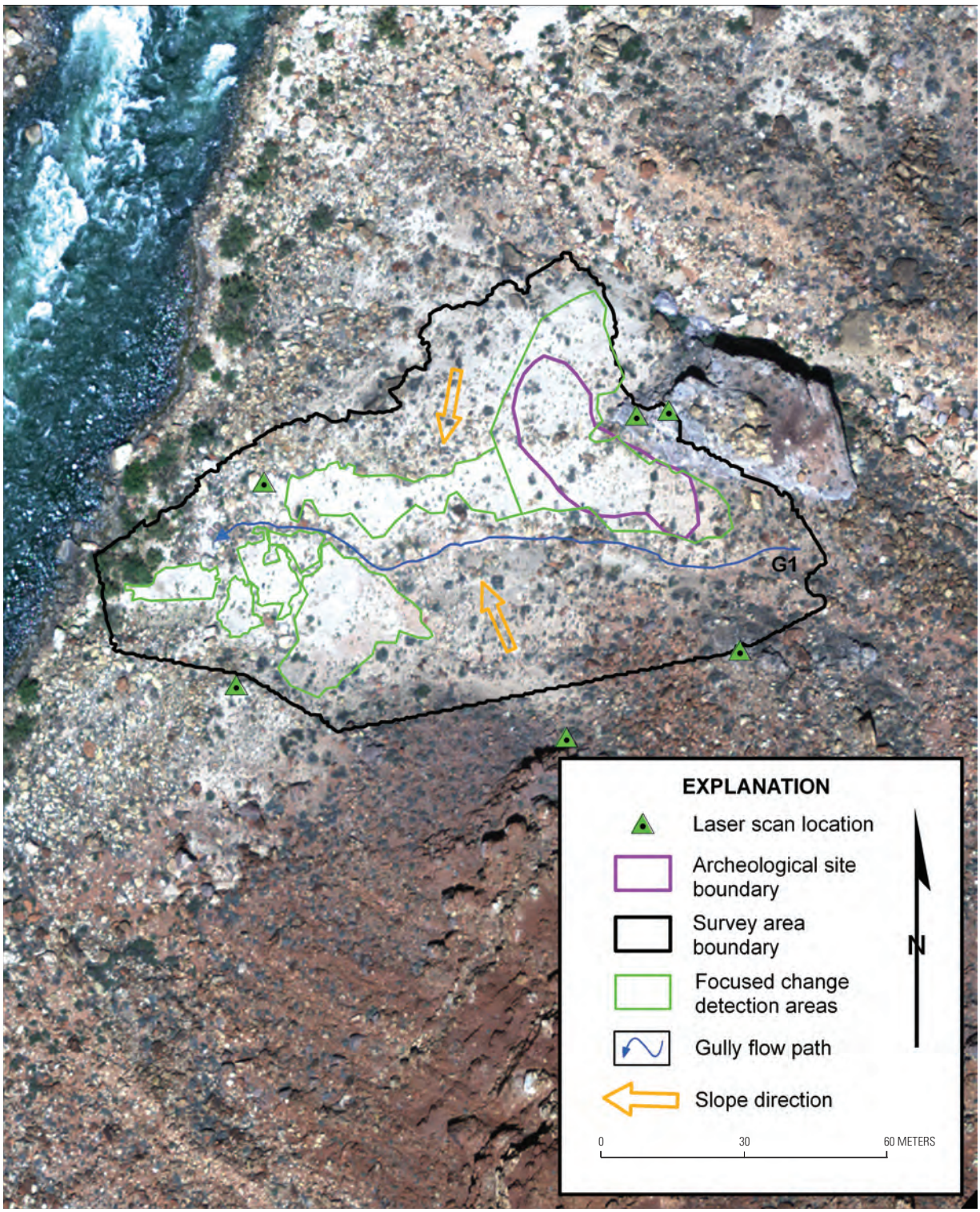

Figure 7. Site AZ:C:05:0031 survey map. Change detection was only analyzed in the focused areas noted.

Figure 8. Site AZ:C:05:0031 survey area photo showing gully location (G1). View is to the southwest.

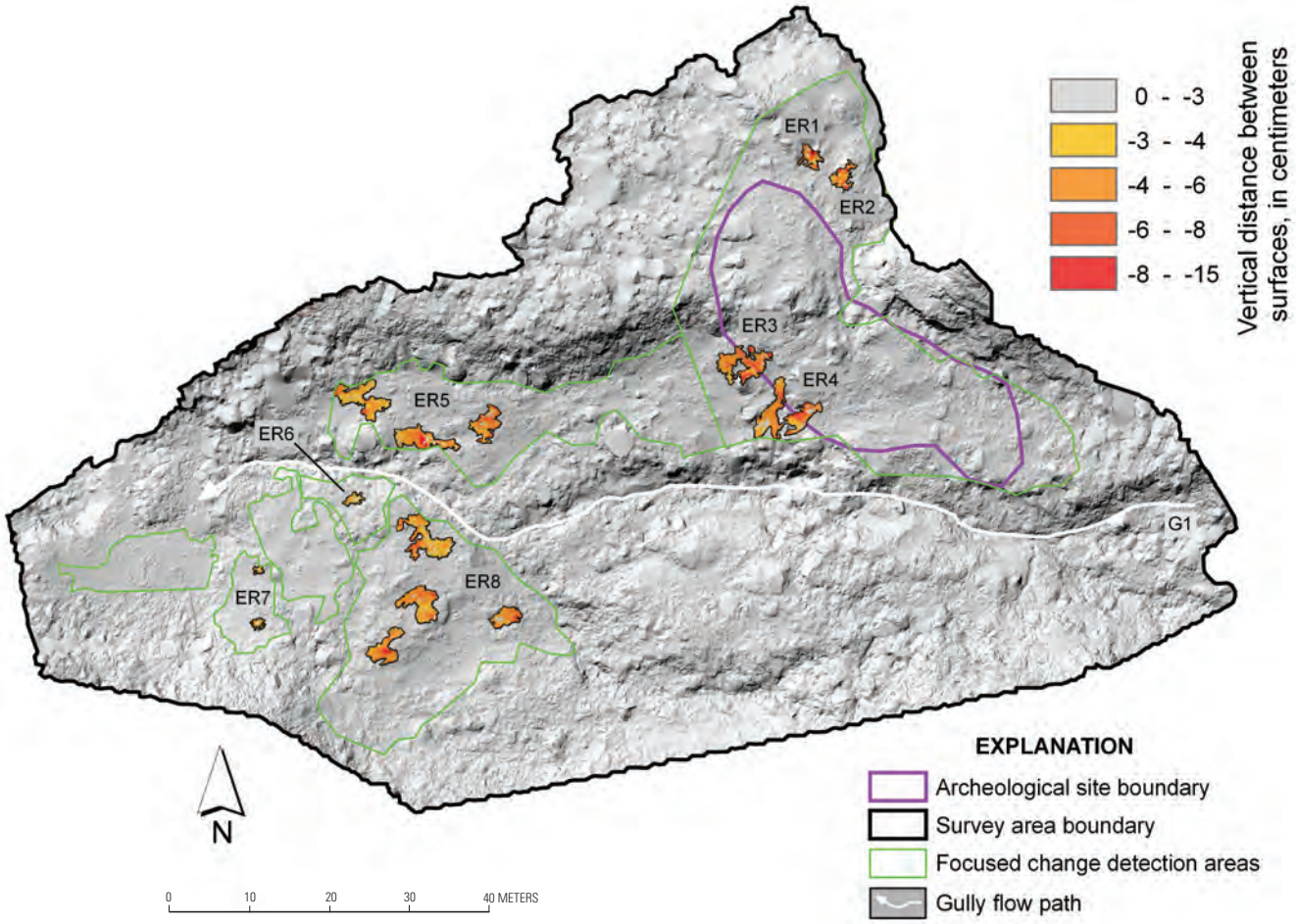

Figure 9. Site AZ:C:05:0031: 5-cm gridded output showing erosion (warm colors, negative) from April 2010 to September 2010. Change detection was only analyzed in focused areas noted. No deposition was detected during this time. Identified change is outlined by polygons, and labels (ER = erosion) are cross-referenced with table 5.

Site AZ:C:13:0006

Site AZ:C:13:0006 has been monitored by terrestrial lidar five times since 2006. The site is an area of Puebloan II (about A.D. 900 to 1100) habitation (Fairley and others, 1994), and although there are no visible habitation structures, the types and varieties of artifacts visible on the site surface suggest that structures may be buried beneath the dune sands in this area. A debris fan covered by alluvium, colluvium, and aeolian dune sands forms the majority of the site area and is bordered on one side by Bright Angel Shale outcrops and on the other by the trunk of a small (~5 m wide) tributary channel that drains directly to the Colorado River (figs. 10 and 11). Three gullies (G1, G2, G3) drain the relatively flat upper site and connect to either the tributary channel (G1, G2) or a lower alluvial terrace that borders the river's edge (G3). Brush and rock check dams were installed in each of these gullies in May 2006 (O'Brien and Pederson, 2009b). Vegetation consists of a mix of bunch grasses and small cacti, chiefly prickly pear (for example, *Opuntia polyacantha* var. *erinacea*), with a few larger mesquite trees (*Prosopis glandulosa* var. *torreyana*) located near the boundaries of the site. O'Brien and Pederson (2009a) identified creep, aeolian transport, overland flow, and rainsplash as the geomorphic processes affecting this site and noted that some of these processes are currently eroding artifacts. Additional site details are included in O'Brien and Pederson (2009a,b).

Change detection analysis results for the first three surveys spanning 2006–2007 are provided by Collins and others (2009). Previously, wide-scale topographic changes consisting of gully erosion and aeolian sand deposition and subsequent erosion were detected here, and a net deposition of sand between May 2006 and September 2007 near gully G2 appeared to smooth the topographic profile at this location (Collins and others, 2009). Overall aggradation within the lower section of this gully was confirmed by total station measurements made by O'Brien and Pederson (2009b). Here, we provide change detection results between September 2007 and the two 2010 datasets.

Surface comparison between September 2007 and April 2010 indicates that change occurred in two areas of the site—one located in a convex area of the lower slope east of gully G2, and the other located in a similar setting east of gully G1 (fig. 12). In neither case can the changes be directly related to processes occurring within the existing gullies at the site. Rather, the first (ER1 through ER4) appears to be related to aeolian transport with minor overland flow in an area previously identified as an active dune slope, whereas the second (ER5 through ER11 and DEP1 through DEP3) appears to be the result of overland flow and soil creep processes in the steepest, convex part of the site. The first erosion area coincides with a section of the site that has undergone both aeolian deposition and subsequent erosion linked to transport of sand from an adjacent sand bar/dune area (Collins and others, 2009). Although visual evidence of overland flow deposits located in the tributary channel below this area constrains the end location for some of the volume eroded, the whereabouts of the aeolian sand removed from the site was not identified. However, in April 2010, we observed very strong (40–50 km/h) wind move sand tens of meters into the air and transport at least some sand to a dune slope on the opposite (south) side of the tributary channel that demarcates the south boundary of the site, suggesting that areas ER1 through ER4 may be losing sand to that location.

It is unclear why the second set of areas (ER5 through ER11) was particularly subject to change—one possibility is that the cryptobiotic crust was destabilized through slope creep and (or) rainsplash processes. Tressler (2011) and Tressler and Pederson (2010) identified creep as an active process at a different area of this site, suggesting that creep may have a significant role in erosion along the steep, convex portions of the site. In addition, there is some visual evidence for new, subtle, channelized flow in parts of this area, but not within a well-formed gully. Whereas the depositional areas can more than likely be linked to their erosion sources located immediately adjacent to them, volumetric comparison of erosion and deposition volumes indicates that a majority of sediment was deposited in the tributary channel immediately below these areas. The large magnitude (more than 10 cm) of erosion (table 6) for some areas is thought to be due to collapse in an oversteepened part of the slope and thus not indicative of more typical erosion previously documented at the site (Collins and others, 2009).

The only change detected between April 2010 and September 2010 was in the active aeolian erosion areas previously identified (ER1 through ER4; fig 13). Here, slope-smoothing processes (most likely from continued aeolian transport) caused subtle erosion to the topography. When this minor amount of erosion is added to that previously measured, and then compared to the volume of sediment deposited in this location between May 2006 and May 2007 (Collins and others, 2009), the overall erosion volume between May 2007 and September 2010 (1.0 m^3, table 6) is still considerably less than the amount of deposition, so there has been a net depositional gain in this area of the site between May 2006 and September 2010.

Table 6. Summary of topographic change at Site AZ:C:13:0006.

Area number	Time period (m/yyyy)	Area (m^2)	Average depth (cm)	Volume (m^3)
AZ:C:13:0006 – ER1	9/2007-4/2010	2.0	14	-0.29
AZ:C:13:0006 – ER2	9/2007-4/2010	1.3	17	-0.21
AZ:C:13:0006 – ER3	9/2007-4/2010	1.0	16	-0.16
AZ:C:13:0006 – ER4	9/2007-4/2010	1.6	14	-0.22
AZ:C:13:0006 – ER5	9/2007-4/2010	1.3	9	-0.12
AZ:C:13:0006 – ER6	9/2007-4/2010	7.3	13	-0.97
AZ:C:13:0006 – ER7	9/2007-4/2010	1.2	11	-0.12
AZ:C:13:0006 – ER8	9/2007-4/2010	2.6	14	-0.35
AZ:C:13:0006 – ER9	9/2007-4/2010	2.1	10	-0.20
AZ:C:13:0006 – ER10	9/2007-4/2010	0.8	11	-0.09
AZ:C:13:0006 – ER11	9/2007-4/2010	5.8	10	-0.59
AZ:C:13:0006 – DEP1	9/2007-4/2010	2.7	9	0.25
AZ:C:13:0006 – DEP2	9/2007-4/2010	4.2	11	0.43
AZ:C:13:0006 – DEP3	9/2007-4/2010	1.9	8	0.16
AZ:C:13:0006 – ER1	4/2010-9/2010	1.0	10	-0.08
AZ:C:13:0006 – ER2	4/2010-9/2010	0.4	4	-0.01
AZ:C:13:0006 – ER3	4/2010-9/2010	0.4	5	-0.02
AZ:C:13:0006 – ER4	4/2010-9/2010	0.4	5	-0.03

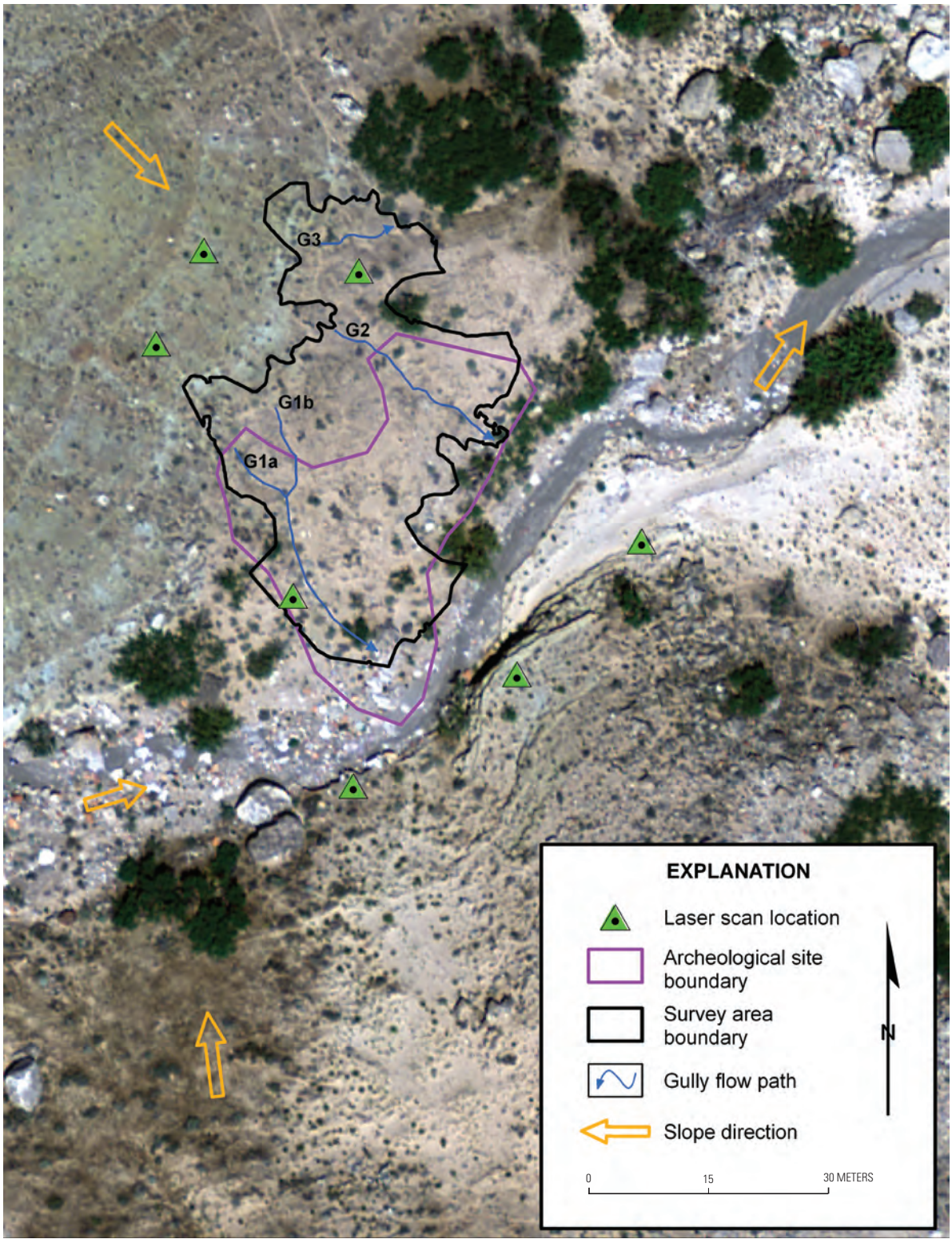

Figure 10. Site AZ:C:13:0006 survey map.

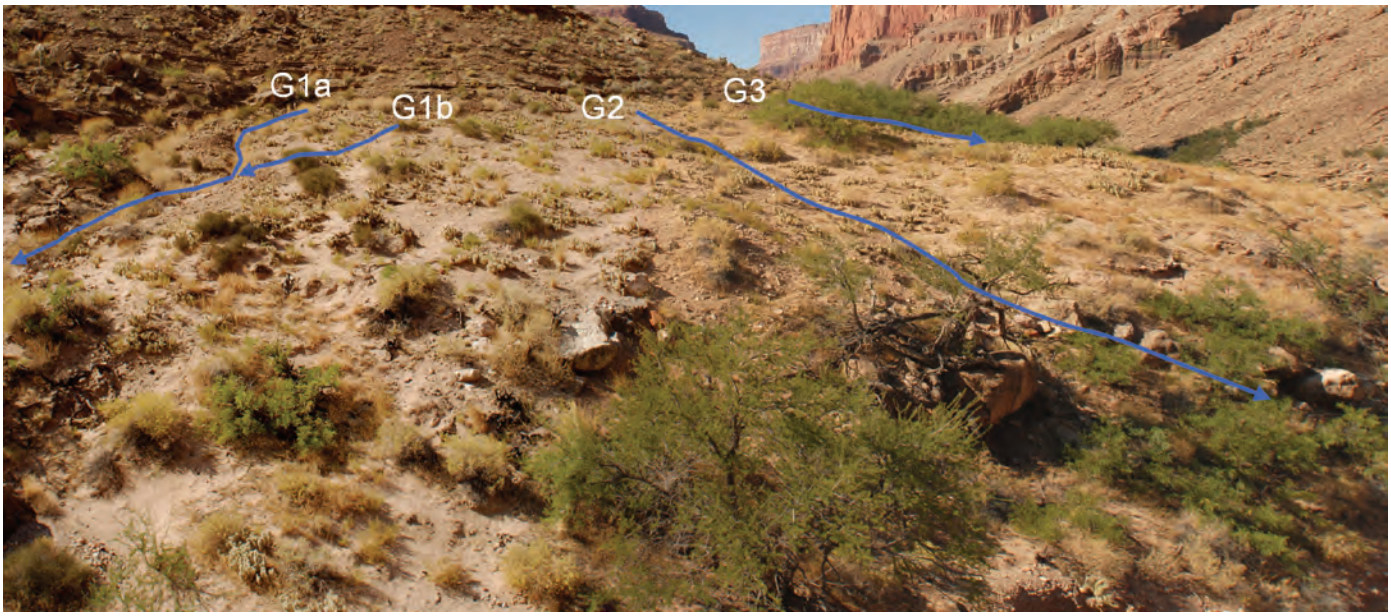

Figure 11. Site AZ:C:13:0006 survey area photo showing gully locations (G1 to G3). View is to the northwest.

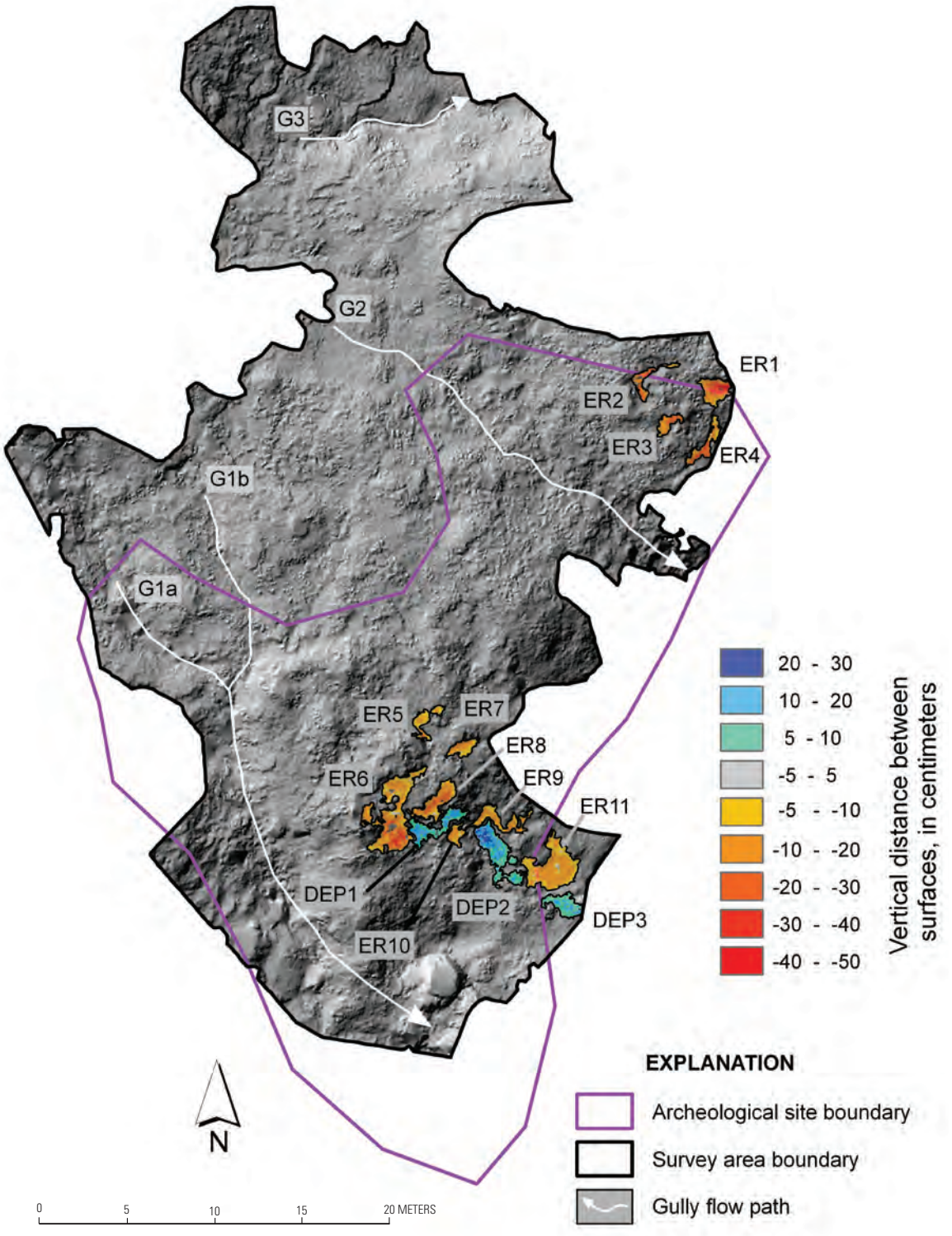

Figure 12. Site AZ:C:13:0006: 5-cm gridded output showing erosion (warm colors, negative) and deposition (cool colors, positive) from September 2007 to April 2010. Identified change is outlined by polygons, and labels (ER = erosion, DEP=deposition) are cross-referenced with table 6.

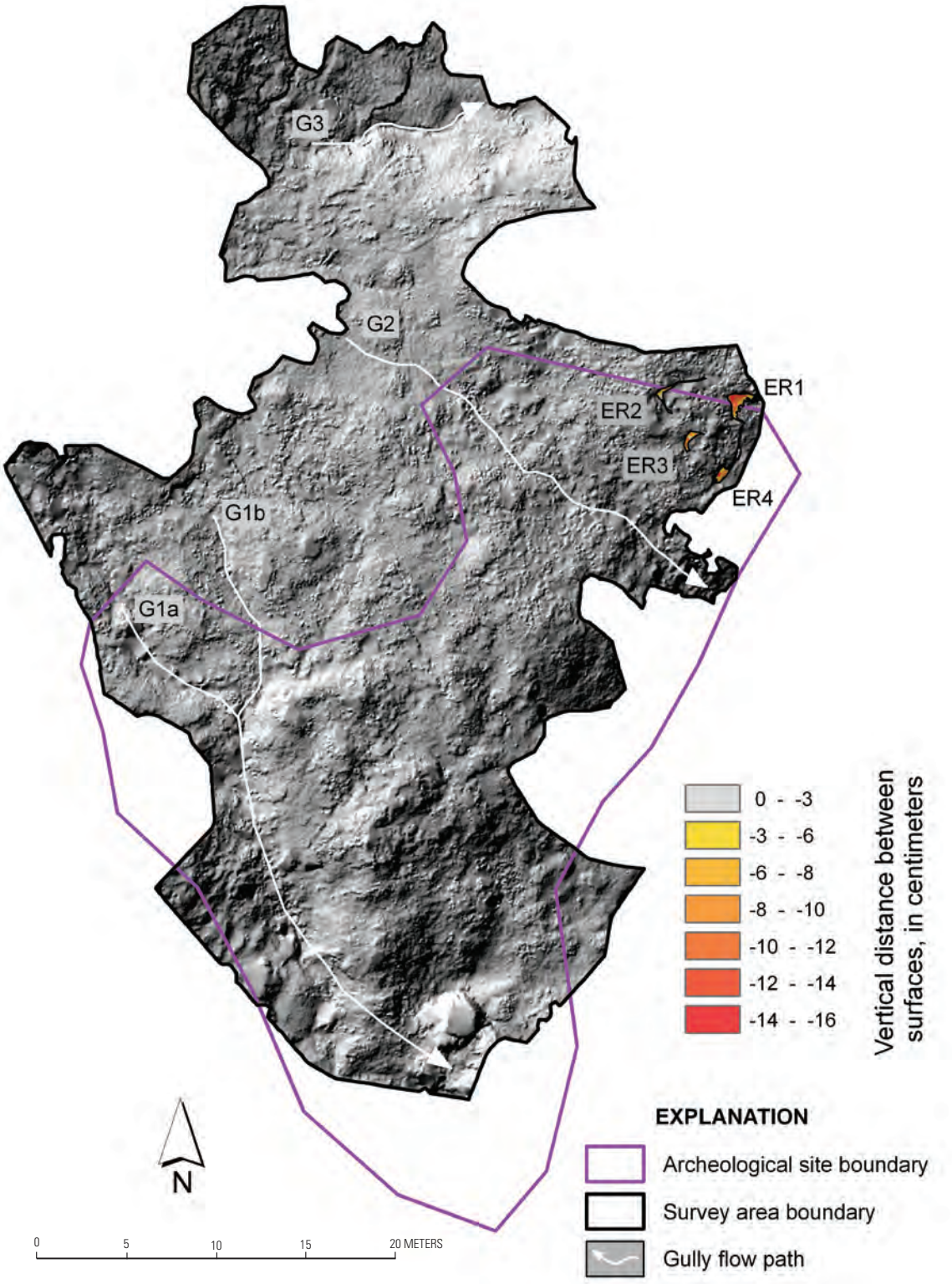

Figure 13. Site AZ:C:13:0006: 5-cm gridded output showing erosion (warm colors, negative) from April 2010 to September 2010. No deposition was detected during this time. Identified change is outlined by polygons, and labels (ER = erosion) are cross-referenced with table 6.

Site AZ:C:13:0336

Site AZ:C:13:0336 is located in the Palisades region of Grand Canyon and has been monitored by terrestrial lidar five times since 2006. The site consists of sparse artifacts and fire-cracked rocks eroding from the face of a low-angle terrace scarp (Fairley and others, 1994). A relatively flat area of flood-deposited sediment immediately to the east of the site is drained by several shallow gullies that spill over the terrace scarp onto a lower fluvial terrace mantled by aeolian sand (figs. 14 and 15). Check dams of brush and rock were installed within the main gully (gully G2) at the site in 2007 to prevent ongoing erosion (O'Brien and Pederson, 2009a,b) Vegetation consists of irregularly spaced grasses, shrubs, and prickly pear cacti (for example, *Opuntia polyacantha* var. *erinacea*) in the flatter upper portion of the site and mesquite trees (*Prosopis glandulosa* var. *torreyana)* several meters in height located at the edges of the site. These trees are a major control on stabilization of coppice dunes that border the site. O'Brien and Pederson (2009a) identified gullying, rilling, creep, overland flow, and aeolian transport as the geomorphic processes affecting this site and noted that creep processes were incrementally eroding artifacts here. Additional site details are included in O'Brien and Pederson (2009a,b).

Change detection analysis results for the first three surveys spanning 2006–2007 for this site are provided by Collins and others (2009). Previously, one area of deposition was identified behind a small brush check dam within a shallow gully (G2—figs. 14 and 15) that bisects the site. This was confirmed by total station measurements made by O'Brien and Pederson (2009b), who measured overall thalweg aggradation during the same period (May 2006 to September 2007). Here, we provide change detection results between September 2007 and the two 2010 datasets.

Surface comparison between September 2007 and April 2010 indicates that 10 areas underwent erosion and 1 area underwent deposition during this period (fig. 16, table 7). In addition, deposition over an area of 2.2 m^2 (labeled "DEP2?" in fig. 16) was identified in the same area as that in which previous deposition occurred during the 2006–2007 surveys (Collins and others, 2009). However, as a result of the laser instrument being located at an oblique angle to this area, the data-point density for this small area was insufficient to conclude that this deposition signal was real. It is therefore not included in table 7, but it is highlighted in figure 16 with the label "DEP2?" because of its importance with regard to existing check dams located in this area.

The 10 identified erosion areas (fig. 16) are located throughout the site and consist of a mix of unvegetated, open-sand areas likely reworked by aeolian processes (for example, ER1, ER2, ER3, ER8, ER10) and by channelized gully processes (for example, ER6, ER7, ER9). Two areas (ER4, ER5) could not be positively linked to a particular geomorphic process because of their close proximity to both aeolian sand deposits and a channel thalweg terminus (near where gully G1 and gully G2 meet). The areas likely associated with channelized overland flow are particularly interesting, especially ER9. Here, a new gully (G3), not very well formed during the time of previous surveys (that is, 2006–2007; Collins and others, 2009), now appears well developed and actively eroding. Because the erosion is confined to the channel, the change mechanism is most likely channelized flow. However, this area, along with ER10, is in close proximity to informal hiking trails used by visitors, so an anthropogenic contribution cannot be ruled out. The ER7 area within gully G2 shows evidence that gully downcutting and channel wall widening have occurred. This area is located above a series of rock check dams (rcd, see fig. 15), suggesting that the channel protection has either reached its capacity or is no longer functioning properly (that is, flow may be circumventing the check dam). Site observations indicate that at least some degree of infilling has occurred, but it is below the error threshold for the presented lidar surveys during this time period (5 cm). Finally, we observe that because no significant volumes of sediment deposition were identified at any of the gully termini within a larger area of alluvial sediments (well landward of the river), the sediment contributed by gully erosion must have been transported out of the surveyed site boundaries, with the exception of the potential deposition outlined by "DEP2?" in figure 16.

The one deposition area (DEP1) is located immediately adjacent to the ER10 area that underwent aeolian erosion. Our observations indicate that this area is also a product of aeolian processes and, in fact, is composed of an almost identical volume of sediment as was removed from ER10. This suggests that the ER10 and DEP1 areas are geomorphologically linked through aeolian sand transport, although it is possible that these features are linked to other areas of erosion and deposition.

Between April 2010 and September 2010, we identified 10 areas of erosion and 1 area of deposition (fig. 17, table 7). Many of these were located in areas of previous activity identified in the September 2007 to April 2010 comparison and are likely linked to aeolian activity on unvegetated patches of sand. Most pronounced was the erosion that occurred at the September 2007 to April 2010 ER9 area, which continued between April 2010 and September 2010 with an additional 4 cm of downcutting (ER7, table 7). Whereas overland flow related transport out of the gully system likely occurred, evidence of aeolian activity is also clearly evident from photo comparison analysis. However, similarly to our previous conclusions for this site, an anthropogenic cause (that is, surface disturbance by hikers) cannot be ruled out. The one deposition area (DEP1) furthers the case for active, ongoing aeolian transport at this site; deposition on the order of 3 cm occurred along an area bordering gully G3 and is most likely linked to the aeolian erosion areas (ER6, ER8) immediately upgully to the south and east.

Table 7. Summary of detailed topographic change at Site AZ:C:13:0336.

Area number	Time period (m/yyyy)	Area (m^2)	Average depth (cm)	Volume (m^3)
AZ:C:13:0336 – ER1	9/2007-4/2010	7.1	7	-0.60
AZ:C:13:0336 – ER2	9/2007-4/2010	3.5	6	-0.26
AZ:C:13:0336 – ER3	9/2007-4/2010	0.6	8	-0.04
AZ:C:13:0336 – ER4	9/2007-4/2010	1.0	7	-0.06
AZ:C:13:0336 – ER5	9/2007-4/2010	1.3	7	-0.09
AZ:C:13:0336 – ER6	9/2007-4/2010	1.6	6	-0.11
AZ:C:13:0336 – ER7	9/2007-4/2010	4.6	7	-0.37
AZ:C:13:0336 – ER8	9/2007-4/2010	0.7	8	-0.06
AZ:C:13:0336 – ER9	9/2007-4/2010	17.0	6	-1.84
AZ:C:13:0336 – ER10	9/2007-4/2010	1.7	7	-0.14
AZ:C:13:0336 – DEP1	9/2007-4/2010	2.2	7	0.16
AZ:C:13:0336 – ER1	4/2010-9/2010	0.6	3	-0.02
AZ:C:13:0336 – ER2	4/2010-9/2010	0.4	3	-0.01
AZ:C:13:0336 – ER3	4/2010-9/2010	0.2	3	-0.01
AZ:C:13:0336 – ER4	4/2010-9/2010	0.6	3	-0.02
AZ:C:13:0336 – ER5	4/2010-9/2010	0.4	3	-0.01
AZ:C:13:0336 – ER6	4/2010-9/2010	1.3	4	-0.05
AZ:C:13:0336 – ER7	4/2010-9/2010	8.3	4	-0.32
AZ:C:13:0336 – ER8	4/2010-9/2010	3.7	4	-0.16
AZ:C:13:0336 – ER9	4/2010-9/2010	0.9	4	-0.03
AZ:C:13:0336 – ER10	4/2010-9/2010	0.1	3	-0.01
AZ:C:13:0336 – DEP1	4/2010-9/2010	1.5	3	0.05

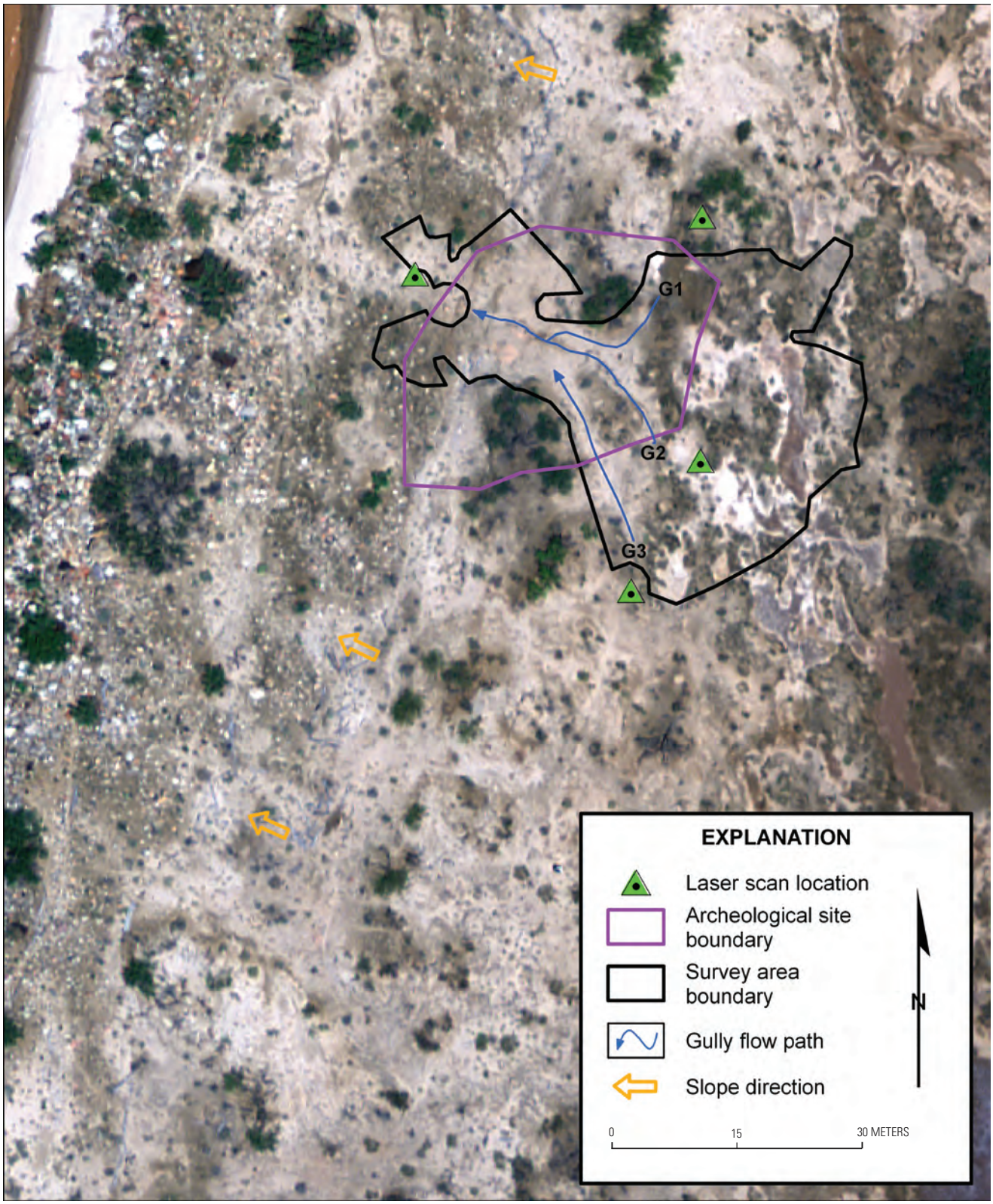

Figure 14. Site AZ:C:13:0336 survey map.

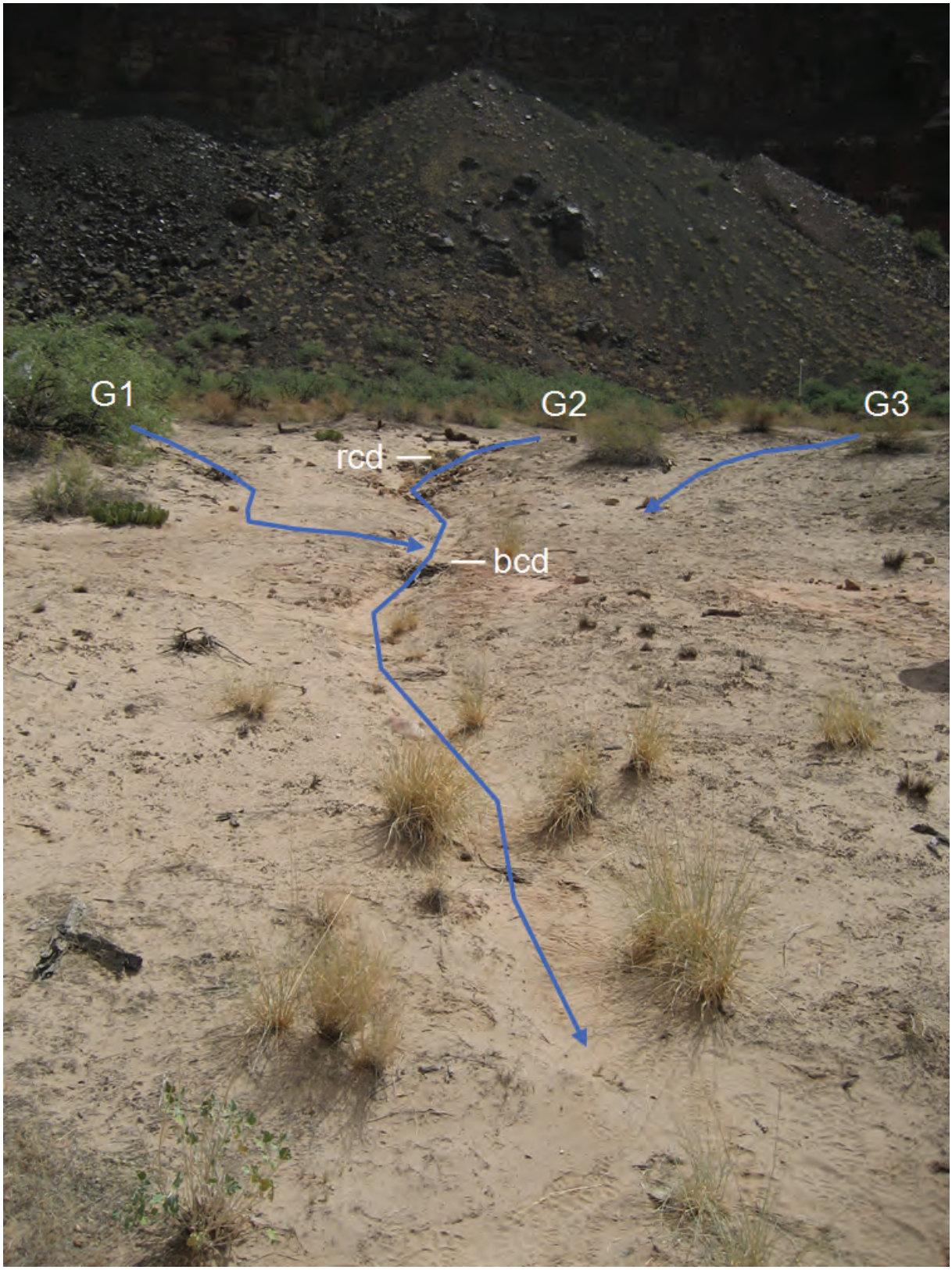

Figure 15. Site AZ:C:13:0336 survey area photo showing gully locations (G1 to G3), and brush (bcd) and rock check dams (rcd). View is to the southeast.

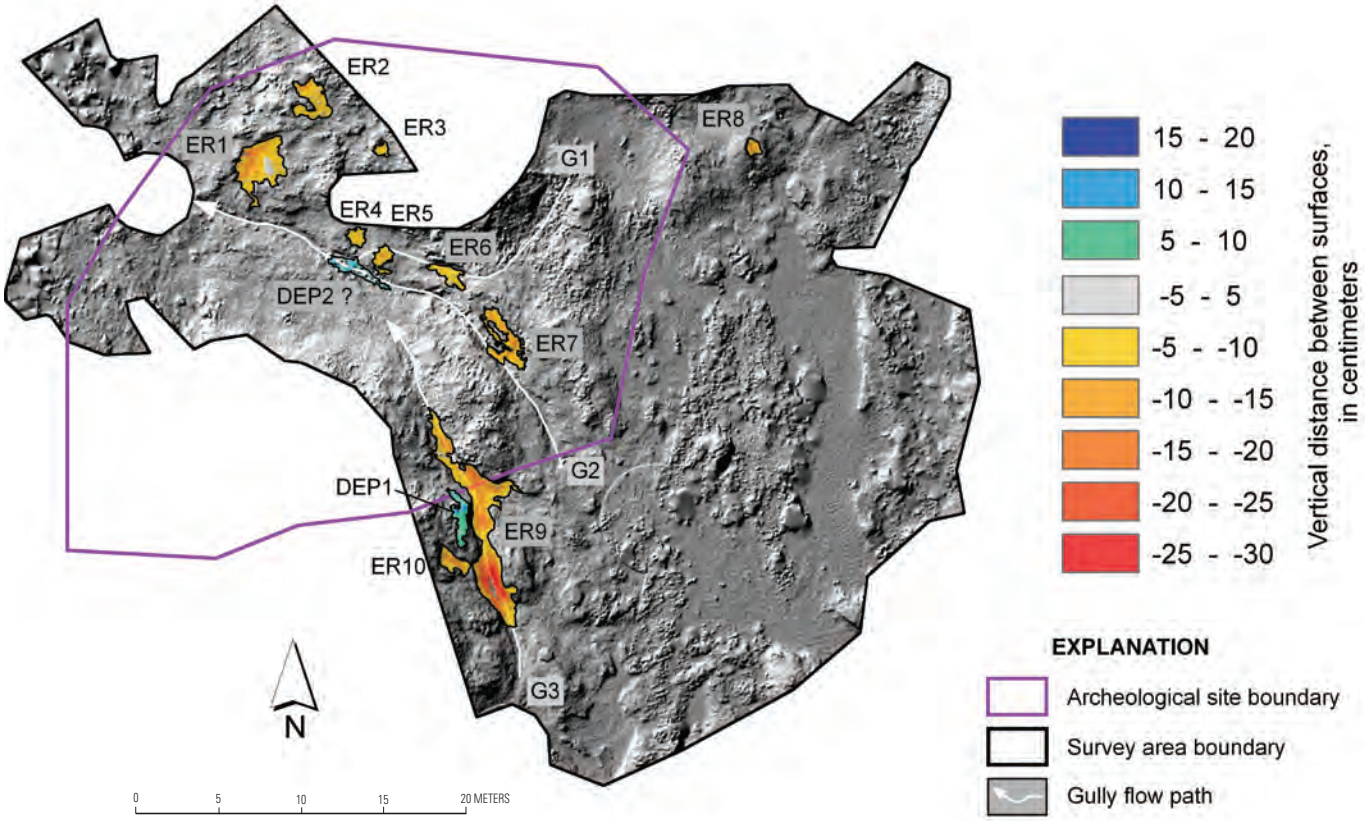

Figure 16. Site AZ:C:13:0336: 5-cm gridded output showing erosion (warm colors, negative) and deposition (cool colors, positive) from September 2007 to April 2010. Identified change is outlined by polygons, and labels (ER = erosion, DEP=deposition) are cross-referenced with table 7. Area outlined by DEP2? indicates probable deposition in the gully channel, but depth and volume cannot be verified because of low lidar point density in the channel.

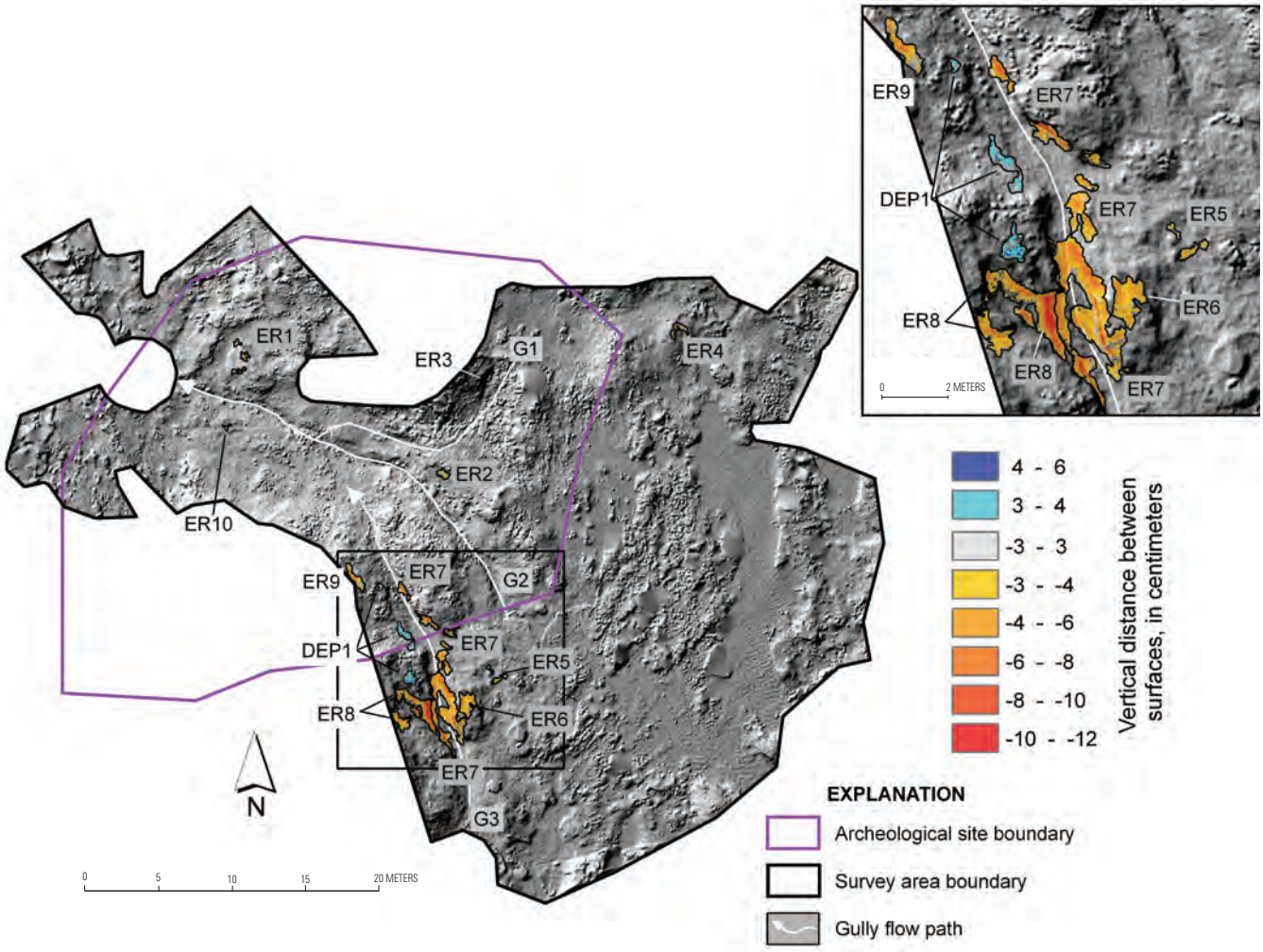

Figure 17. Site AZ:C:13:0336: 5-cm gridded output showing erosion (warm colors, negative) and deposition (cool colors, positive) from April 2010 to September 2010. Identified change is outlined by polygons, and labels (ER = erosion, DEP=deposition) are cross-referenced with table 7.

Site AZ:C:13:0099

Site AZ:C:13:0099 in the Palisades region has been monitored by terrestrial lidar five times since 2006. The site is archeologically important because of the high density of early-middle Pueblo II artifacts and habitation structures found here, with evidence of a pre-Puebloan occupation as well (Fairley and others, 1994). In addition, buried structures and a variety of artifacts have been exposed by gully sidewall erosion in recent years. The site is located north of Site AZ:C:13:0336, in and around a deeply (>1 m) incised gully system (figs. 18 and 19) that drains much of this area and begins as a series of smaller shallow tributary drainages to the east at the base of a steep talus slope. Rock check dams have been used in the past to mitigate ongoing erosion at several locations within this site. Vegetation occurs throughout the site, including large (several meters in canopy diameter) mesquite trees (*Prosopis glandulosa* var. *torreyana*) and smaller shrubs and grasses. O'Brien and Pederson (2009a) identified gullying, aeolian transport, and piping as the geomorphic processes affecting this site and noted that archeological resources were being destroyed by gullying here. Additional site details are included in O'Brien and Pederson (2009a)

Change detection analysis results for the first three surveys spanning 2006–2007 for this site are provided by Collins and others (2009). Previous surveys detected deposition and erosion at this site related to aeolian and gullying processes.

Because of the presence of ancestral Puebloan structures and artifacts buried in the vicinity and the imminent destruction of parts of the site by gullying erosion, the site was excavated by the National Park Service and Museum of Northern Arizona in spring 2008 to record and document the archeological history of the site (Anderson and Neff, 2011). Following these activities, the excavations were backfilled and the site topography was restored as close as possible to preexcavation site contours. Thus, lidar-derived change detection at this site provides a means to discriminate the preexcavation and postexcavation topography and to determine if any other nonanthropogenic changes occurred at the site during the April 2010 to September 2010 time interval.

We identified at least 13 areas of erosion and 5 areas of deposition between September 2007 and April 2010 (fig. 20, table 8). Most of these areas (for example, ER1, ER11, DEP4) are known to have been modified by excavation activities (Anderson and Neff, 2011); most areas of erosion coincide with locations of excavation, and areas of deposition are where backdirt from the excavation units was piled and screened. Whereas some areas of change may have been caused by natural agents, given the magnitude of the excavation activities and the amount of hiker traffic that occurs in this area, anthropogenic causes for all of the detected change cannot be ruled out. No further attempt has been made at understanding the causal geomorphologic factors affecting the site during this time frame (September 2007 to April 2010).

Between April 2010 and September 2010, we identified one area of erosion and four areas of deposition (fig. 21). The erosion area is located on the bank of the main gully, in an area of aeolian sediments, and coincides with the ER3 area from the September 2007 to April 2010 interval that also underwent erosion during that time period. The four identified areas of deposition between April 2010 and September 2010 are all located within, and at the bottom of, the gully channels. Photo comparison between April 2010 and September 2010 indicate that aeolian transport is potentially responsible for at least some of the deposition. However, careful review of photos indicates that some bank erosion located in difficult-to-model (and therefore unquantified) overhanging channel walls occurred during this time period. This suggests that channelized flow led to bank collapses, and these collapses may be responsible for the additional in-channel deposition. In general, although both the erosion and deposition areas are relatively small, they indicate that geomorphic processes continue to be active at this site, even over short time intervals (5 months).

Table 8. Summary of detailed topographic change at Site AZ:C:13:0099.

Area number	Time period (m/yyyy)	Area (m^2)	Average depth (cm)	Volume (m^3)
AZ:C:13:0099 – ER1	9/2007-4/2010	41.6	25	-10.39
AZ:C:13:0099 – ER2	9/2007-4/2010	3.3	21	-0.49
AZ:C:13:0099 – ER3	9/2007-4/2010	2.0	10	-0.19
AZ:C:13:0099 – ER4	9/2007-4/2010	9.7	7	-0.96
AZ:C:13:0099 – ER5	9/2007-4/2010	4.3	8	-0.42
AZ:C:13:0099 – ER6	9/2007-4/2010	2.0	8	-0.15
AZ:C:13:0099 – ER7	9/2007-4/2010	2.0	7	-0.18
AZ:C:13:0099 – ER8	9/2007-4/2010	6.6	14	-1.02
AZ:C:13:0099 – ER9	9/2007-4/2010	2.7	8	-0.22
AZ:C:13:0099 – ER10	9/2007-4/2010	0.8	7	-0.05
AZ:C:13:0099 – ER11	9/2007-4/2010	18.5	14	-1.97
AZ:C:13:0099 – ER12	9/2007-4/2010	5.5	15	-0.88
AZ:C:13:0099 – ER13	9/2007-4/2010	4.0	11	-0.37
AZ:C:13:0099 – DEP1	9/2007-4/2010	4.8	8	0.39
AZ:C:13:0099 – DEP2	9/2007-4/2010	2.6	8	0.25
AZ:C:13:0099 – DEP3	9/2007-4/2010	3.0	15	0.44
AZ:C:13:0099 – DEP4	9/2007-4/2010	3.2	20	0.70
AZ:C:13:0099 – DEP5	9/2007-4/2010	8.9	11	1.00
AZ:C:13:0099 – ER1	4/2010-9/2010	0.4	4	-0.02
AZ:C:13:0099 – DEP1	4/2010-9/2010	0.2	4	0.01
AZ:C:13:0099 – DEP2	4/2010-9/2010	0.6	5	0.02
AZ:C:13:0099 – DEP3	4/2010-9/2010	0.4	6	0.01
AZ:C:13:0099 – DEP4	4/2010-9/2010	0.4	6	0.01

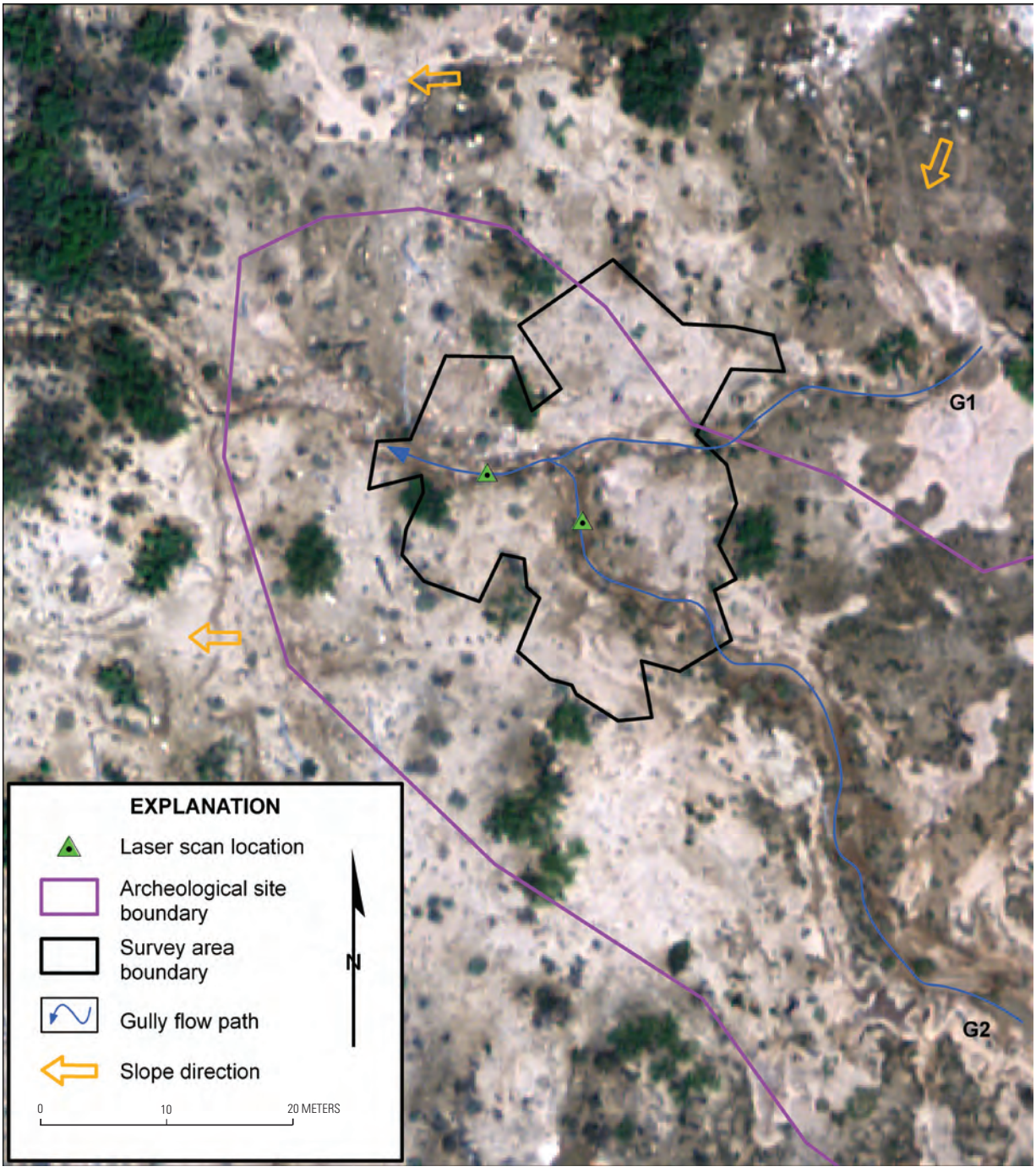

Figure 18. Site AZ:C:13:0099 survey map.

Figure 19. Site AZ:C:13:0099 survey area photo showing gully locations (G1 and G2). View is to the east.

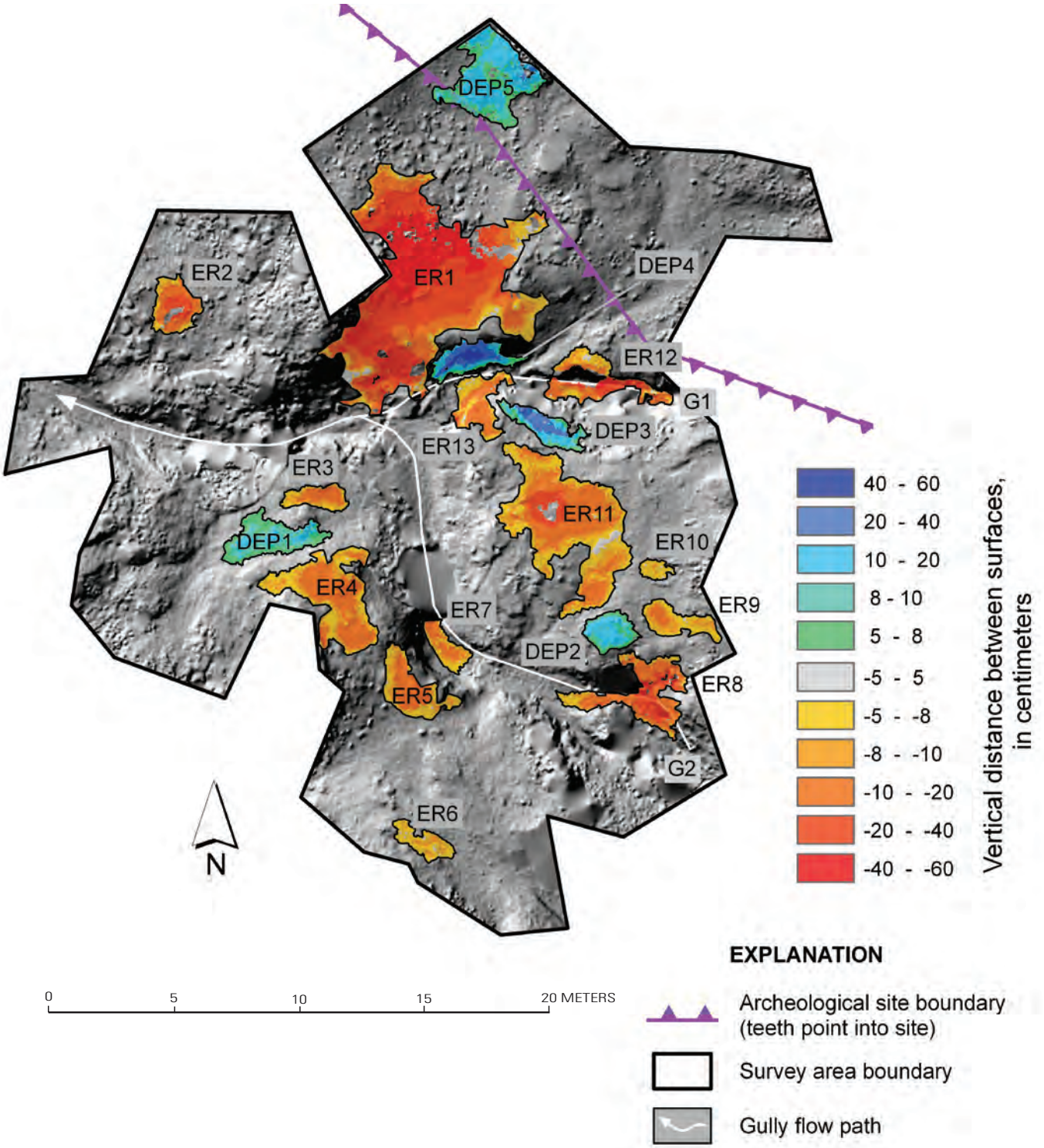

Figure 20. Site AZ:C:13:0099: 5-cm gridded output showing erosion (warm colors, negative) and deposition (cool colors, positive) from September 2007 to April 2010. Identified change is outlined by polygons, and labels (ER = erosion, DEP=deposition) are cross-referenced with table 8.

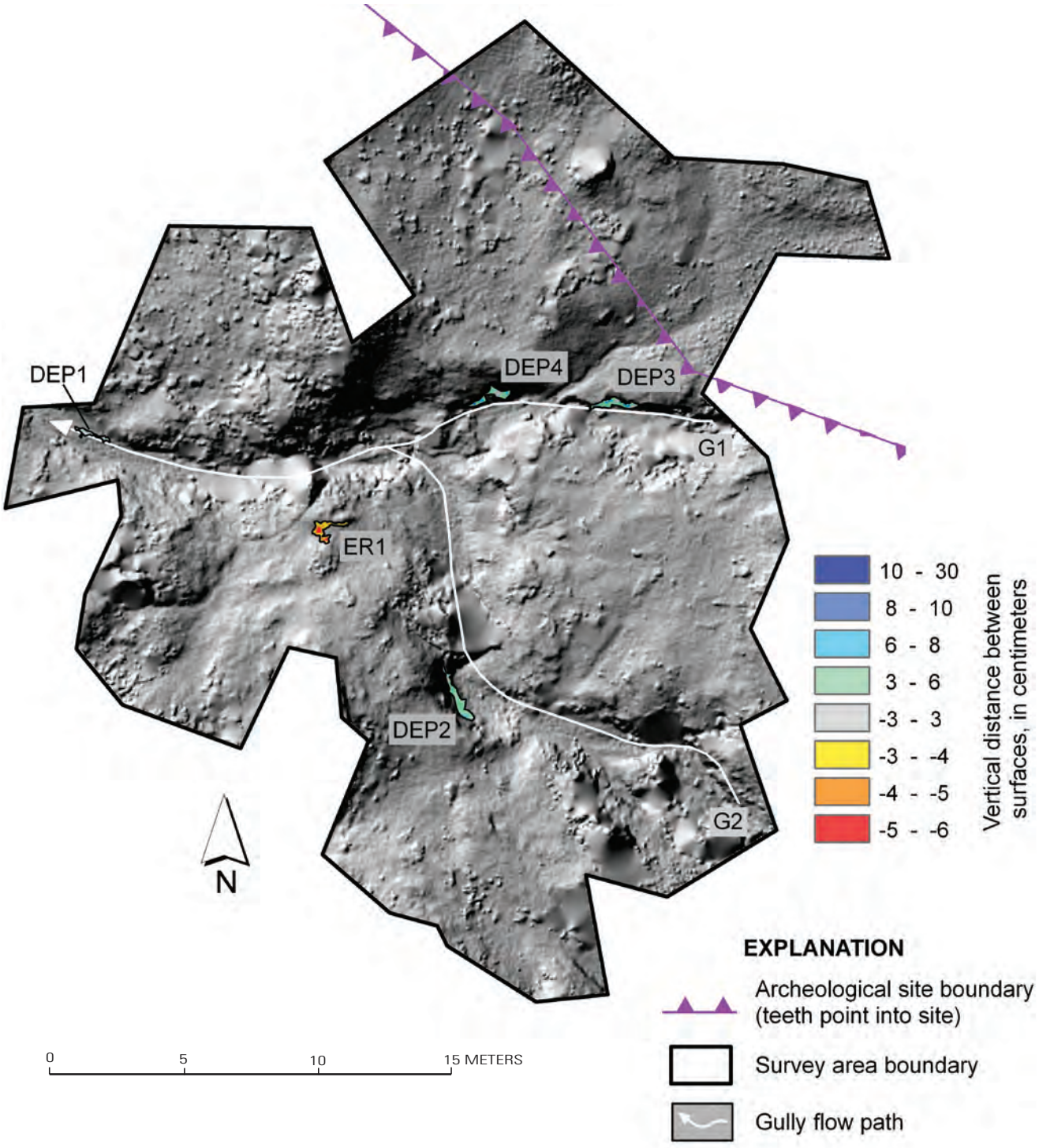

Figure 21. Site AZ:C:13:0099: 5-cm gridded output showing erosion (warm colors, negative) and deposition (cool colors, positive) from April 2010 to September 2010. Identified change is outlined by polygons, and labels (ER = erosion, DEP=deposition) are cross-referenced with table 8. Areas of large-magnitude (>10 cm) deposition within the boundaries of DEP3 and DEP4 are approximately 100 cm^2 in size and are too small to show clearly.

AZ:C:13:0099 Playa Area

Upstream of the AZ:C:13:0099 gully system is a formerly ponded area, now infilled by wind-blown sand and water-deposited silts and clays, colloquially called a "playa." The area is a former backwater channel of the Colorado River and is a relatively flat surface in which water has ponded and evaporated (figs. 22 and 23). A hard-pan, evaporite-rich, fine grained crust covers most of the site, potentially providing at least some protection to rapid gullying from overland flow. The playa area has been monitored by terrestrial lidar five times since 2006. Although not an archeological site in itself, several such sites border the playa, and evidence of ongoing channelized flow erosion indicates that this area could be an indicator for potential change at these other archeological sites. Overland flow on the playa surface has created several shallow channels that drain to a single major channel that runs through the playa (fig. 22) and into the AZ:C13:0099 site (gully G2, fig. 18). Isolated rockfall deposits, consisting of large boulders several meters in maximum dimension, are located throughout the area and generally redirect the paths of smaller drainages that converge at the north end of the playa. Whereas the playa itself is devoid of any vegetation, mature mesquite trees (*Prosopis glandulosa* var. *torreyana*) border it in many locations. We identified overland flow as the primary geomorphic process affecting this site.

Change detection analysis results for the first three surveys spanning 2006–2007 for this area are provided by Collins and others (2009). Previous surveys detected only one minor area of erosion related to channel widening between May 2006 and May 2007. Here, we provide change detection results between September 2007 and the two 2010 datasets.

Surface comparison between September 2007 and April 2010 datasets identify six small areas of erosion and one area of deposition (fig. 24, table 9). The six erosion areas are all centrally located and formed in the largest of the shallow channels that traverse the playa. The depth of erosion (between 6 and 8 cm) is roughly coincident with the existing channel depth, suggesting that erosion took place through channel widening rather than channel deepening during channelized flow events. The one area of deposition is also located in the central channel on an inside bend, directly across from an erosion area. It is very likely that some of the sediment eroded from ER1, ER2, and (or) ER3 was redeposited here, whereas the remainder and that from erosion areas ER4, ER5, and ER6 was carried further downstream, out of the playa area, as evidenced by the lack of other depositional areas within the study region. These observations and measurements suggest that whereas channelized flow processes are actively shaping the playa area, the hardened evaporative crust has thus far successfully prevented additional downcutting. Therefore, channel widening from surface water runoff during storm events appears to be the current major geomorphic process affecting this area.

Between April 2010 and September 2010, we identified only one minor area of erosion (fig. 25, table 9). The erosion was located in the same vicinity of the September 2007 to April 2010 ER1 area (see above discussion) and consisted of approximately 5 cm of channel sidewall widening. Like the erosion areas identified between September 2007 and April 2010, the location of this erosion, in an outside bend near the first instance of significant channel incision, reflects the continued role of channelized flow in shaping the playa surface.

Table 9. Summary of detailed topographic change at AZ:C:13:0099 playa survey area.

Area number	Time period (m/yyyy)	Area (m^2)	Average depth (cm)	Volume (m^3)
AZ:C:13:0099 Playa – ER1	9/2007-4/2010	0.3	6	-0.02
AZ:C:13:0099 Playa – ER2	9/2007-4/2010	1.2	6	-0.08
AZ:C:13:0099 Playa – ER3	9/2007-4/2010	0.1	6	-0.01
AZ:C:13:0099 Playa – ER4	9/2007-4/2010	0.8	8	-0.05
AZ:C:13:0099 Playa – ER5	9/2007-4/2010	0.5	6	-0.03
AZ:C:13:0099 Playa – ER6	9/2007-4/2010	0.7	8	-0.05
AZ:C:13:0099 Playa – DEP1	9/2007-4/2010	0.4	6	0.02
AZ:C:13:0099 Playa – ER1	4/2010-9/2010	0.02	5	-0.001

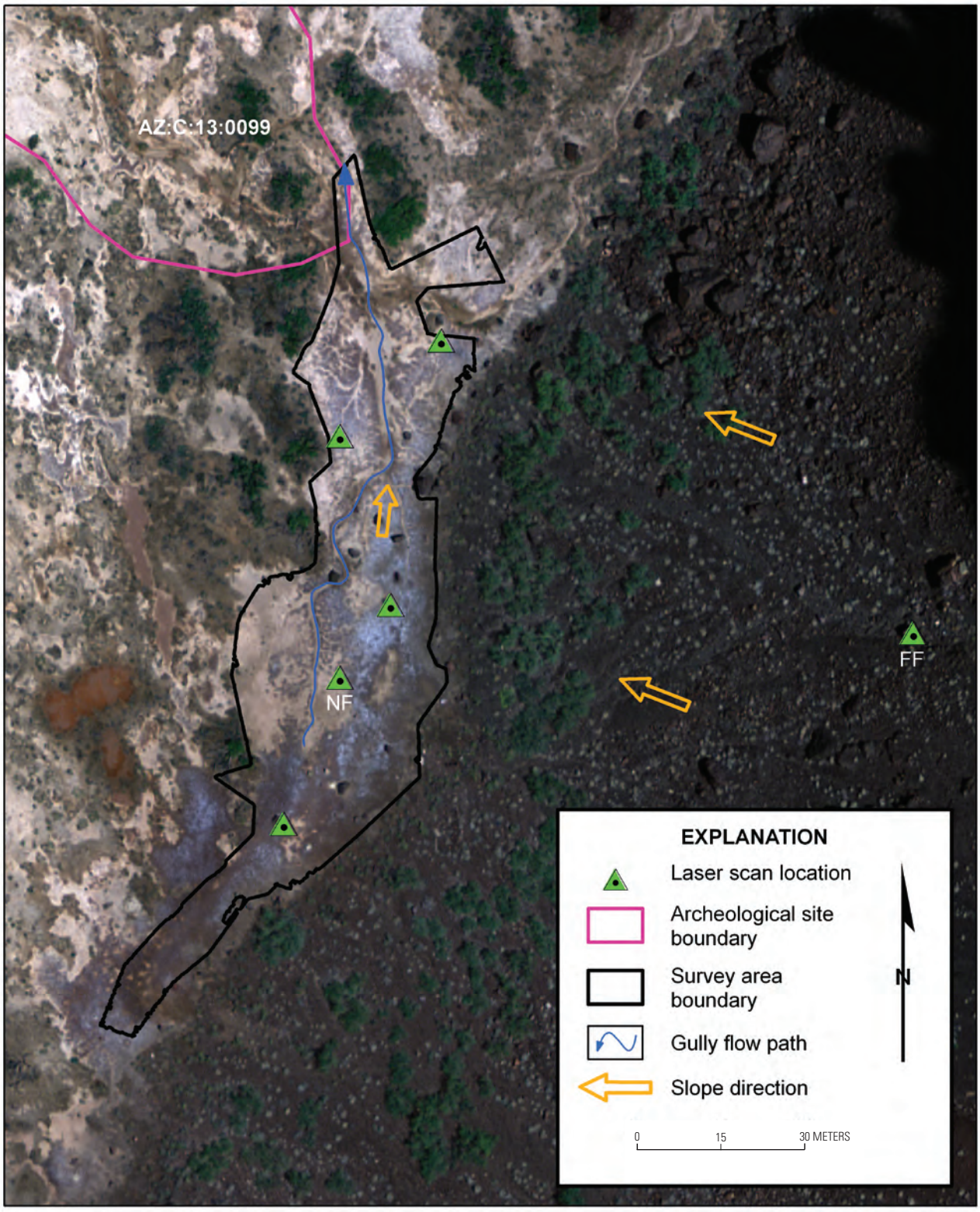

Figure 22. AZ:C:13:0099 playa area survey map. Laser scan locations used for additional lidar point density analysis (NF and FF) are shown for reference.

Figure 23. AZ:C:13:0099 playa survey area photo showing location of main channel (blue line). View is to the south.

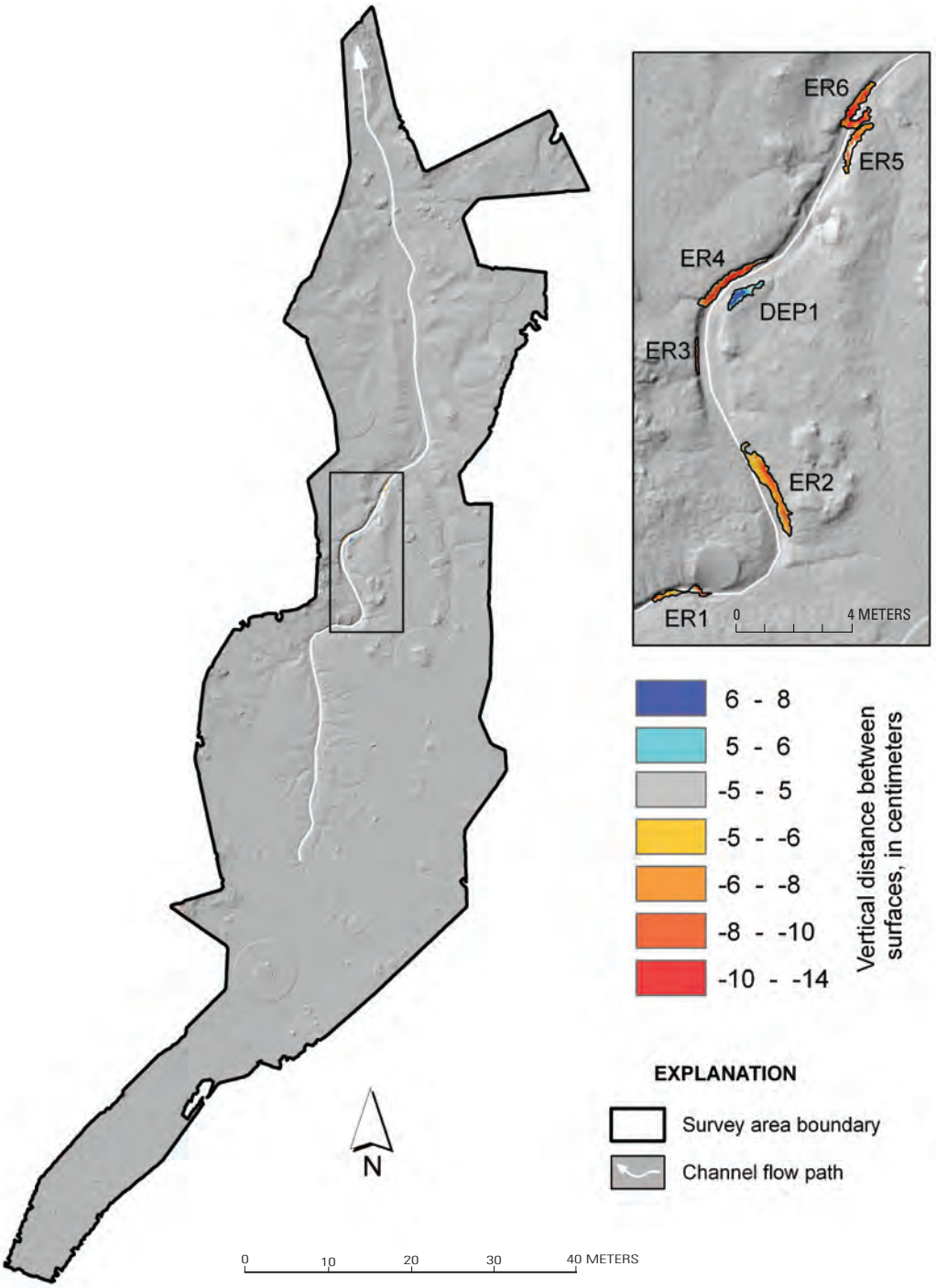

Figure 24. AZ:C:13:0099 playa area: 5-cm gridded output showing erosion (warm colors, negative) and deposition (cool colors, positive) from September 2007 to April 2010. Identified change is outlined by polygons, and labels (ER = erosion, DEP=deposition) are cross-referenced with table 9. Faint "circles" apparent in this and other DEMs included in the results are artifacts of the surface-building algorithms; because they are below the error threshold they are not of consequence.

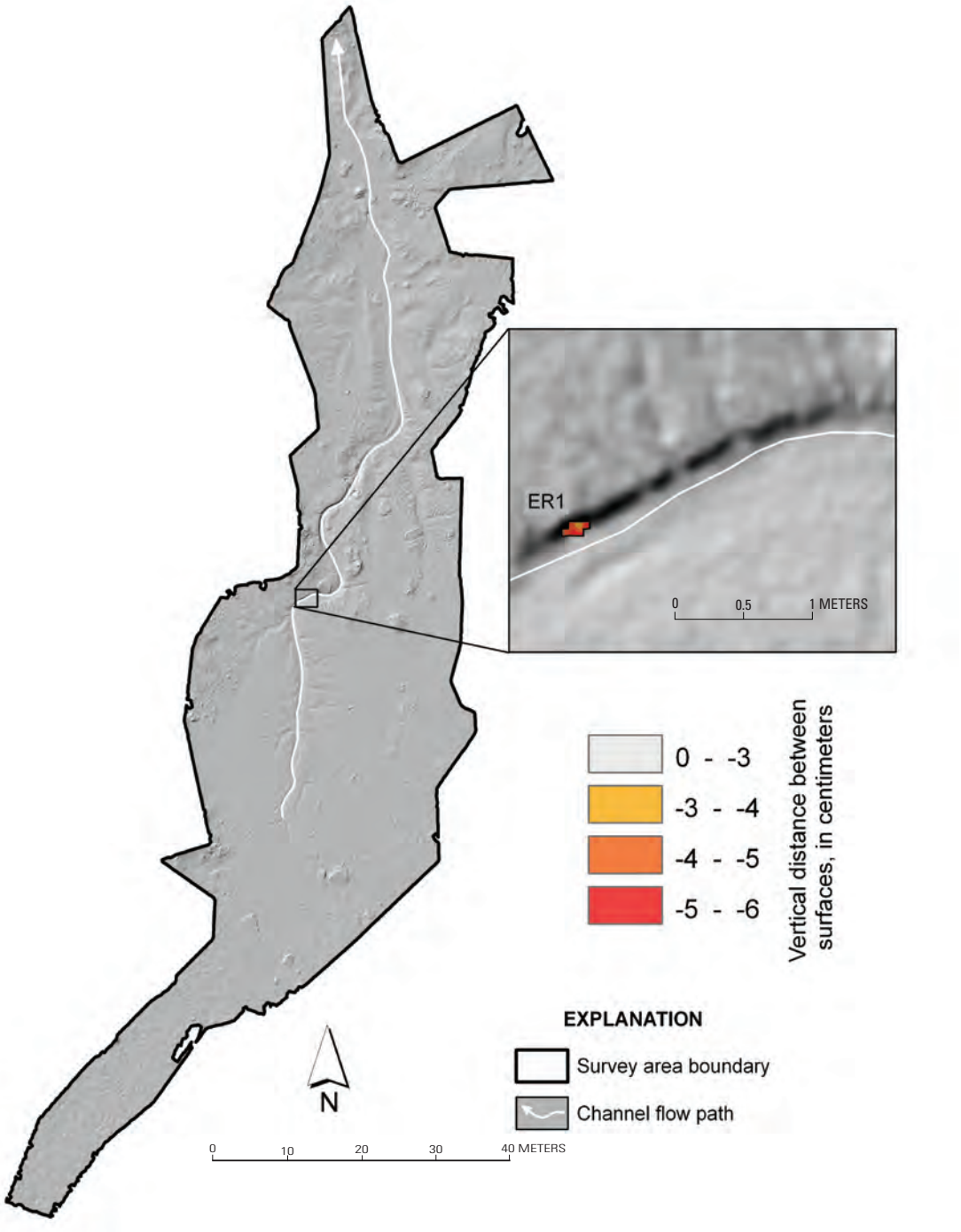

Figure 25. AZ:C:13:0099 playa area: 5-cm gridded output showing erosion (warm colors, negative) from April 2010 to September 2010. No deposition was detected during this time. Identified change is outlined by polygon, and label (ER = erosion) is cross-referenced with table 9.

Site AZ:C:13:0321

Site AZ:C:13:0321 was not investigated by previous lidar surveys, and therefore the April and September 2010 surveys presented the first opportunity for detailed change detection analysis. The site is located very close (~ 60 m) to the Colorado River within an active dune area that receives sediment from a neighboring river sand bar (figs. 26 and 27). An archeologically important slab-lined roasting feature, which contains fire-cracked rocks, ash, and wood charcoal, is located within the sand dunes and just above the lowest part of a channel-shaped hollow formed between the dunes (Fairley and others, 1994). The feature is intermittently buried by aeolian sand, and thus its protection is tied directly to the geomorphology of the nearby sand bar. The hollow between the dunes slopes towards the river's edge, but no indications of overland flow are readily evident (O'Brien and Pederson, 2009a). This hollow is often used as a hiking path by river runners accessing terrain inland from a popular camping beach. Whereas the site is predominantly located within dune sands, several areas of gravel-pebble slope wash are also located in the hollow bottom. Western honey mesquite trees (*Prosopis glandulosa*) with a full spectrum of maturity (that is, some dying, others with healthy vigor) surround the site. Within the site, a wide variety of isolated vegetation is established within the dune sands and gravel substrate, including globemallow (*Sphaeralcea* sp.), arrow weed (*Pluchea sericea*), four-wing saltbush (*Atriplex* sp.), sand verbena (*Abronia elliptica*), and nonnative Russian thistle (*Salsola tragus*) (Draut, 2011). O'Brien and Pederson (2009a) identified aeolian transport as the primary geomorphic process affecting this site. They also noted that aeolian removal of sand can sometimes expose archeological artifacts, making them vulnerable to anthropogenic trailing. Additional site details are included in O'Brien and Pederson (2009a).

We performed change detection throughout the immediate area of the hollow bottom, focusing on areas in and around one of the archeological features (fig. 26). This area has been the subject of additional investigation focusing on the development of sandbars that result from high flow experiments and on the effect that aeolian processes may have in moving sediment from river sand bars to archeological sites (Draut and others, 2010a,b).

Surface comparison between the April 2010 and September 2010 datasets identified two areas of erosion within the analyzed site boundary (fig. 28, table 10), consisting of an area (ER1) along the upper length of the hollow, directly adjacent to the slab-lined roasting feature, and several smaller disconnected areas (ER2) towards the river to the south. Because of the long length (~ 8 m) over which erosion occurred and recent (2010) observed aeolian activity immediately downhollow (towards the river), we suggest that aeolian processes were the most likely agent for this erosion. However, because the majority of the erosion area also coincides with a path used by hikers traversing the site, anthropogenic effects such as surface compaction from foot traffic cannot be ruled out as a contributing factor.

Table 10. Summary of topographic change at Site AZ:C:13:0321.

Area number	Time period (m/yyyy)	Area (m^2)	Average depth (cm)	Volume (m^3)
AZ:C:13:0321 – ER1	4/2010-9/2010	9.7	4	-0.36
AZ:C:13:0321 – ER2	4/2010-9/2010	4.2	4	-0.24

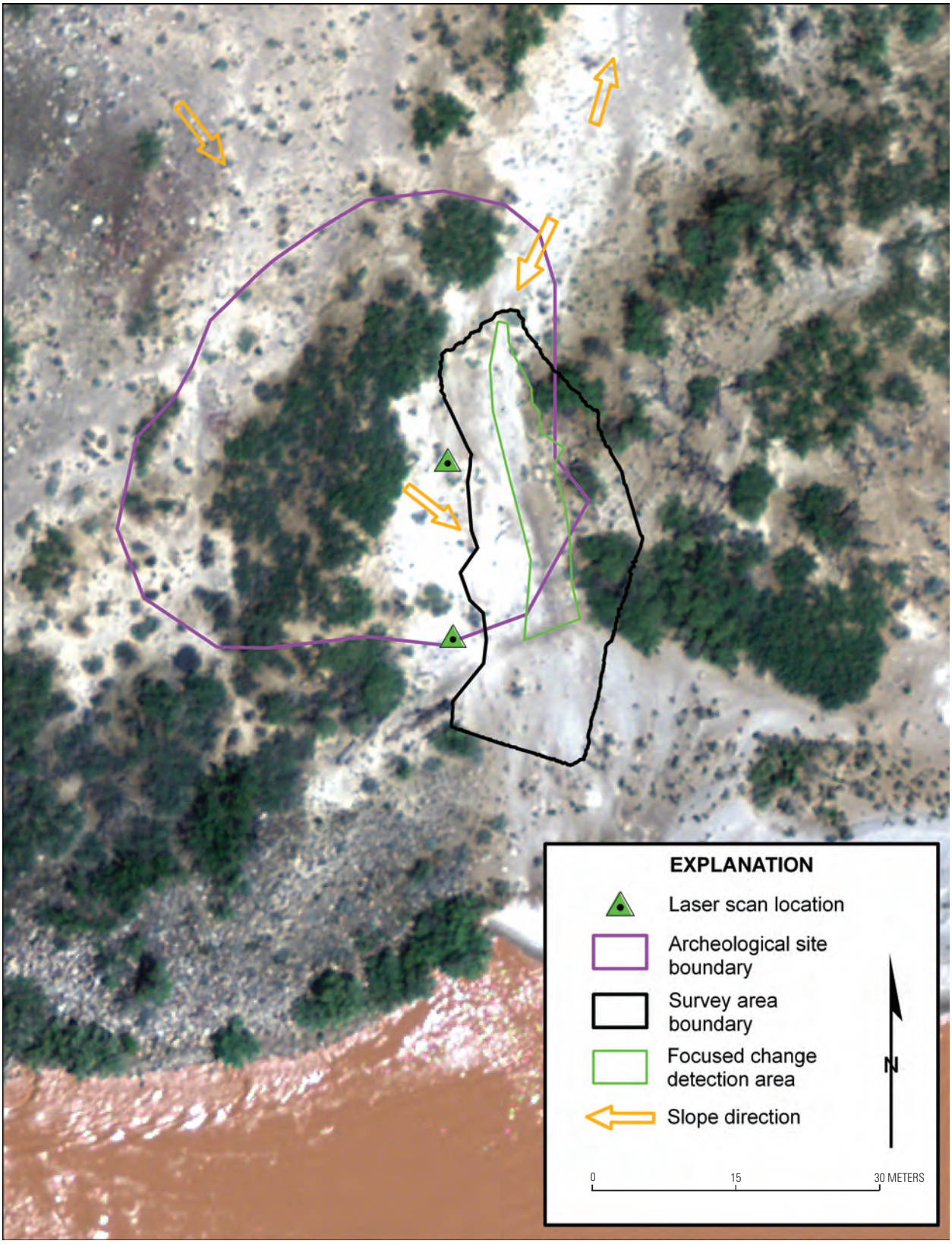

Figure 26. Site AZ:C:13:0321 survey map. Change detection was only analyzed in focused area noted.

Figure 27. Site AZ:C:13:0321 survey area photo. View is to the north.

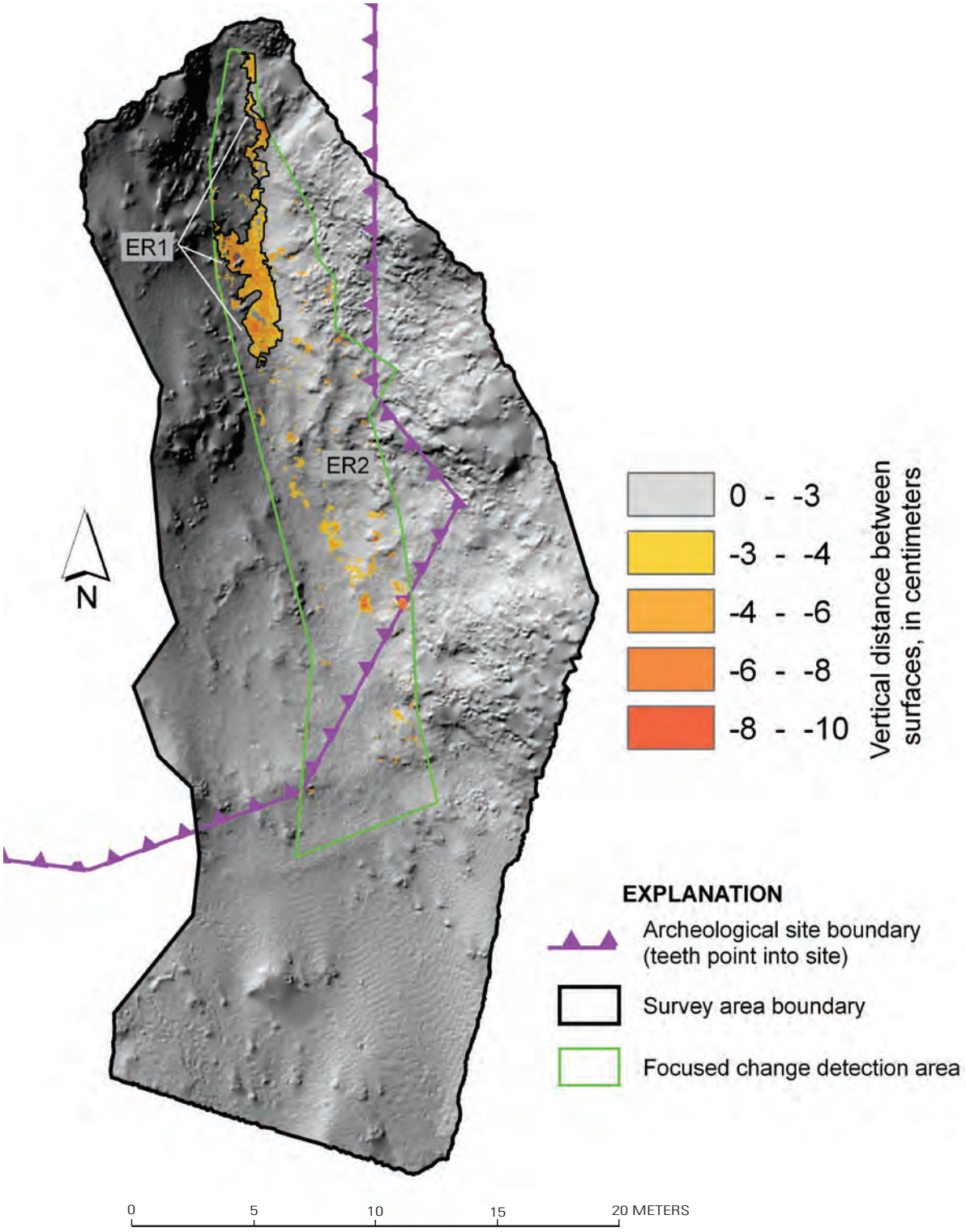

Figure 28. Site AZ:C:13:0321: 5-cm gridded output showing erosion (warm colors, negative) from April 2010 to September 2010. Change detection was only analyzed in focused area noted. No deposition was detected during this time. Identified change is outlined by polygons, and labels (ER = erosion) are cross-referenced with table 10. ER2 polygons encompass all areas of erosion outside of the ER1 polygon.

Sites AZ:C:13:0346 and AZ:C:13:0348

Sites AZ:C:13:0346 and AZ:C:13:0348 (both of which are referred to collectively as AZ:C:13:0348 when reporting change detection analysis results) are two adjoining sites that have been monitored by terrestrial lidar four times since 2006. The sites are archeologically important as an area of Puebloan II habitation and contain remains of jacal-type structures, built by planting wood posts in the ground, weaving sticks between the posts, and plastering the wooden framework with mud (Fairley and others, 1994). The area also contains dense deposits of surface artifacts, including pottery sherds and stone tools. The combined site areas include the terminus of a broad alluvial fan of slope-wash deposits that grades into an alluvial terrace scarp adjoining a former flood plain of the Colorado River (figs. 29 and 30). Three small gullies (G1, G2, and G3) traverse the sites and terminate on the alluvial terrace, which in turn grades into an area of sand dunes that cap the terrace along the river's edge. Brush and rock check dams have been used in gullies G1 and G3 in the past to mitigate ongoing erosion at several locations within this site (O'Brien and Pederson, 2009b). Vegetation consists of irregularly spaced, small desert seepweed bushes (*Suaeda moquinii*) and larger mesquite trees (*Prosopis glandulosa* var. *torreyana*), which in some cases are sufficiently dense to partially obscure gullies from overhead observations. O'Brien and Pederson (2009a) identified gullying, aeolian transport, and overland flow as the geomorphic processes affecting these sites but also observed that visitor-induced trailing was also causing erosion. They also noted that whereas the majority of the site appeared stable with respect to erosion of archeological resources, additional gullying could lead to negative site impacts. Additional site details are included in O'Brien and Pederson (2009a,b).

Change detection analysis results for the first three surveys spanning 2006–2007 are provided by Collins and others (2009). Previously, two potential areas of erosion had been identified in gully G1 and G2 between May 2007 and September 2007. Total station measurements of gully thalwegs by O'Brien and Pederson (2009b) confirmed an overall erosion signal in gully G1 during this time and also noted overall, but difficult to quantify, aggradation in gully G3 between May 2006 and September 2007. Here, we provide change detection results between September 2007 and September 2010.

Surface comparison between September 2007 and September 2010 identified 13 areas of erosion and 3 areas of deposition (fig. 31, table 11). In general, the changed areas are located throughout the sites but in close proximity to existing pockets of either loose dune sands or immature cryptobiotic crust areas. Noting that the change detection threshold for these sites is 5 cm, it is possible that some of these pockets of change are larger in area and linked to one another through areas with change of less than 5 cm. Most areas (for example, ER5, ER6, ER8, ER9, ER11) show visual evidence that suggests aeolian erosion as the dominant geomorphic process (table 11). Three areas (ER7, DEP2, DEP3) are likely linked to alluvial fan processes—here outwash sediments appear to have been transported by overland flow. Overall, these results identify that both geomorphic agents continue to reshape the topography of these sites.

We note that additional change areas may also have occurred at these sites. During the September 2010 survey, the laser instrument was positioned at slightly different locations compared to previous survey efforts (Collins and others, 2009). This had the effect of reducing the point density of some areas of the sites, including the majority of the gullies that traverse the central slope, and resulted in low confidence change-detection determination in several areas. In addition, extremely windy conditions in advance of a storm front in September 2010 resulted in collection of some data with poor precision, thereby preventing identification of all potential areas of change. However, these areas were estimated to be minor in size compared to the areas where change was positively detected. Thus, the results presented here should be taken as reliable, but also as the minimum change that occurred during this time period.

Table 11. Summary of topographic change at Sites AZ:C:13:0346 and AZ:C:13:0348.

Area number[1]	Time period (m/yyyy)	Area (m^2)	Average depth (cm)	Volume (m^3)
AZ:C:13:0348 – ER1	9/2007-9/2010	4.3	7	-0.29
AZ:C:13:0348 – ER2	9/2007-9/2010	3.7	8	-0.28
AZ:C:13:0348 – ER3	9/2007-9/2010	8.1	10	-0.79
AZ:C:13:0348 – ER4	9/2007-9/2010	3.3	8	-0.27
AZ:C:13:0348 – ER5	9/2007-9/2010	10.5	9	-0.94
AZ:C:13:0348 – ER6	9/2007-9/2010	12.9	10	-1.24
AZ:C:13:0348 – ER7	9/2007-9/2010	16.7	16	-2.62
AZ:C:13:0348 – ER8	9/2007-9/2010	3.1	8	-0.25
AZ:C:13:0348 – ER9	9/2007-9/2010	5.2	13	-0.65
AZ:C:13:0348 – ER10	9/2007-9/2010	3.7	9	-0.33
AZ:C:13:0348 – ER11	9/2007-9/2010	8.5	6	-0.53
AZ:C:13:0348 – ER12	9/2007-9/2010	2.3	9	-0.20
AZ:C:13:0348 – ER13	9/2007-9/2010	3.0	8	-0.24
AZ:C:13:0348 – DEP1	9/2007-9/2010	3.6	6	0.24
AZ:C:13:0348 – DEP 2	9/2007-9/2010	1.4	8	0.12
AZ:C:13:0348 – DEP 3	9/2007-9/2010	16.2	6	0.95

[1] Area number prefix (i.e., AZ:C:13:0348) refers to areas located in both AZ:C:13:0346 and AZ:C:13:0348.

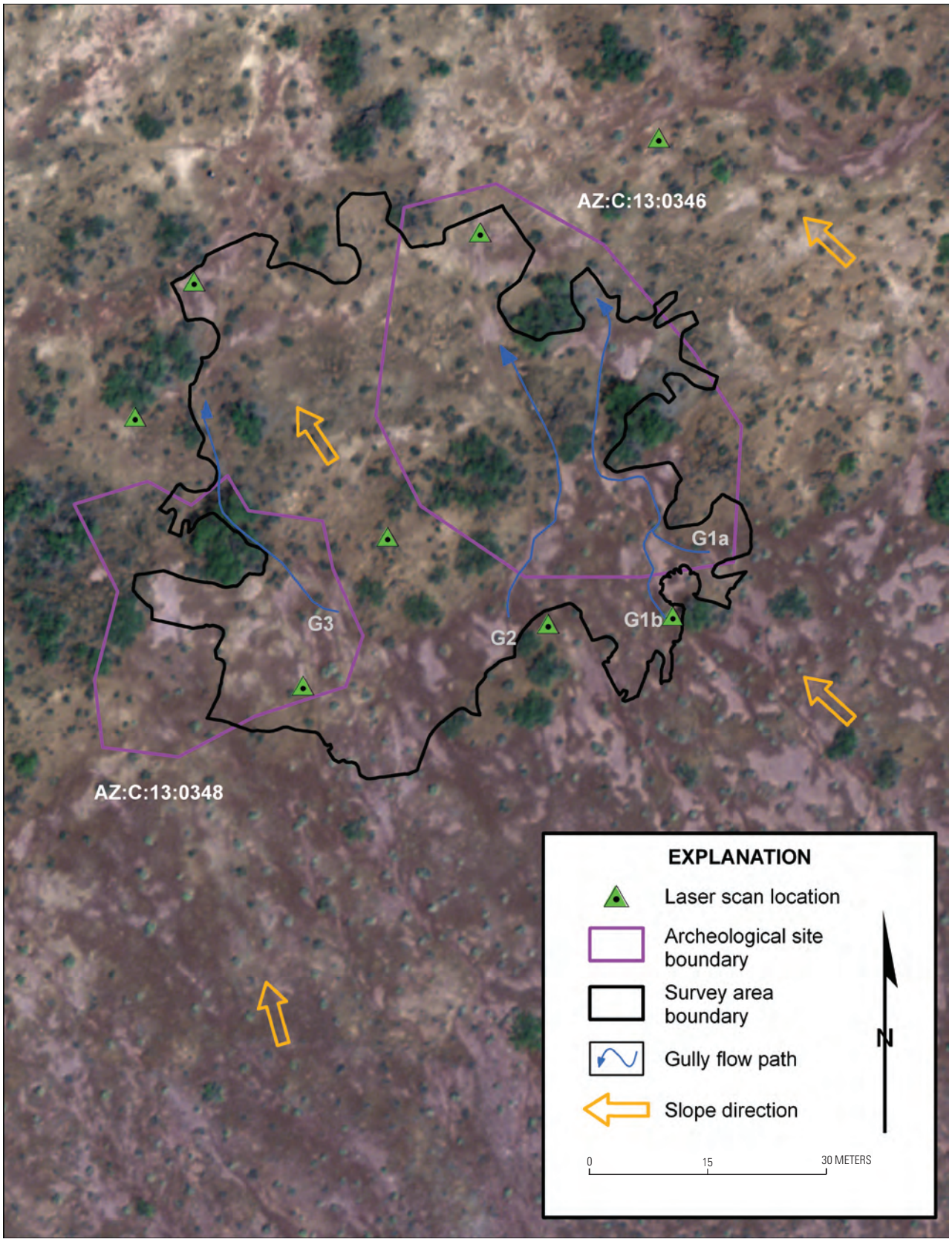

Figure 29. Site AZ:C:13:0346 and AZ:C:13:0348 survey map.

Figure 30. Sites AZ:C:13:0346 and AZ:C:13:0348 survey area photo showing gully locations (G1 to G3). View is to the south.

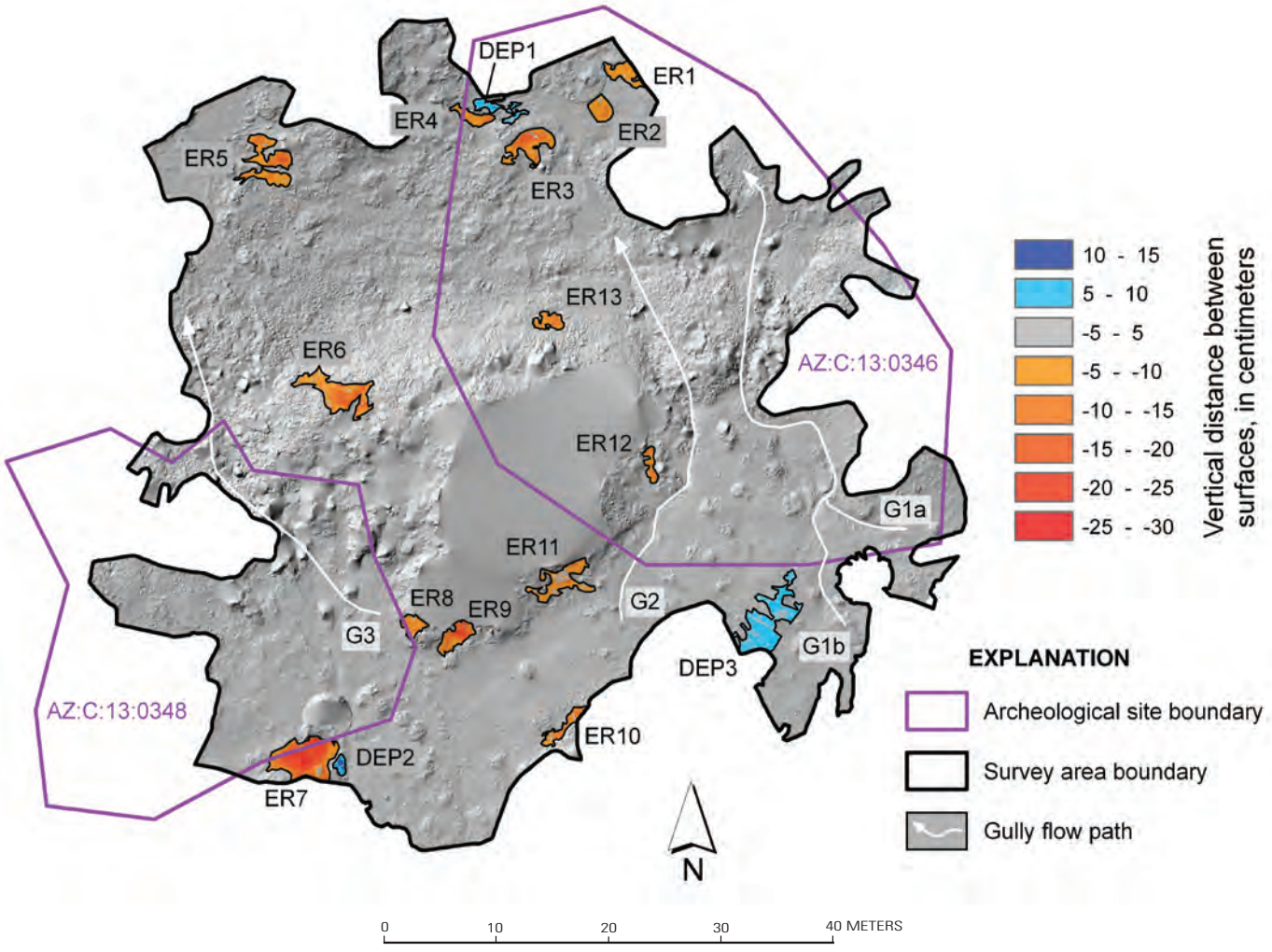

Figure 31. Site AZ:C:13:0346 and AZ:C:13:0348: 5-cm gridded output showing erosion (warm colors, negative) and deposition (cool colors, positive) from September 2007 to September 2010. Identified change is outlined by polygons, and labels (ER = erosion, DEP=deposition) are cross-referenced with table 11.

Site AZ:B:10:0225

Site AZ:B:10:0225 was previously surveyed only once, in September 2007. Thus, the most recent September 2010 survey data presented the first opportunity to conduct detailed change detection analysis at this site. The site is very close (~ 30 m) to the Colorado River and is located on a sand ramp that is backed by steep and sometimes overhanging Tapeats Sandstone ledges (figs. 32 and 33). The ledges formed shelters for the prehistoric people that formerly inhabited the area, and the slope below these shelters is littered with pottery sherds, lithic debitage, fire-cracked rocks, and other artifacts (Fairley and others, 1994). Two large gullies (G1 and G2) traverse the edges of the site and fall steeply over sandstone ledges, terminating near the river's edge in a deposit of large (~20 cm to 1 m diameter) boulders. The gullies are infilled with aeolian sand transported from nearby dunes and potentially from a large river sand bar located directly across the river from the site. Area vegetation includes isolated catclaw acacia (*Acacia greggii*), prickly pear (*Opuntia* sp.), goldenbush (*Isocoma acradenia*), ephedra (*Ephedra* sp.), brittlebush (*Encelia* sp.), trixis (*Trixis californica*), and perennial bunch grasses such as Indian rice grass (*Achnatherum hymenoides*). Tamarisk (*Tamarix ramosissima*) and arrowweed (*Pluchea sericea*) border the site near the river's edge and lower dune areas. O'Brien and Pederson (2009a) identified gullying, overland flow, aeolian transport, and creep as the geomorphic processes affecting this site and noted that both gullying and creep were incrementally eroding artifacts here. Additional site details are included in O'Brien and Pederson (2009a).

Although no pre-September 2007 datasets are available for analysis, on-site observations of a large storm event immediately prior to the September 2007 survey bracket the time frame in which formation of the existing gullied topography at this site, and particular in gully G2, must have occurred. Surface comparison between September 2007 and September 2010 indicates that additional major changes occurred to this site during this 3-year period, consisting of 11 areas of erosion and 7 areas of deposition (fig. 34, table 12). On the sideslope of G1, erosion of as much as 50 cm and deposition of as much as 32 cm occurred, most likely from aeolian processes. Net sediment volume removed was approximately 1.6 m^3, consisting of five areas of erosion (ER1 through ER5) and four areas of deposition (DEP1 through DEP4). Whereas gully G1 was already eroded to bedrock (Tapeats Sandstone ledges or slope wash boulders) throughout the majority of the gully bottom in September 2007, gully G2 was founded on slope wash boulders only in the upper section of the gully. In the lower section of gully G2, weakly lithified dune sands formed sharp, vertical sidewalls as much as 1 m deep in September 2007 (see cover image). By September 2010, massive gully erosion and sidewall slumping had occurred, removing 114.8 m^3 of sediment (areas ER 8 and ER9), with average and maximum depths of erosion of 52 cm and 160 cm, respectively. Side slopes in September 2010 were smoothed to the sand's angle of repose, and infilling had begun to reshape the gully bottom (DEP5). Net volumetric erosion in G2 (that is, ER8 + ER9 - DEP5) was 105.6 m^3. The geomorphic processes that occurred at G2 are gully erosion (ER8 and ER9) followed by aeolian sand infilling (DEP5) and topographic smoothing.

Additional minor erosion and deposition also occurred within the central slope area, located between gullies G1 and G2 (DEP6, DEP7, ER10), that forms the bulk of the archeological site area. The likely geomorphic agent for these changes is aeolian sand transport. The minor area of erosion located between the gullies (ER11) could have been caused by soil creep processes; O'Brien and Pederson (2009a) identified creep as one of the dominant processes at this site. It is possible that minor additional change also occurred throughout this area; however, regularly spaced low-lying grasses and shrubs growing on the dune slope prevented additional detailed analysis of this area. If changes did occur, they are judged to have been relatively minor (that is, smaller in area and volume than ER11).

Table 12. Summary of detailed topographic change at Site AZ:B:10:0225.

Area number	Time period (m/yyyy)	Area (m^2)	Average depth (cm)	Volume (m^3)
AZ:B:10:0225 – ER1	9/2007-9/2010	0.2	9	-0.02
AZ:B:10:0225 – ER2	9/2007-9/2010	3.1	12	-0.41
AZ:B:10:0225 – ER3	9/2007-9/2010	8.9	14	-1.38
AZ:B:10:0225 – ER4	9/2007-9/2010	2.1	22	-0.43
AZ:B:10:0225 – ER5	9/2007-9/2010	1.3	30	-0.35
AZ:B:10:0225 – ER6	9/2007-9/2010	14.3	16	-2.22
AZ:B:10:0225 – ER7	9/2007-9/2010	2.2	22	-0.49
AZ:B:10:0225 – ER8	9/2007-9/2010	101.5	52	-53.03
AZ:B:10:0225 – ER9	9/2007-9/2010	117.5	52	-61.74
AZ:B:10:0225 – ER10	9/2007-9/2010	2.7	7	-0.19
AZ:B:10:0225 – ER11	9/2007-9/2010	0.4	7	-0.03
AZ:B:10:0225 – DEP1	9/2007-9/2010	3.2	15	0.45
AZ:B:10:0225 – DEP2	9/2007-9/2010	2.7	13	0.33
AZ:B:10:0225 – DEP3	9/2007-9/2010	0.7	15	0.10
AZ:B:10:0225 – DEP4	9/2007-9/2010	0.6	17	0.09
AZ:B:10:0225 – DEP5	9/2007-9/2010	55.0	16	9.22
AZ:B:10:0225 – DEP6	9/2007-9/2010	2.6	9	0.22
AZ:B:10:0225 – DEP7	9/2007-9/2010	16.5	6	0.82

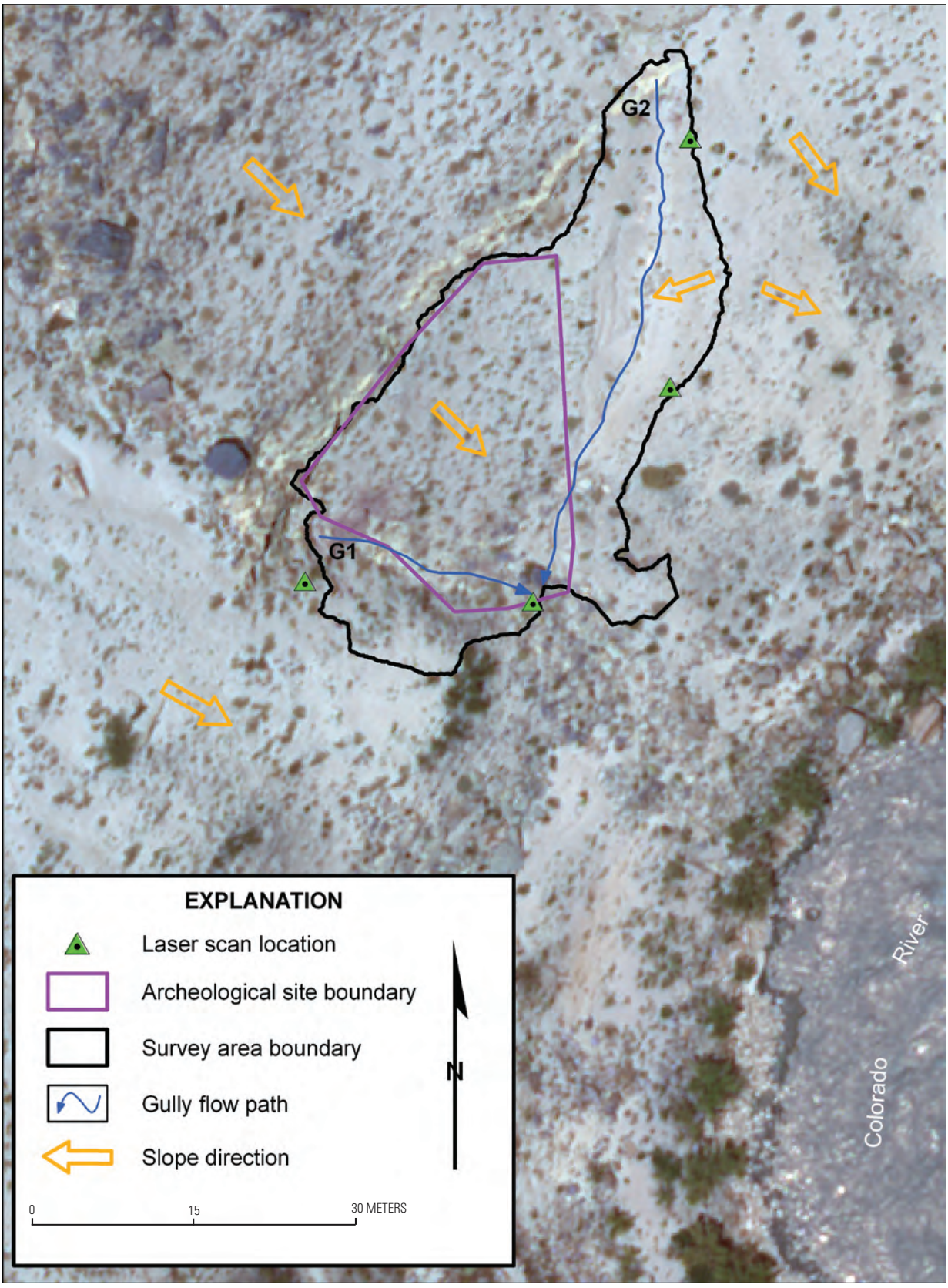

Figure 32. Site AZ:B:10:0225 survey map.

Figure 33. Site AZ:B:10:0225 survey area photo showing gully locations (G1 and G2). View is to the southwest.

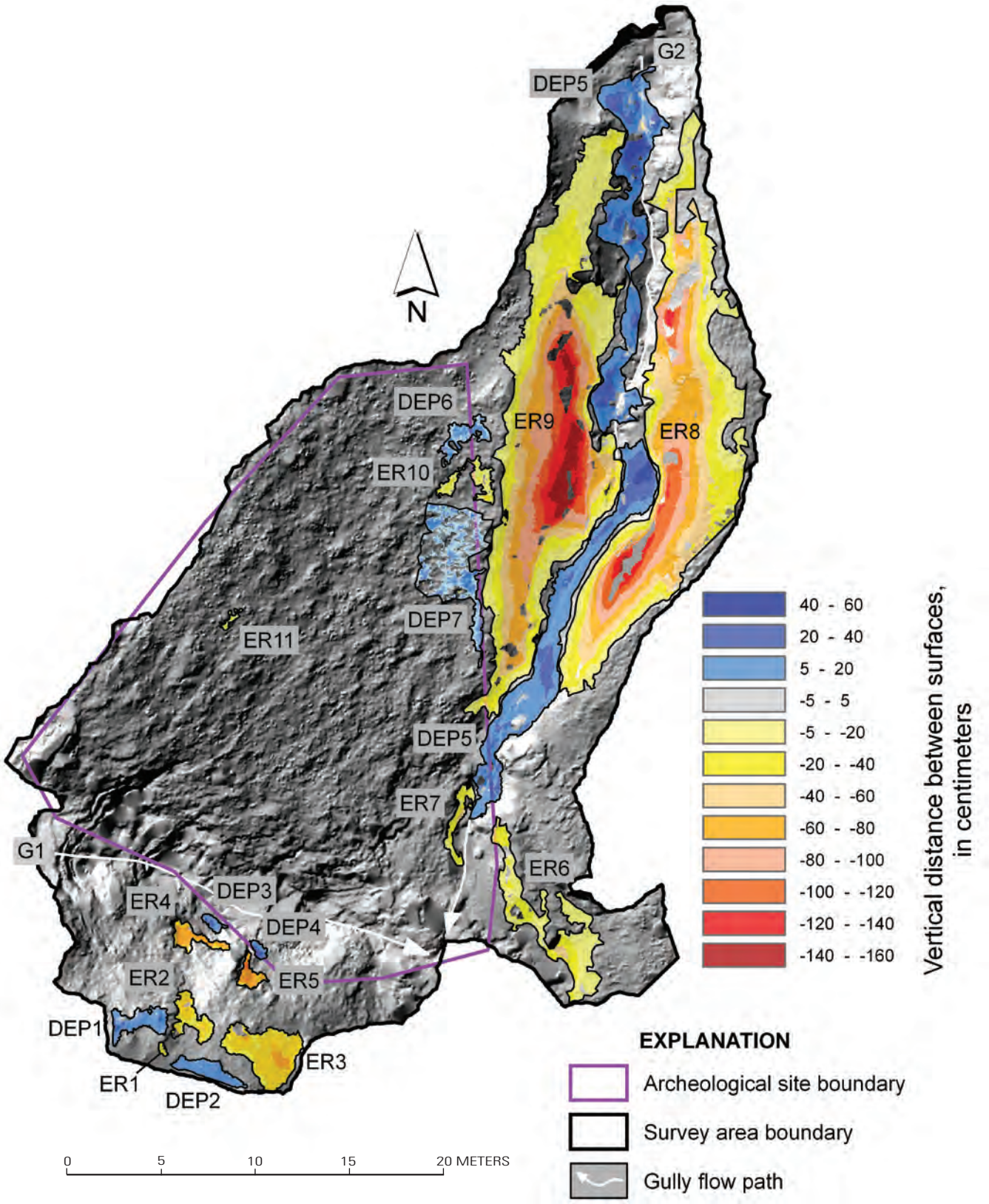

Figure 34. Site AZ:B:10:0225: 5-cm gridded output showing erosion (warm colors, negative) and deposition (cool colors, positive) from September 2007 to September 2010. Identified change is outlined by polygons, and labels (ER = erosion, DEP=deposition) are cross-referenced with table 12.

Site AZ:G:03:0072 US

Site AZ:G:03:0072 US (upstream) and site AZ:G:03:0072 DS (downstream) form a single archeological site but were divided into two survey areas because of their large spatial extent. The entire site has been monitored by terrestrial lidar four times since 2006. This site is a prehistoric and protohistoric habitation area containing sparse surface artifacts and numerous agave roasting pits (Fairley and others, 1994). The upstream survey area (AZ:G:03:0072 US) consists of a convex hillslope that bounds an alluvial terrace that slopes down to the Colorado River, and it is further bounded on one side by a boulder-choked channel and on the other by steep slopes and outcrops of basalt cliffs (figs. 35 and 36). Three gullies traverse this part of the site; two (G1 and G2) are founded on alluvial fill cobbles and boulders, whereas the other (G3) cuts through an active sand dune. The sand dune extends from gully G2 to the western edge of the site near the boulder-choked channel. Brush check dams were installed in gully G2 in May 2006 (O'Brien and Pederson, 2009b). Vegetation consists of clumps of grasses, smaller bushes, and prickly pear cactus (*Opuntia basilaris*), along with taller groups of ocotillo (*Fouquieria splendens*), cholla (*Cylindropuntia acanthocarpa*), and larger creosote (*Larrea tridentata* var. *tridentata*) and catclaw acacia (*Acacia greggii*) several meters in height. O'Brien and Pederson (2009a) identified gullying, creep, aeolian transport, and overland flow as the geomorphic processes affecting this site and noted that archeological features were actively being eroded by these processes. Additional site details are included in O'Brien and Pederson (2009a,b).

Change detection analysis results for the first three surveys spanning 2006–2007 are provided by Collins and others (2009). Previously, substantial erosion was detected distributed throughout all three gullies in addition to the dune slope between G2 and G3. O'Brien and Pederson (2009b) also measured significant erosion in gully G2 and minimal erosion in G1 between May 2006 and September 2007. Here, we provide change detection results between September 2007 and September 2010.

Surface comparison between September 2007 and September 2010 indicate that major changes continued to occur at this site, consisting of erosion in two of the three gullies and throughout the mid-area sand dune field (fig. 37, table 13). In total, 14 areas of erosion and 6 areas of deposition were identified. Whereas average erosion and deposition depths were 11 and 16 cm, respectively, maximum values reached between 50 and 60 cm. The vast majority of the erosion and deposition within the mid-area dune field and in the gully G3 vicinity more than likely occurred as a result of aeolian processes. In general, the spatial pattern of aeolian erosion and deposition indicates a southwest to northeast transport vector (for example, from ER5 to DEP1 and from ER14 to DEP5). Significant erosion and deposition also occurred within gully G3 (ER8, ER10, ER11, DEP2, DEP3, DEP4, DEP6), and our observations indicate that both overland flow and aeolian processes were active in this area. Massive bank failure (ER11, fig. 37) and smoothing of the upper gully surface (DEP2 and DEP3) are indicated by the data and site observations. The only change detected in the gully G1 and G2 areas was a small bank collapse in gully G2 (ER1, fig. 37). This is consistent with the generalized characteristics within this area (grassy vegetated and cryptobiotic soil crusts), indicating a more stable site condition here.

Table 13. Summary of detailed topographic change at Site AZ:G:03:0072 US.

Area number	Time period (m/yyyy)	Area (m^2)	Average depth (cm)	Volume (m^3)
AZ:G:03:0072 US – ER1	9/2007-9/2010	0.4	8	-0.04
AZ:G:03:0072 US – ER2	9/2007-9/2010	3.1	11	-0.36
AZ:G:03:0072 US – ER3	9/2007-9/2010	10.6	8	-0.93
AZ:G:03:0072 US – ER4	9/2007-9/2010	0.5	8	-0.04
AZ:G:03:0072 US – ER5	9/2007-9/2010	47.4	16	-7.74
AZ:G:03:0072 US – ER6	9/2007-9/2010	1.8	10	-0.17
AZ:G:03:0072 US – ER7	9/2007-9/2010	0.8	10	-0.06
AZ:G:03:0072 US – ER8	9/2007-9/2010	0.2	6	-0.01
AZ:G:03:0072 US – ER9	9/2007-9/2010	3.5	8	-0.28
AZ:G:03:0072 US – ER10	9/2007-9/2010	2.2	22	-0.46
AZ:G:03:0072 US – ER11	9/2007-9/2010	12.4	20	-2.66
AZ:G:03:0072 US – ER12	9/2007-9/2010	1.6	9	-0.13
AZ:G:03:0072 US – ER13	9/2007-9/2010	4.0	11	-0.45
AZ:G:03:0072 US – ER14	9/2007-9/2010	3.6	13	-0.48
AZ:G:03:0072 US – DEP1	9/2007-9/2010	34.2	12	3.87
AZ:G:03:0072 US – DEP2	9/2007-9/2010	4.7	16	0.70
AZ:G:03:0072 US – DEP3	9/2007-9/2010	1.9	10	0.19
AZ:G:03:0072 US – DEP4	9/2007-9/2010	3.2	25	0.78
AZ:G:03:0072 US – DEP5	9/2007-9/2010	4.9	11	0.47
AZ:G:03:0072 US – DEP6	9/2007-9/2010	1.9	22	0.39

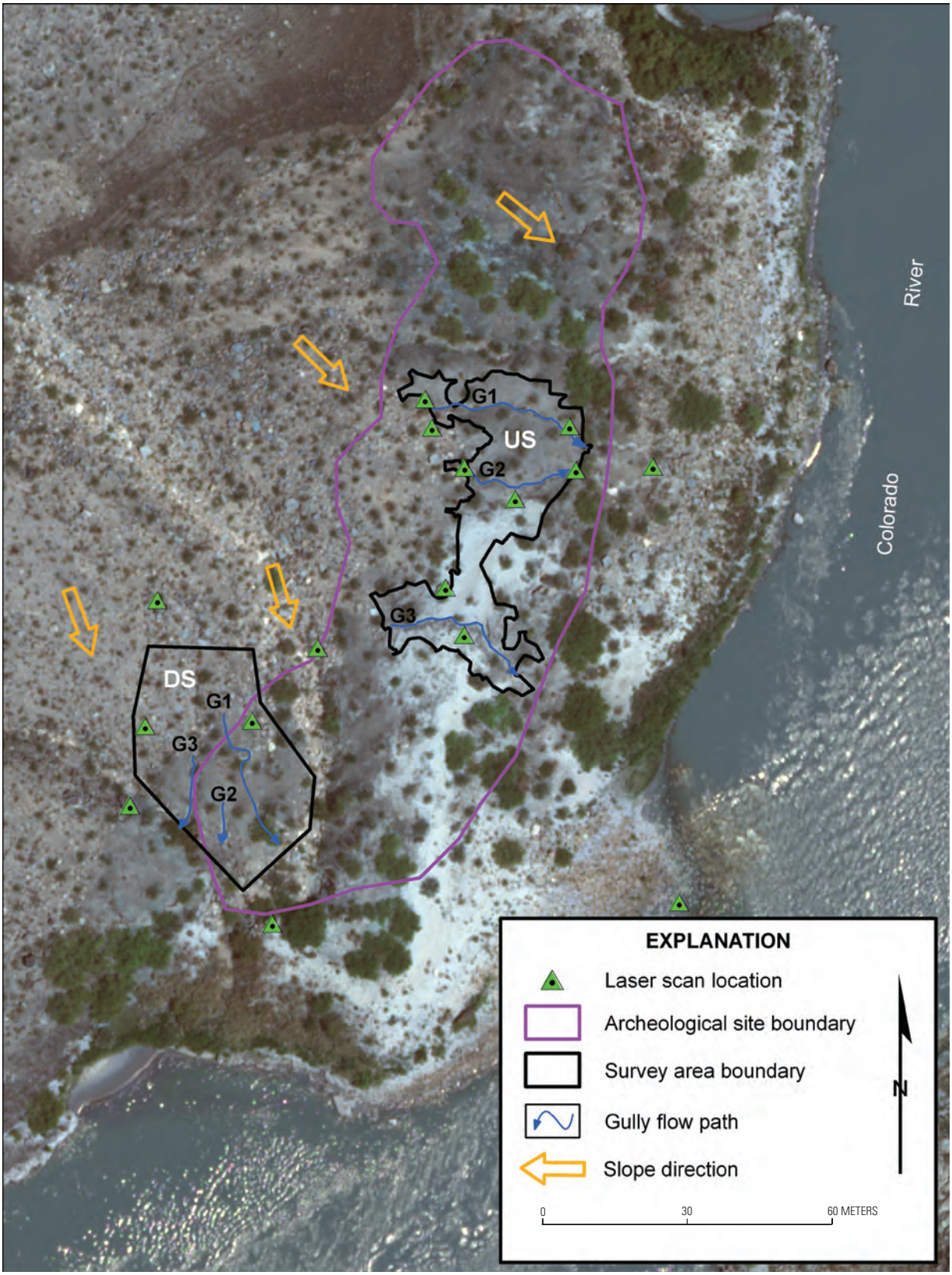

Figure 35. Site AZ:G:03:0072 survey map for upstream (US) and downstream (DS) areas.

Figure 36. Site AZ:G:03:0072 US survey area photo showing gully locations (G1 to G3). View is to the west.

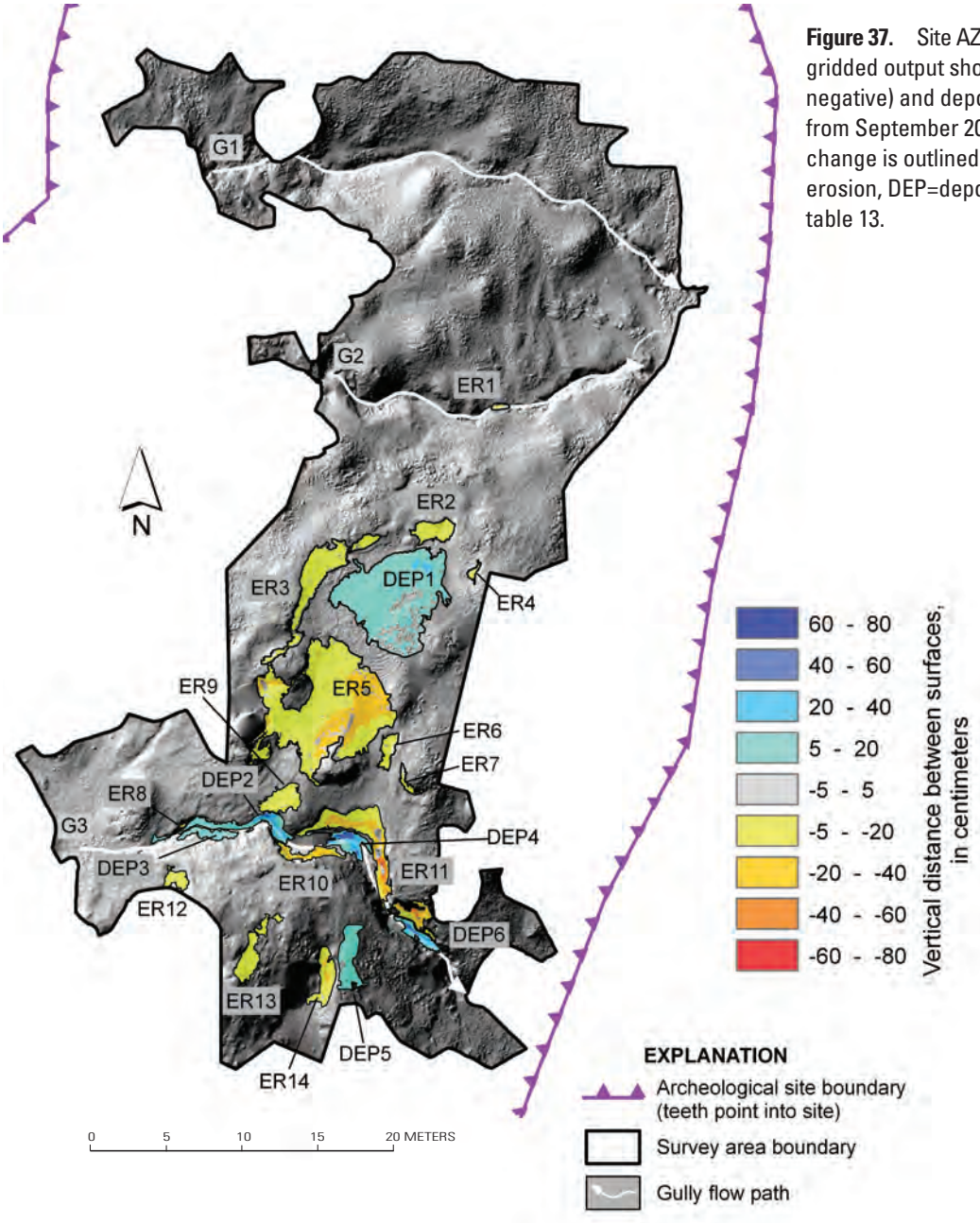

Figure 37. Site AZ:G:03:0072 US survey area: 5-cm gridded output showing erosion (warm colors, negative) and deposition (cool colors, positive) from September 2007 to September 2010. Identified change is outlined by polygons, and labels (ER = erosion, DEP=deposition) are cross-referenced with table 13.

Site AZ:G:03:0072 DS

The downstream area of site AZ:G:03:0072 (AZ:G:03:0072 DS) has been monitored by terrestrial lidar four times since 2006. Identically to the upstream area, this part of the site contains abundant evidence of prehistoric and protohistoric habitation (Fairley and others, 1994). The area consists of a convex hillslope bounded by two larger, boulder-filled channels (figs. 35 and 38). The upper part of the slope is relatively flat, and three small gullies traverse this area, steepening as they join the bordering channels below. Rock check dams exist in the steepest sections of some of these gullies. Vegetation includes a broad mix of cacti, including prickly pear (*Opuntia basilaris*) and ocotillo (*Fouquieria splendens*), as well as several larger mesquite (*Prosopis glandulosa* var. *torreyana*) and catclaw acacia (*Acacia greggii*) trees. In the gullies, large vegetation is generally absent, but soils appear to be stabilized by both grasses and cryptobiotic crust. O'Brien and Pederson (2009a) identified gullying, creep, aeolian transport, and overland flow as the geomorphic processes affecting this site and noted that archeological features were actively being eroded by these processes. Additional site details are included in O'Brien and Pederson (2009a,b).

Change detection analysis results for the first three surveys spanning 2006–2007 are provided by Collins and others (2009). Previously, no significant change was detected at this site. Here, we provide change detection results between September 2007 and the two 2010 datasets.

Surface comparison between September 2007 and September 2010 indicate that no significant changes occurred during this time (fig. 39). In general, this area of site AZ:G:03:0072 appears stable with regard to existing gullies—most channel substrates are either bedrock-controlled or protected by dense grasses, thereby preventing substantial erosion. In addition, no recent aeolian sand deposits are present here—most areas are stabilized by cryptobiotic crust or are covered by grasses and larger vegetation.

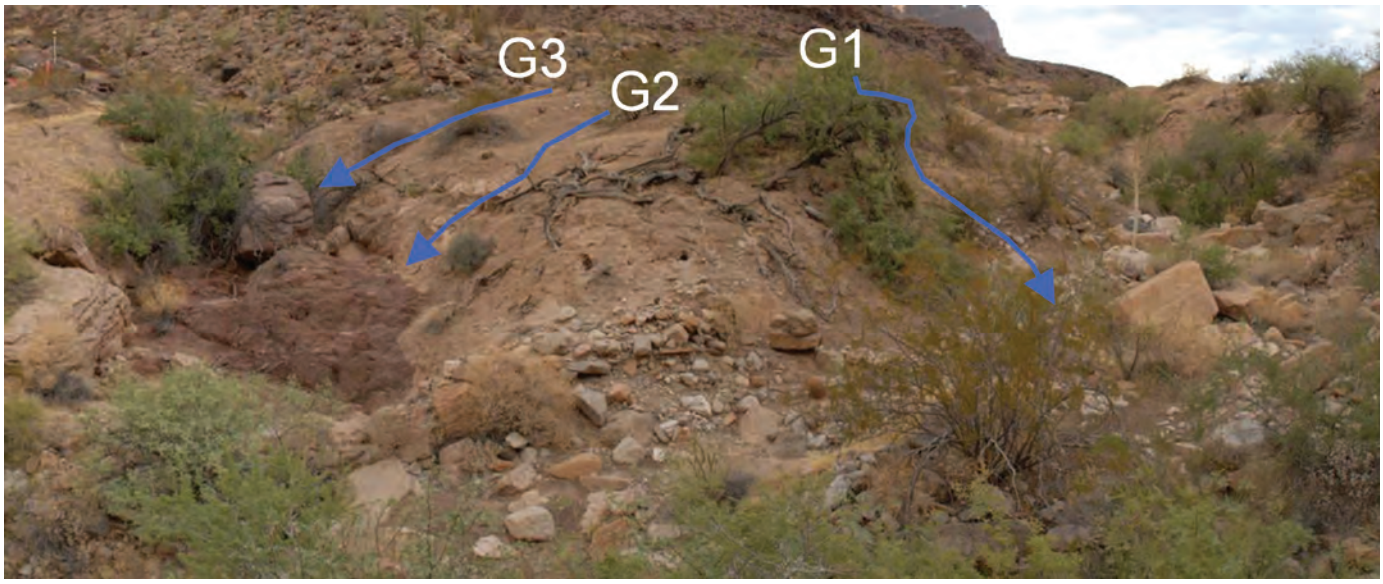

Figure 38. Site AZ:G:03:0072 DS survey area photo showing gully locations (G1 to G3). View is to the north.

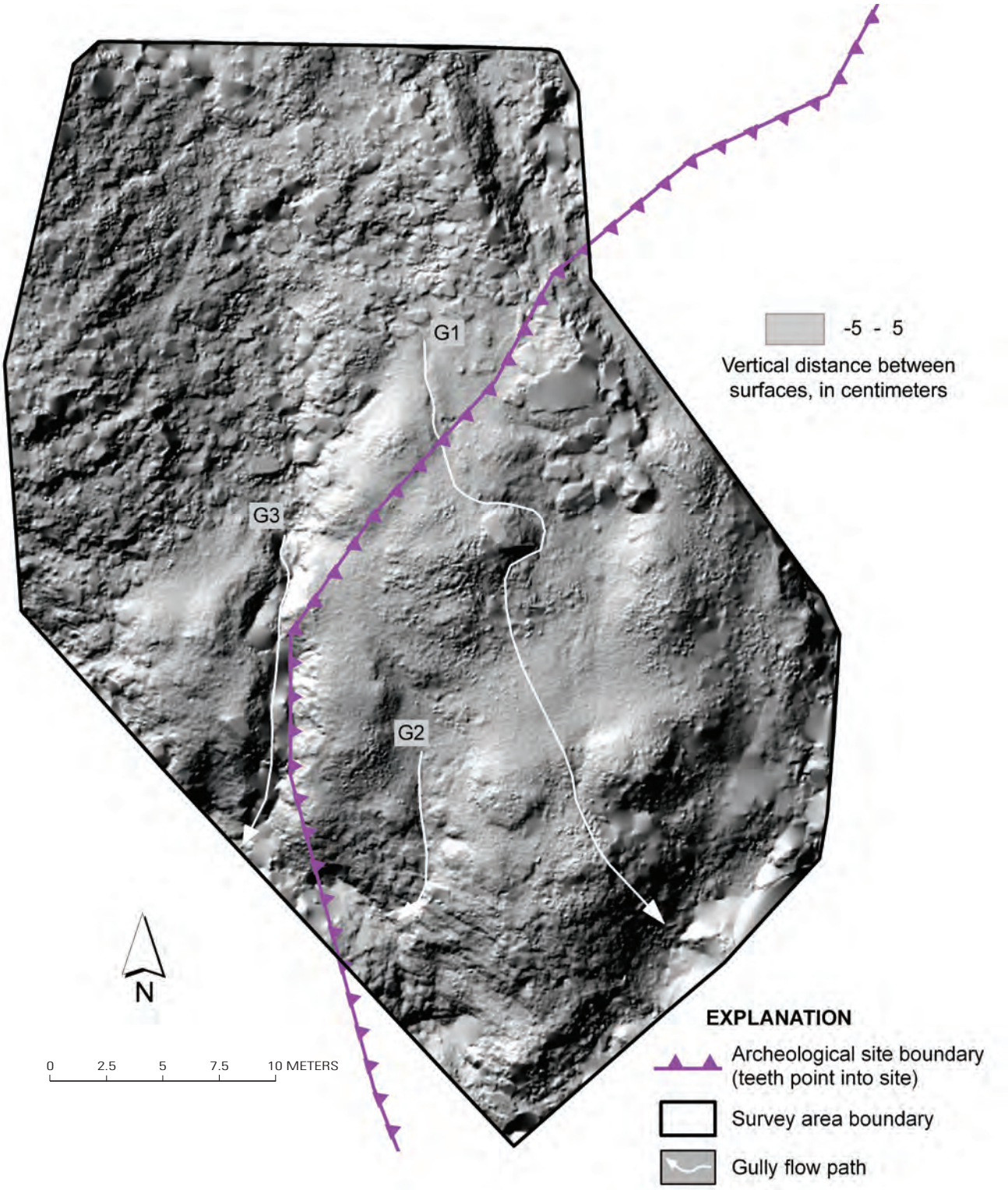

Figure 39. Site AZ:G:03:0072 DS survey area: 5-cm gridded output showing no significant change from September 2007 to September 2010.

Analysis and Optimization of Other Metrics of Archeological Site Stability

Whereas the bulk of this research is aimed at increasing the accuracy of topographic change detection on archeological sites along the Colorado River corridor, we also undertook several studies to investigate and optimize additional applications of lidar surveying for monitoring other types of changes at archeological sites. These studies are more than simply new directions to push this technology—they address existing science questions that have eluded answers because of the difficulty in collecting the high-accuracy data needed to shed light on processes affecting site stability. These questions include:

- Are archeological structures stable or actively deteriorating, and if deteriorating, where and by how much?
- Are surface artifacts moving position, and if so, by how much?
- Are cryptobiotic soil crusts changing (expanding or shrinking), and if so, by how much?

They also address several technique-specific questions such as:

- Can lidar-linked photography be used to model gully thalwegs as an indicator of site change, above and beyond existing, traditional survey methods?
- How can lidar scan positioning be optimized with respect to point density to model archeological site change most efficiently and with the least amount of site disturbance?

We address each of these questions separately here.

Monitoring Archeological Structure Stability

With the increased accuracy of the latest generation of laser scanners, monitoring even subtle changes in topography is now achievable. This provides an important avenue for change detection studies, including monitoring the stability of structures and the movement of individual structural elements (for example, many habitation sites in Grand Canyon have above-ground structures with walls formed from stacked rocks). At some sites, stacked rock walls have been built abutting steep slopes that may be subject to soil creep as a dominant process (see, for example, Tressler, 2011; Tressler and Pederson, 2010); this suggests that monitoring this process using high-accuracy surveys can lead to increased awareness of potential site instability. Whereas some lasers (that is, those with a phase-based laser mechanism) can collect data at the submillimeter scale, performing change detection on objects, especially those in a natural setting, remains challenging because of inaccuracies in global coordinate positioning. In most cases, at best, reoccupying laser scan and control point locations is generally only achievable at the centimeter scale.

To test the application of terrestrial lidar change detection on habitation structures, we performed consecutive temporal lidar surveys of several rock walls that formed habitation structures used by prehistoric farmers in the 11th and 12th centuries (Fairley and others, 1994) at site AZ:C:13:0009 (figs. 40 and 41). The site is located on an alluvial terrace bounded on one side by a side canyon arroyo and on the other by dunes adjacent to the Colorado River. Dune sands mantle parts of the site, along with slope wash boulders and scattered clumps of vegetation. Vegetation includes brittlebush (*Encelia farinosa*), western honey mesquite (*Prosopis glandulosa*), prickly pear cactus (*Opuntia* sp.), and a variety of perennial bunch grasses. O'Brien and Pederson (2009a) identified gullying, creep, and aeolian transport as the primary geomorphic processes affecting this site and noted that these processes are currently destroying archeological resources at the site. Additional site details are included in O'Brien and Pederson (2009a).

We collected four scans of the area both in April 2010 and again in September 2010, focusing specifically on capturing the detailed topography of seven areas where the remains of habitation structures are visible on the surface. Data were processed identically as described previously for the other 2010 datasets. Following processing, specific rocks or groups of rocks that represent the remains of habitation structures were identified and isolated for analysis. We analyzed the three-dimensional change at each area by two methods. First, we calculated the distance between each set (April 2010 and September 2010) by computing the mean distance between each group of points that represent the same set of rocks (fig. 42). Second, we constrained the mean distance comparison to only those data that represent the best fit between the two sets of data. This represents a slight improvement in relative fit, in that unmatched points are not used in the data comparison (that is, the numbers of points used for comparison are less than the first method—see table 14). We note that the two algorithms are essentially the same, with the first analysis using all the points and the second using only those points that represent the best fit.

The results (table 14) show that the three-dimensional distances (that is, the changes in position) between sets of rocks are all on the order of 1 to 3 cm. Standard deviations were less than 1 cm in most cases. Because these distances are also on the order of the previously established empirical error thresholds (that is, 3 cm for change detection between the April 2010 and September 2010 datasets), we conclude that either (1) the rocks representing the remains of the habitation structures did not move during the monitoring time period, or (2) if the rocks did move, it was on a magnitude less than the error threshold of 3 cm. With either selection, the main conclusion is that monitoring of habitation structures using the methods presented herein (that is, using repeat, temporally distinct survey and control point locations) is not capable of determining change detection at the 1 to 2 cm scale. As previously mentioned, phase-based scanners might be used in the future as an improvement if subcentimeter change detection were required, but with the majority of the errors linked to georeferencing and registration, the use of permanently fixed, repeatedly occupied, monuments for setting up survey and control point locations would likely be required.

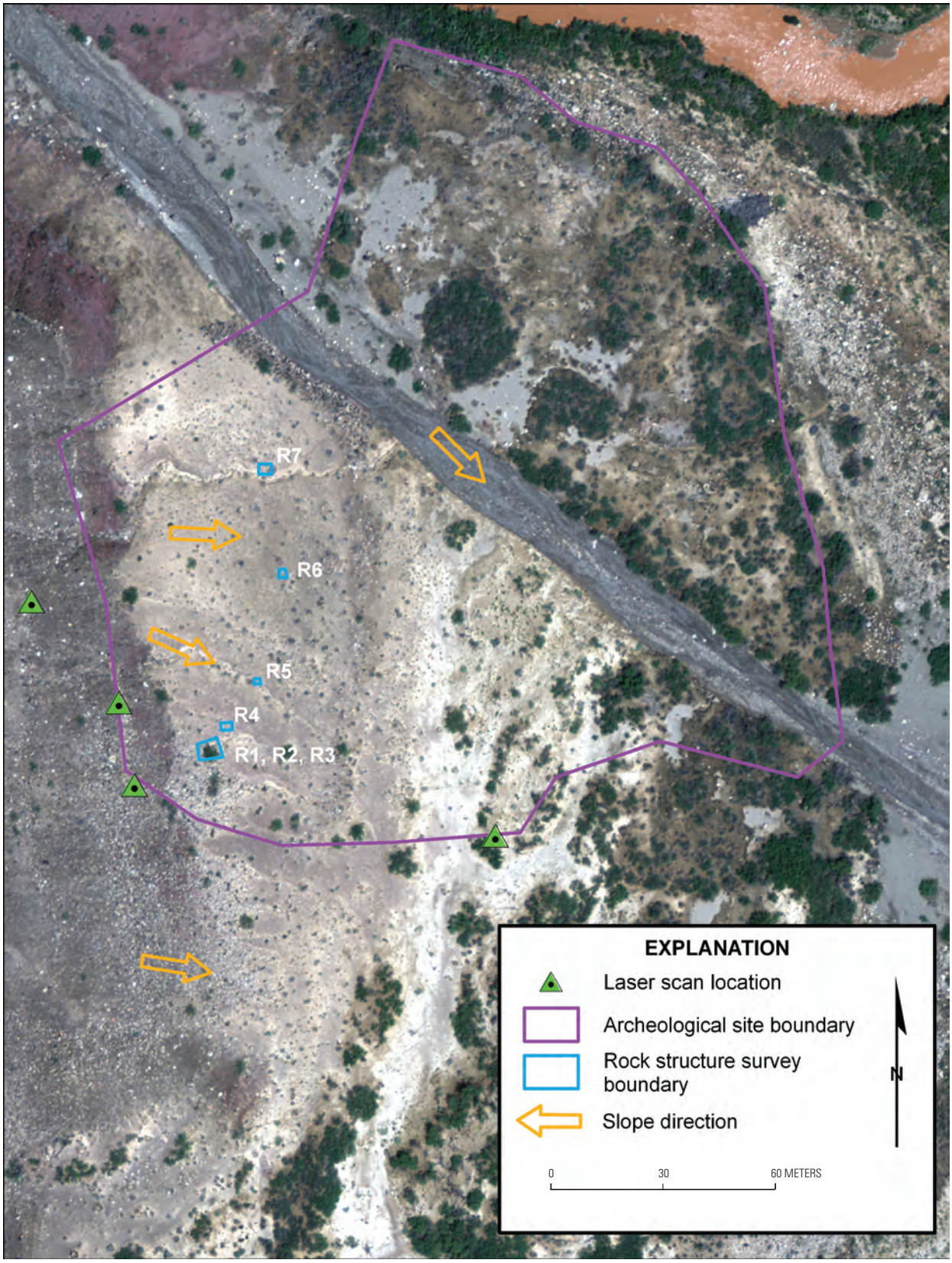

Figure 40. Site AZ:C:13:0009 survey map showing locations of rock habitation structures (R1 to R7) monitored for movement.

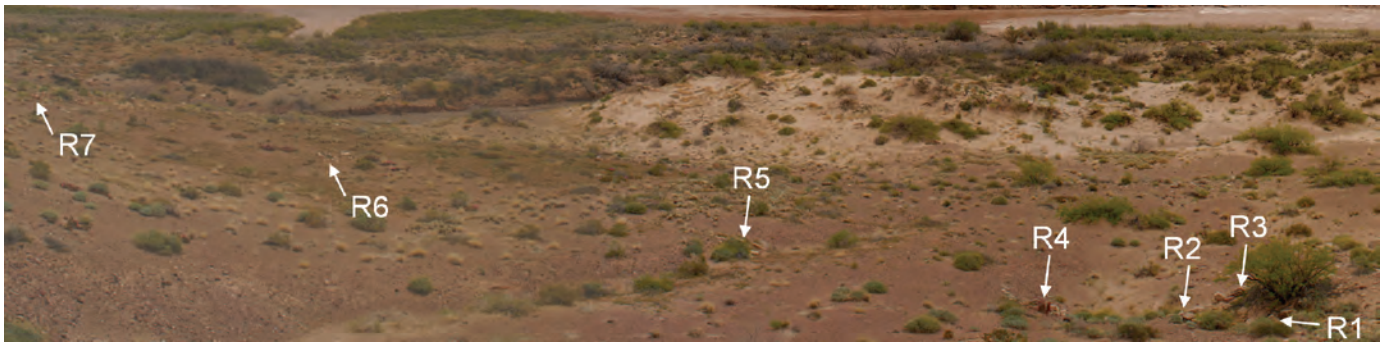

Figure 41. Site AZ:C:13:0009 survey area photo showing rock habitation structures R1 to R7. View is to the east. See figure 40 for scale.

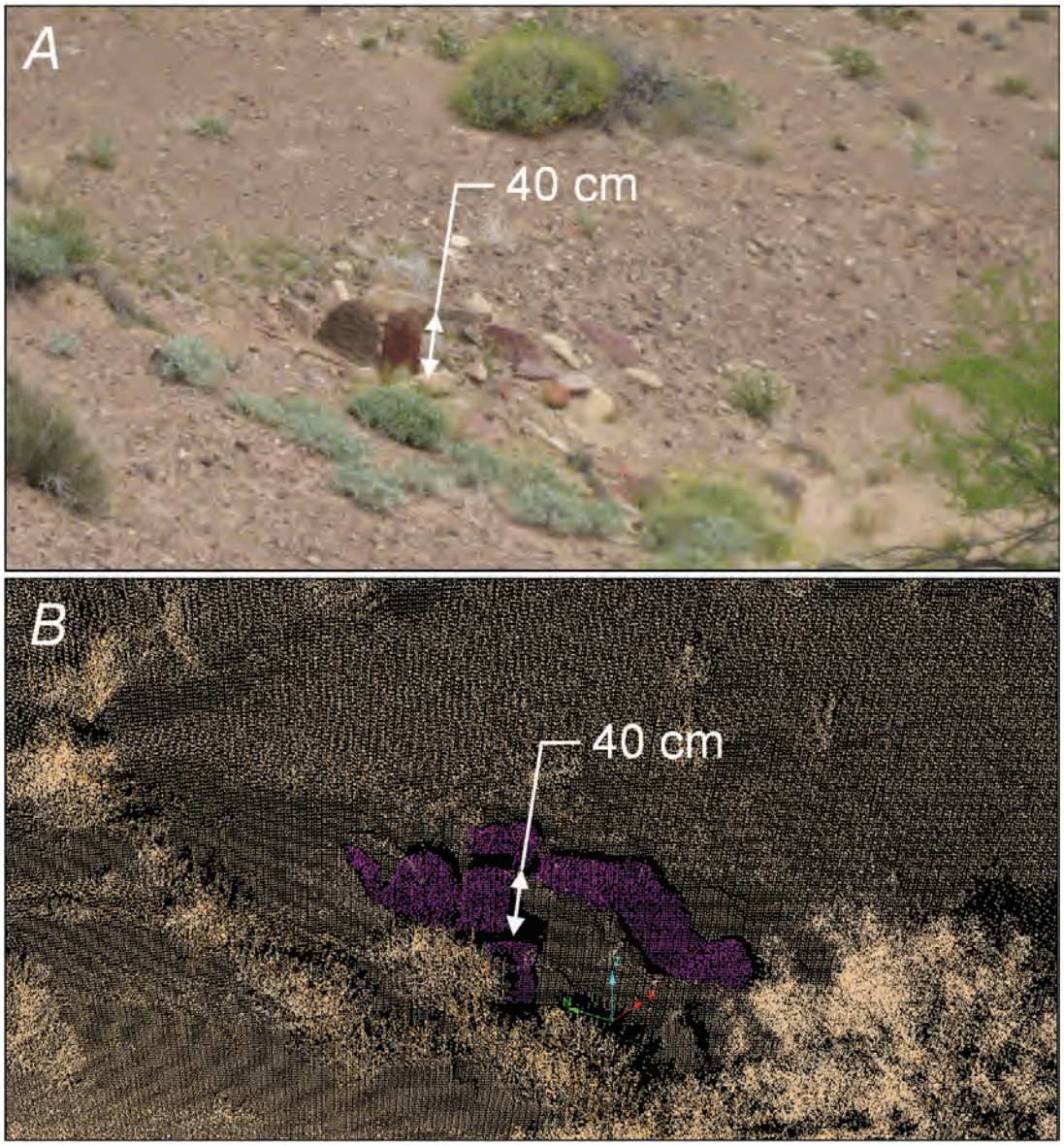

Figure 42. Change detection of rock habitation structure R4 at Site AZ:C:13:0009. *A*, Photo of rock habitation structure walls (view is to the northeast). *B*, Rocks (purple) identified in point cloud data from April 2010.

Table 14. Change detection analysis for rock habitation structures at Site AZ:C:13:0009.

Survey area and rock structure number	Time period (m/yyyy)	Number of points used in all point analysis	Number of points used in best-fit analysis	Mean distance between all points (cm)	Mean distance between best-fit points (cm)
AZ:C:13:0009 – R1	4/2010-9/2010	2,637	2,497	1.5	1.4
AZ:C:13:0009 – R2	4/2010-9/2010	2,921	2,033	2.0	1.8
AZ:C:13:0009 – R3	4/2010-9/2010	2,724	2,004	3.0	2.5
AZ:C:13:0009 – R4	4/2010-9/2010	6,781	3,502	1.8	1.6
AZ:C:13:0009 – R5	4/2010-9/2010	2,304	1,796	2.0	1.6
AZ:C:13:0009 – R6	4/2010-9/2010	1,143	1,095	2.2	2.1
AZ:C:13:0009 – R7	4/2010-9/2010	3,904	3,343	2.8	2.6
Average		3,202	2,324	2.2	1.9

Monitoring Artifact Movement

For archeological sites with surface artifacts (for example, pieces of pottery or piles of fire-cracked rock) quantitative tracking of changes in artifact position could provide a useful metric related to archeological site stability. Tressler (2011) and Tressler and Pederson (2010) showed that tracking small rocks at a fine scale could be used as a proxy for measuring soil creep, which might govern some aspects of site stability. Tracking changes on this scale (subcentimeter) requires that: (1) artifacts be recognizable both in photos and in lidar point clouds and (2) the point density be sufficient to clearly delineate artifacts of interest. Although the lidar survey data analyzed in this report were not purposefully collected at sufficiently high density to perform this level of change detection, we performed directed analyses for a simple case where artifacts were within range of a nearby scan position from a neighboring site. Here, we present analysis results for a small subset of data from site AZ:C:13:0334 (fig. 43*A*), located in the Palisades region. The site has essentially the same characteristics as that previously described for the AZ:C:13:0099 playa area, with the addition that aeolian transport is also an active process here. Additional site details are included in O'Brien and Pederson (2009a).

The lidar data for our analyses consist of a single scan collected from each of the April and September 2010 surveys at an approximate range of between 21 m and 24 m and focused on an area containing a sizable concentration of individual rock fragments; each fragment measured approximately 1 to 4 cm in longest dimension. These georeferenced data, cropped to an area of approximately 4,250 m^2, are accurate to a mean point-to-point matching error of 8 mm, with 6 mm standard deviation. Thus, the data are only sufficiently accurate to perform change detection at a scale of 1 to 2 cm, at best. Despite this limitation, we performed lidar-directed change detection analysis for the two datasets in hope that artifacts could be at least visible in the point cloud data. Unfortunately, despite the generally close range between artifacts and scanner location, we determined that the point density (0.05 to 0.11 points/cm^2 or approximately 3 to 5 cm spacing) was insufficient to delineate individual objects (fig. 43*B*).

Increased point density was not specifically collected at this site because of our focus on whole-site (large-area) data collection. However, other studies (for example, Tressler and Pederson, 2010) using data from our previous surveys (Collins and others, 2009) have shown that sufficient point density (4 points/cm^2) can be collected using short-range (~4 m) instrument locations and used to track centimeter-scale rock clast movement. Thus, the obvious conclusion is that point density must be maximized to at least the 2-points/cm^2 range (subcentimeter point spacing) to detect artifacts of this type at this range, and a metric relating an artifact of any size to the required point density can easily be calculated for a specific area of interest. Whereas this might be within the range of some topographically directed terrestrial lidar instruments, it might also exceed the instruments' accuracy specifications. Our recommendations, therefore, are to use either phase-based laser scanning instruments with both improved (millimeter-scale) accuracy and resolution or close-range (<10 m) digital photogrammetry. However, georeferencing errors may still be the greatest limitation when using lidar methods and would require a local (that is, site-scale) network of permanent control points to be established and repeatedly occupied for all initial and subsequent surveys.

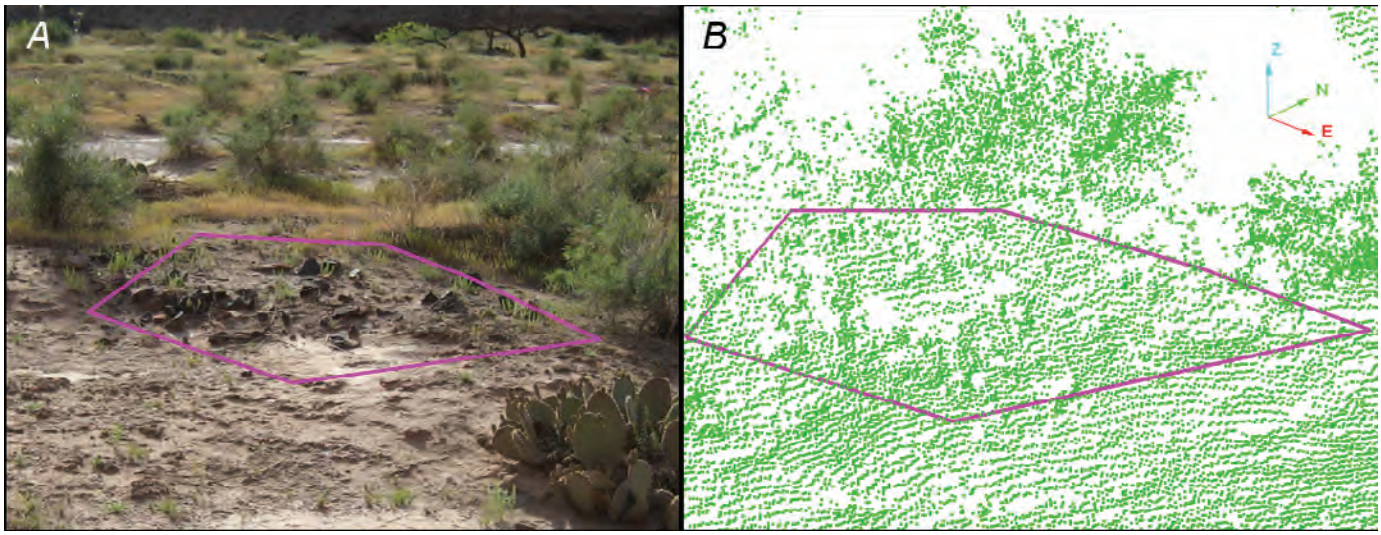

Figure 43. An artifact concentration at site AZ:C:13:0334. *A,* Image. *B,* Point cloud. The point density (~0.1 point/cm^2) is insufficient to track potential movement of individual artifacts or single rocks, precluding detailed change detection.

Detection and Mapping of Cryptobiotic Soil Crust

Biological soil crusts (herein referred to interchangeably as cryptobiotic soil crusts or cryptobiotic crusts) are important components of desert ecosystems (Belnap and others, 2001), including those found at many archeological sites in Grand Canyon. Cryptobiotic crusts form at the soil surface and are composed of living bacteria, algae, fungi, lichens, and mosses (Belnap and others, 2001). They are generally resilient in some respects (for example, they can withstand drying and wetting) but are susceptible to damage from compaction (for example, by footsteps), which can destroy the crust-forming organisms, thereby disrupting growth. The presence or absence of cryptobiotic crust at an archeological site can be indicative of site stability and the degree to which surficial erosion processes are active at a site, because crusts keep wind from transporting sediment out of sites, prevent rainsplash- and runoff-induced erosion, and are often precursors to the establishment of vegetation that may then further inhibit both aeolian and overland flow erosion. Knowing and tracking the areal extent of cryptobiotic crust in and near archeological sites is therefore a potentially important component of archeological site stability monitoring.

Existing methods of mapping cryptobiotic crusts are generally implemented by visual techniques—soils are inspected in the field and several classes of development are distinguished from one another according to established protocols (for example, Tongway and Smith, 1989; Belnap and others, 2001). The areal extent of cryptobiotic crust at a particular site can be mapped directly on a photographic base map, such as a low-altitude orthophotograph, or can be mapped by survey boundary methods, such as GPS or total station. Whereas these techniques are likely the most conclusive ways to determine what is and what is not a cryptobiotic crust, they may cause disturbance to the archeological and/or biologic properties of a site through human impacts (for example, from footprints and survey rod imprints). Mapping techniques using airborne and satellite remote sensing techniques already exist (for example, Karnieli and others, 2001; Chen and others, 2005), but these are generally more suited for large-scale (that is, hundreds of square kilometers) investigations. Use of smaller scale remote sensing methods, such as terrestrial lidar, may therefore offer a means of minimizing potential impacts during cryptobiotic crust surveys at the scale of an individual archeological site. Already, the use of combined photomapping with terrestrial lidar has been applied to geologic outcrop mapping (for example, Bellian and others, 2005), and close-range hyperspectral imaging has been combined with terrestrial lidar mapping (for example, Kurz and others, 2011). This technology is therefore moving rapidly forward.

We examine the use of terrestrial lidar for mapping cryptobiotic soils through an example taken from Site AZ:C:05:0031 using the April 2010 data. Here, both uncrusted, loose dune sands and cryptobiotic-crusted sands are located in discrete locations within the general area of the archeological site. In addition to positional (x, y, z) and color channel (red, green, blue) data, our laser system also collected laser signal amplitude data. Laser signal amplitude is a measure of signal return strength and is dependent on target material type, range between target and laser, and laser incident angle. The use of laser signal amplitude for determining the areal extent of a particular substrate, such as cryptobiotic crust, is therefore not ideal because remote sensing campaigns should be range-independent. That is, they should only be based on the material type—an attribute that could potentially be more appropriately extracted if the laser reflective intensity were measured. When collected, the data can very often be discretized and range

normalized (see, for example, Kaasalainen and others, 2011). Unfortunately, most existing time-of-flight terrestrial lidar systems (including the type used in our study) are not capable of measuring reflective intensity and therefore cannot be used for this purpose. Currently, some aerial lidar sensors, phase-based terrestrial scanners, and only the newest generation of time-of-flight terrestrial lidar units offer this capability (so-called "full waveform" measurements). Despite this equipment-based limitation, we explored the use of terrestrial lidar for cryptobiotic crust mapping by examining the laser strength amplitude for a narrow range of point cloud data from the archeological site. This resulted in normalizing the effect of laser range over the investigated area (that is, comparable at this range only), but it was then not applicable to the entire archeological site considered as a whole. Our methodology consisted of:

1. Visually identifying areas of both highly developed (that is, level of development > 4; Belnap and others, 2008) cryptobiotic crusted and uncrusted dune sands at a similar laser range (approximately 35 m) both through high-resolution digital images (figs. 44 *A,B*) and through on-site mapping (Amy Draut, written commun., August 2011). Areas with minimal to no vegetation were purposely selected. An approximately similar area (roughly 6 to 8m^2) was used for each substrate by integrating three smaller dune sand areas to be of approximate equivalent areal extent as the one cryptobiotic crust area (table 15).

2. Digitally outlining the identified cryptobiotic crust and uncrusted dune sand areas in the point cloud data from a single vantage point and single point cloud to minimize laser incidence effects (fig. 44*C*).

3. Filtering the point clouds to contain only those points within the cryptobiotic crust and uncrusted dune sand boundaries.

4. Querying the segregated point cloud statistics (for example, mean, standard deviation) for laser return amplitude, as a measure of signal strength for each substrate (table 15).

5. Filtering the entire point cloud by the mean plus one standard deviation for each substrate (cryptobiotic crust or sand) to see if there is a quantitative distinction for areas covered with cryptobiotic crust (fig. 45).

The results indicate that there is a clear laser signal amplitude distinction (measured on a relative scale from 0, low, to 65,535, high) between the cryptobiotic crust and uncrusted dune sand areas (table 15). The mean value for cryptobiotic crust is approximately 450 amplitude units above that for the uncrusted sand areas, and at one standard deviation there is almost no overlap between pixels with identical signal strengths. Mapping of the point cloud using a mean +/- one standard deviation (that is, $\pm 1\sigma$) threshold shows that the different amplitudes effectively segregate the cryptobiotic crust areas from the uncrusted dune sand areas (fig. 45). Thus, this exercise shows that a clear distinction in identifying cryptobiotic soil crust from uncrusted dune sands based on laser amplitude was achievable for at least a small patch of data at a single range. These results are substantiated by previous work on this subject using slightly different techniques (for example, identifying different rock lithology with combined photo-lidar methods, see Bellian and others, 2005). However, as previously discussed, a thorough comparison of the entire site (that is, at different ranges) is not possible because of the effects of range on signal amplitude and because vegetation and other substrates (for example, rocks, see fig. 45) impair a clear evaluation of the amplitude signal over a larger region. The use of a full waveform laser that collects reflective intensity data, especially if collected from an airborne platform, would likely alleviate these issues.

Table 15. Laser amplitude analysis of areas of cryptobiotic crust vs. uncrusted dune sand at Site AZ:C:05:0031.

Area (see fig. 44)	Number of points in crypto or sand area	Mean range from laser origin (m)	Mean signal amplitude[1]	Standard deviation of signal amplitude	Minimum signal amplitude	Maximum signal amplitude
Crypto area A	4,346	36	9,947	209	7,938	11,011
Sand area avg.	4,869	33	9,494	258	7,170	10,498

[1] Signal amplitude units are measured on a relative basis between 0 and 65,535.

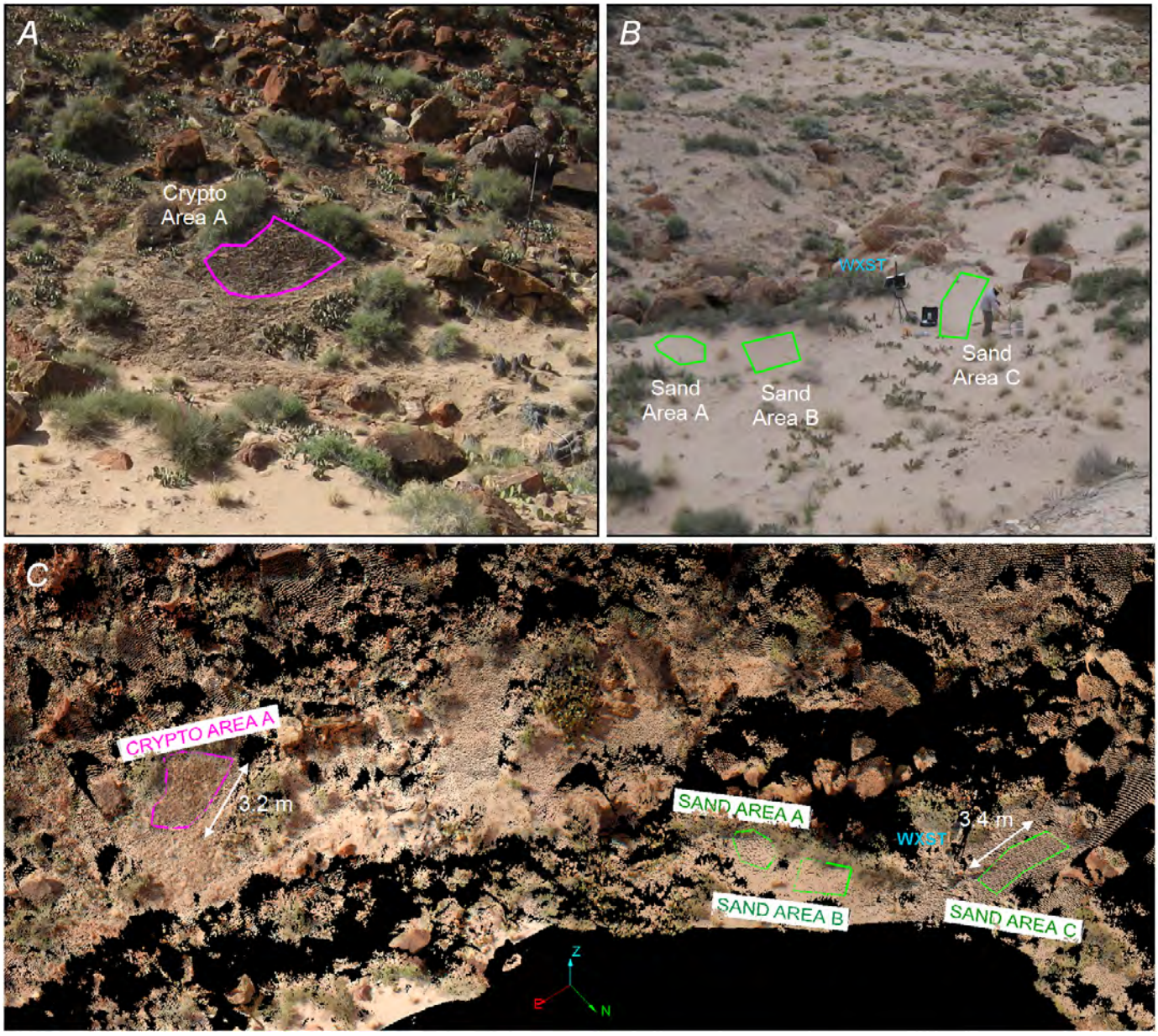

Figure 44. Overview photos of (*A*) cryptobiotic crust area (view is to the south – see fig. 7) and (*B*) uncrusted dune sand areas (view is to the southwest – see fig. 7) at site AZ:C:05:0031 from April 2010. *C*, Point cloud data of same areas showing proximity and scale (WXST = weather station).

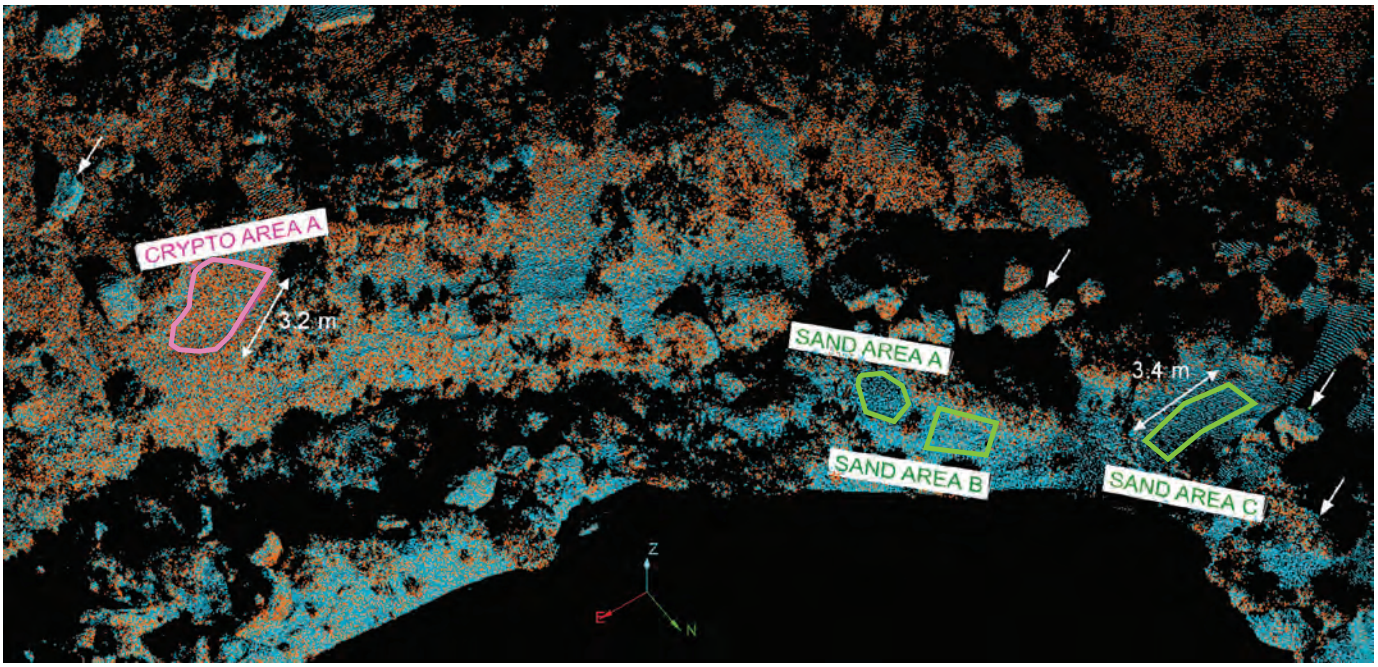

Figure 45. Laser-strength amplitude-filtered point cloud for cryptobiotic crust area (orange, with amplitude range of 9,738–10,156 units) and uncrusted dune sand area (blue, with amplitude range of 9,236–9,752 units) effectively segregates the mapped areas from one another. Other areas with vegetation or boulders (for example, identified with single-headed arrows), are not effectively segregated by this classification.

Gully Thalweg Determination From Combined Lidar-Photography

One of the most visible signs of archeological site change in the Colorado River corridor is the ongoing erosion of gully channels that traverse through these sites. Researchers (for example, Hereford and others, 1991; Fairley and others, 1994; Leap and others, 1997; Pederson and others, 2006) have documented the incision and formation of gullies, and some of these gullies are now effectively removing artifacts from their original locations and transporting them into the Colorado River to be lost downstream. Although the debate on the cause and the long-term rate of incision of these gullies is a broader topic reflecting the relative influences of natural verses anthropogenic sources for the erosion, knowledge of their location and change over time is needed for an informed analysis of this subject. Whereas existing survey methods (for example, conventional total station surveys) exist for obtaining these data (for example, Hazel and others, 2008; O'Brien and Pederson, 2009b), the accuracy and relatively high impact of these methods (that is, requiring a person to stand in, and traverse through, an archeological site) prompted a reevaluation of remotely sensed methods by the USGS to obtain this type of data.

In 2006, Collins and others (2008) performed a study to compare the use of terrestrial lidar methods verses total station methods in generating high-resolution, accurate long profiles of gully thalwegs at archeological sites in the Colorado River corridor. In general, the study showed that lidar can be used as an effective tool, but that the method, as applied in 2006, had limitations regarding the ability to track such fine-scale detail as gully kickpoints in areas of complex topography. Further, the water-drop pathway algorithm utilized (involving automated computational methods to interrogate a surface model and determine the channel flow path) had limitations when the topography was shallow in slope. In these instances, the algorithm did not always determine the lowest, most efficient flow line, thereby creating unrealistically complex and tortuous channel flow paths. Whereas the overall results (mean difference errors of less than 5 cm between total station and lidar) closely mimicked the total vertical analytical error of the lidar and total station instruments used (4.3 cm and 1.3 cm, respectively), standard deviations of the same difference errors (between 5 and 19 cm) highlighted the variability of the data comparison. Collins and others (2008) therefore concluded that feature identification and thalweg mapping using the methods used at that time were not reliable to the degree needed to implement them on a wider, more regular basis for monitoring gully erosion at archeological sites.

With the rapid advancement of lidar technology since the 2006 study (Collins and others, 2008), new instruments (including that used in the present study) have become

available that are more accurate and that offer the ability to perform photo-based mapping on lidar point cloud data. This new technology thereby has the potential to better tackle the thalweg mapping question by use of a remotely sensed methodology. Therefore, as part of the present study, we collected channel thalweg data at approximately 2.5-m intervals (judged as an efficient spacing and of sufficient resolution at this site) using a total station at the AZ:C:13:0099 playa area site (fig. 46; see also figs. 22 and 23) so that a direct comparison of this data to a lidar-extracted thalweg could be made. Because the channel at this site is not technically a gully (not steep walled), it provides a somewhat more robust evaluation (that is, topographic subtleties in its lower overall profile are more difficult to discern). The methodology involved "coloring" the point cloud data using the calibrated high-resolution photographs collected through a Nikon D200 digital SLR camera mounted to the top of the laser (fig. 4). The colored point clouds were then utilized in two ways:

1. A surface model (TIN) was created, colored, and textured using the photos in order to try to determine the thalweg using the now photo-draped model.

2. The colored point cloud was used to virtually map the thalweg at approximately 0.75-m intervals (again, judged efficient and of sufficient resolution for this site) by optical-manual recognition using the combined colored topography.

The first method was unsuccessful in accurately depicting a suitable surface model for channel thalweg extraction. Limitations included the need to filter the dataset to at least some minimum threshold in order to generate a surface model for color and texture modeling. The filtering effectively limited the resolution of the model, such that the thalweg was then "blurred" and difficult to identify. Although photo-draping algorithms are rapidly becoming more sophisticated, we did not find the methods efficient or accurate during the present evaluation.

The second method of direct thalweg mapping on the colored point cloud was much more successful. Here, approximately 100 m of the thalweg was mapped using 136 points (compared to 37 using total station) on a combined colored point cloud consisting of data from five separate scan locations. Horizontal plane accuracy was good (fig. 47), with maximum differences on the order of 20 cm. In general, these were due to the coarser resolution of the total station data. Profile view accuracy was also exceptional (fig. 48), with mean difference errors between the long profiles generated by lidar and total station of only 0.2 cm and 84 percent of the data within a 2-cm vertical error bound. This is therefore a vast improvement over the results obtained by Collins and others (2008), especially so because the thalweg investigated here is relatively flat—such situations had earlier been highlighted as a limitation of lidar methods.

Because the lidar-generated thalweg was based on an order-of-magnitude larger number of points, the long profile is evidently longer and more variable. However, in only two locations (at approximately the 33-m and 65-m distance marks—see fig. 48) were the lidar data significantly different from the total station data. Here, we determined that the differences were due to a lack of point density in the total station data—the differences were located in two low-lying areas of the thalweg where "pools" developed (a result of filling and subsequent drying of the channel), such that the total station likely missed locating these lower visibility features. In summary, the use of photo-colored point clouds for mapping channel thalwegs proved to be a vast improvement over previous attempts to identify subtle topographic features such as these. This method thus shows much promise for mapping geomorphic change in gully systems, as long as the limitations discussed by Collins and others (2008) are avoided (namely, surveying in highly vegetated areas that obscure any view of the gully thalweg).

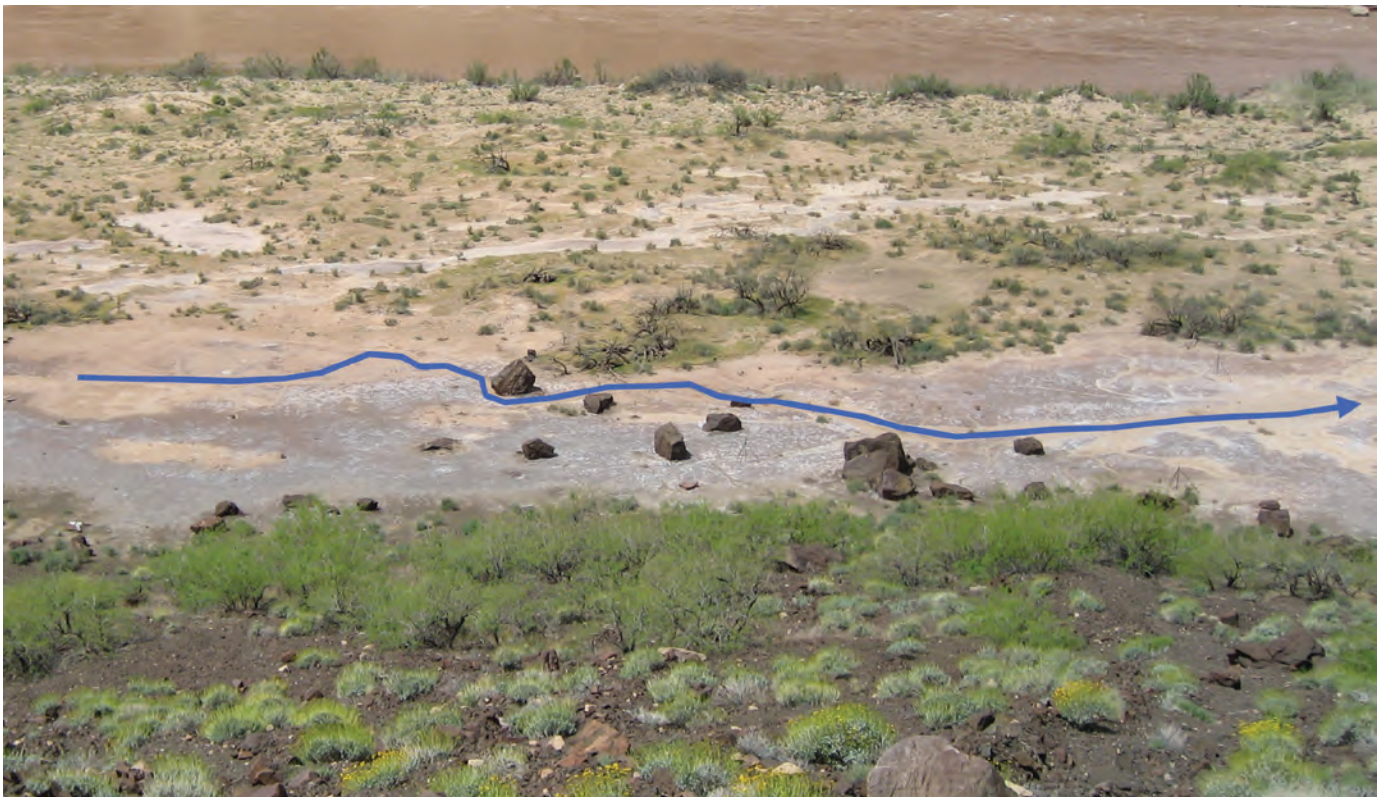

Figure 46. Oblique image overview of AZ:C:13:0099 playa area showing length of main channel thalweg (blue line) for long profile analysis. View is to the west (see fig. 22).

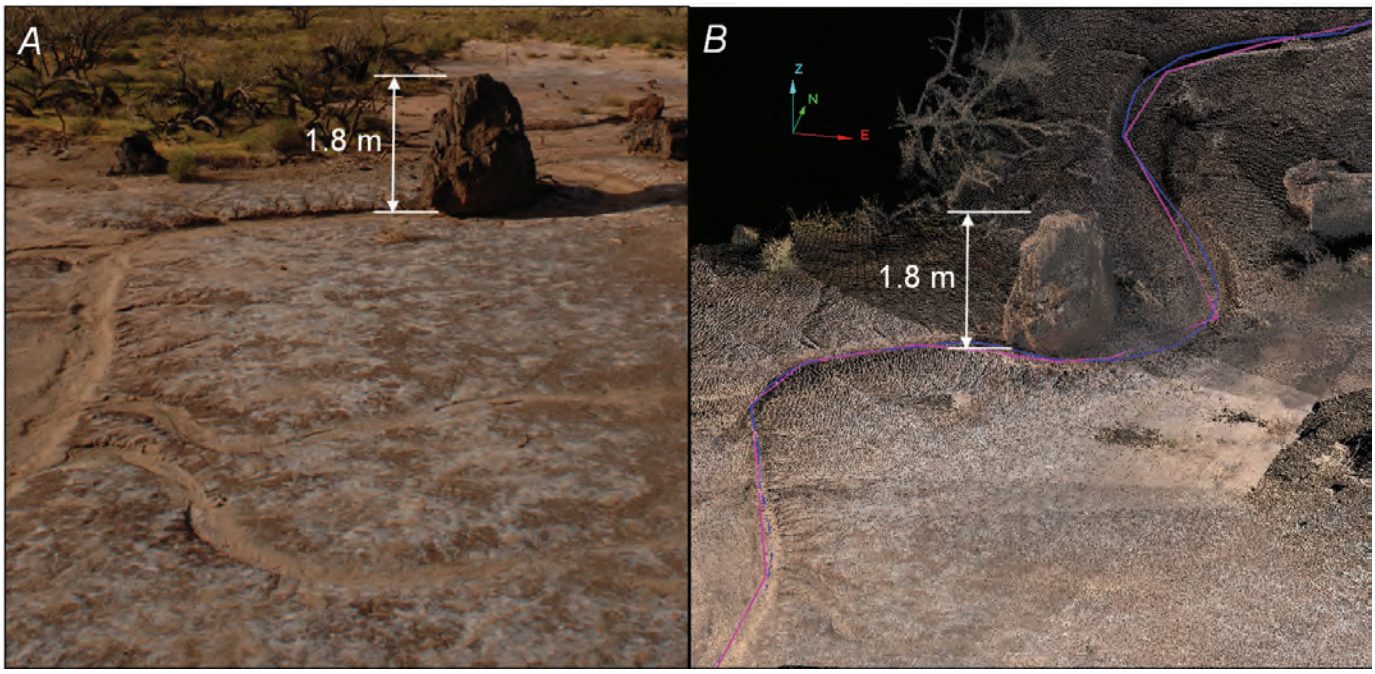

Figure 47. A section of the AZ:C:13:0099 playa area channel as it winds around a large rock. *A*, Oblique image (view is to the north – see fig. 22). *B*, Point cloud data. Pink, coarser resolution line is thalweg derived from total station data. Blue, finer resolution line is thalweg derived from lidar data.

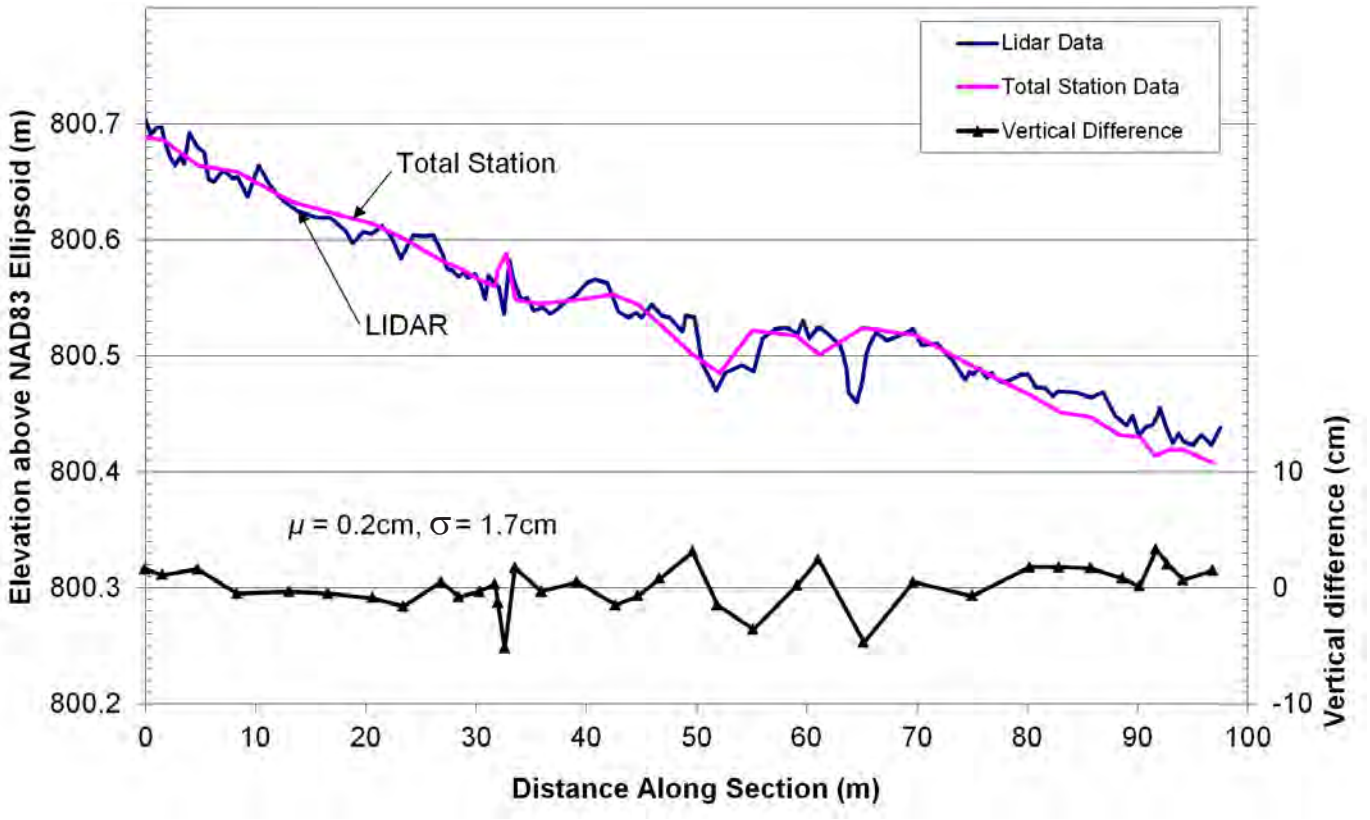

Figure 48. Long profile view of channel thalweg comparison using terrestrial lidar and total station data at AZ:C:13:0099 playa area during April 2010. Mean and standard deviation of differences between lidar and total station data identified by μ and σ, respectively.

Effect of Survey Location on Lidar Point Density

Lidar point density is affected by a suite of factors, including laser specifications, range to target, and obliquity of laser incident angle. In most cases, point density can be optimized by selecting appropriate, overlapping laser scanner survey setup locations with good laser-to-target incident angles. Olsen and others (2009) showed how this can be determined for near-vertical coastal bluffs scanned from evenly spaced beach locations fronting the bluffs. When scanning flatter topography, such as that found in many archeological sites in Grand Canyon, optimizing point density can be difficult because of the lack of suitable scan locations that offer near-perpendicular trajectories to the target. This problem is typically resolved by collecting data from additional scan locations, resulting in more time on site and possibly more site impacts. When surrounding topography offers an overview of a survey area (fig. 49*A*), the best results are often achieved. However, the final point density can decrease if the scan location is positioned beyond a laser-defined distance threshold (that is, as defined by the angular step increment of the laser at far range). Here, we provide results from a study conducted at the AZ:C:13:0099 playa area that verified this effect. The study was conducted to show that whereas far-field (>100 m) scanning from a high vantage point can effectively resolve geomorphic-scale topographic features, near-field (<30 m) scanning is still needed for resolving small, archeological-scale features.

Following existing archeological site lidar monitoring protocols, five near-field scans were collected at the AZ:C:13:0099 playa area. In addition, one far-field scan was collected from the approximate mid-height of a steep talus slope adjacent to the site (fig. 22). The near-field scans collected data at a horizontal and vertical angular resolution of 0.05°, whereas the far-field scan was set to collect data at an angular resolution of 0.02° (the maximum allowed by the laser scanner instrument at this field of view). In general, minimum laser scan incident angles (as measured from the horizontal to the maximum trajectory covering the data collection area) ranged from 8° to 11° for the near-field data and from 16° to 21° for the far-field data. Thus, the far-field setup leads to approximately double the incident angle, thereby improving the quantity of potentially usable laser returns. However, the point density results show that the near-field data far exceeds the far-field data, as expected. For an area 10 m by 10 m within the southern end of the playa (representing a typical

area of interest; fig. 49*A*), the point density from the far-field (from one scan position, see "FF" in fig. 22) is 180 points/m^2 (fig. 49*B*), whereas the point density from the near-field (also from one scan position, see "NF" in fig. 22) is 13,130 points/m^2 (fig. 49*C*), an increase in two orders of magnitude. With the near-field data, geomorphic subtleties such as channel fingering are captured, whereas with the far-field data, only the overarching topography is captured. The tradeoff here is the relative area in which data collection occurs. In this example, the single far-field scan captures the entire area of interest (~10,300 m^2; table 4), whereas the near-field data require five independent scan locations and twice the amount of time (also potentially increasing site impacts) to capture the same area. Further, it is technically possible that a higher degree of accuracy could be obtained using only a single far-field scan because registration errors between multiple scans might be avoided. However, whereas far-field setups are more efficient at data collection, near-field setups are required to monitor and understand geomorphic change at scales of importance for monitoring archeological site stability.

Discussion

This continuing investigation provides new information about the amount and types of topographic changes affecting Colorado River corridor archeological sites in Grand Canyon National Park. In addition, the results present newly refined techniques for collecting and evaluating topographic and other types of change data for use in monitoring overall archeological site stability. These new findings are summarized below.

Archeological Site Change Detection

We detected statistically significant change (greater than either ±3 cm or ±5 cm, depending on survey dates) at 9 of 10 survey areas, including all 9 archeological sites investigated in the current study (table 16). The only survey area not showing signs of change was the downstream part of site AZ:G:03:0072. For the remainder of the surveyed areas, changes tended to be of larger magnitude between September 2007 and April 2010 than between April 2010 and September 2010, consistent with expectations regarding the length of time in which changes could have occurred (that is, over longer time intervals, multiple events could be responsible for the measured changes). Detected changes range from areas with large-scale aeolian sand erosion and deposition (for example, the upstream part of site AZ:G:03:0072) to those with massive gully erosion generated by overland flow (site AZ:B:10:0225). Investigation and comparison of specific areas of change detected between 2006–2007 (Collins and others, 2009) and detected between 2007–2010 (this report) indicate that some sites changed consistently (that is, with the same general location and magnitude), whereas other sites changed under new configurations (that is, change occurred at either a different magnitude or location than previously documented). For example, at site AZ:C:13:0336, erosion occurred in a gully that had previously eroded, and also at a new gully location. These results highlight the dynamic geomorphology of the Colorado River corridor and the need to monitor sites regularly and repeatedly to understand the geomorphologic effects on site condition. Overall, and ignoring the results from Site AZ:C:13:0099 between September 2007 and April 2010, which were clearly influenced by an unusual anthropogenic cause (the excavation of the site in 2008), total measured erosion was greater both in area and volume (669 m^2 and 157 m^3, respectively) compared to total measured deposition (169 m^2

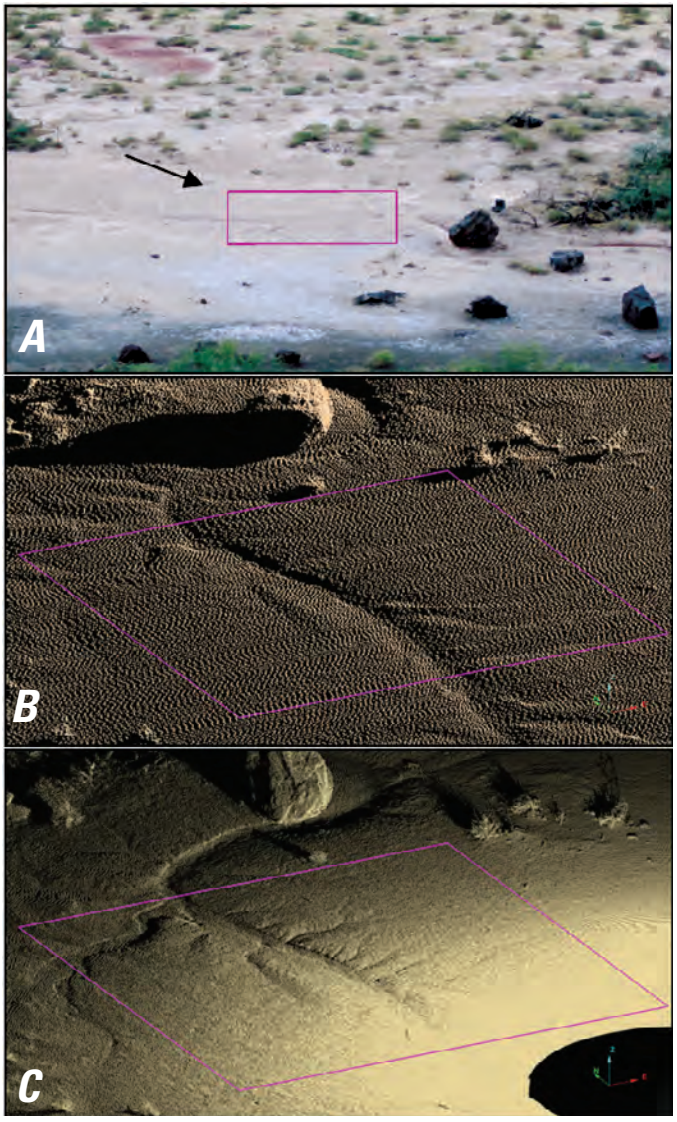

Figure 49. Comparison of far-field and near-field data for a 10 m by 10 m area of the AZ:C:13:0099 playa. *A,* Photo (view is to the west—see fig. 22). Arrow indicates look angle for *B* and *C*. *B,* Far-field (FF) lidar point density. *C,* Near-field (NF) lidar point density.

and 20 m^3, respectively) during the September 2007 to September 2010 time period. It should be noted that not all areas within the investigated archeological sites were monitored for change. However, although these conclusions are only technically applicable to the specific areas monitored, they more than likely correctly capture the overall trend—that of archeological site erosion throughout the Colorado River corridor.

In general, we documented the causes of detected changes as being related to two primary processes: aeolian transport and overland/channelized flow. In at least one case (AZ:C:13:0099 between September 2007 and April 2010), anthropogenic actions influenced the erosion and deposition patterns. From the magnitude of changes surmised to be due to both overland flow erosion and aeolian sand erosion and deposition processes, back-analysis of the meteorological events that caused these changes should be possible where records of rainfall and wind direction and speed are available for the time frame in which the changes occurred (for example, Draut and others, 2009a,b; 2010b). For example, examination of local rainfall and wind records may identify particularly significant events that could have caused the magnitude of changes observed and detected from the data (that is, large-scale gullying or aeolian sand transport). Whereas this type of analysis is beyond the scope of this report, if undertaken in the future it would serve to bracket potential empirical thresholds for the magnitudes of processes that cause these types of site changes. Unfortunately, comparison of these results with expected and modeled results from the 2008 High Flow Experiment (HFE) (Melis, 2011), which may have affected the archeological sites monitored here, is not possible because of the 2½-year gap between the dates on which our data were collected. That is, whereas the September 2007 and April 2010 dates bracket the 2008 HFE in March of that year, they do not bracket the experiment closely enough to be able to link changes specifically to effects of the HFE.

Lidar Change Detection Monitoring

Several components of the lidar surveying method used in this study warrant discussion. First, we note that the accuracy thresholds used for all change detection analyses are a significant improvement from previous efforts and currently represent the best achievable limits at this scale. Performing repeat topographic change detection at below a 3-cm threshold in a remote setting without the use of permanently installed reoccupiable control points, which generally necessitate at least some archeological site disturbance, will require significant improvements in both laser and GPS/total station accuracy. Whereas lidar technology continues to evolve, more accurately surveying control point locations would require significant technological advancements that have thus far not been introduced in rugged field instrumentation.

Second, this study investigated several additional metrics for evaluating archeological site change that could prove to be useful with additional advances in technology (for example, monitoring structural walls, tracking artifact movement, monitoring cryptobiotic soil crust cover). Here, we introduced available methods of analysis, but also discovered significant limitations (for example, overall inaccuracy of time-of-flight lasers for these monitoring purposes, lack of full wave-form analysis with most current available laser scanners). However, we also suggest that different and newer instrumentation already available may be able to address these limitations in some cases. Thus, although this study showed that tracking some of these site metrics was not possible using the instruments available at the time of data collection, we also posit that the limitations may be overcome with new technology.

Finally, we show that technological advances have already been helpful in addressing some previous limitations. Namely, we conclusively identified a gully thalweg running through relatively flat topography to a degree of accuracy better than established in previous studies. The use of photo-colored point clouds is certainly a step in the right direction for this type of analysis, and we expect that additional advances will make such analyses still more accurate in the future.

Conclusions

Archeological sites within the Colorado River corridor of Grand Canyon National Park offer a window into the lives of the people who occupied this region long ago. Given that many archeological sites are located in areas subject to rapid geomorphologic change, such as alluvial terraces subject to gullying processes and active aeolian dune fields, understanding the magnitude and causes of these changes is important for monitoring and managing both short-term and long-term archeological site stability. High-resolution topographic change detection using terrestrial lidar techniques, coupled with site-specific geomorphologic analysis of archeological sites, provides much of the necessary detailed information needed to understand rates of change and to guide management decisions. Further, high-resolution, highly accurate data at the scale presented in this report are required in order to track fine site changes that might be precursors to larger scale, destructive erosion events. This information can assist in addressing open questions regarding what role, if any, sediment-depleted flows from Glen Canyon Dam have on site stability and what effects visitor use might have on site deterioration.

In this study, we build upon existing data to generate new topographic change maps and infer related geomorphologic causes of archeological site change at 10 survey areas covering 9 archeological sites throughout the length of the Colorado River corridor over a 3-year period from September 2007 to September 2010. Eight areas were monitored for change at a 5-cm detection threshold between September 2007 and either April or September 2010, and six areas (including some of the eight previously studied) were monitored for change at a 3-cm detection threshold between April and September 2010. Our results indicate that 9 of the 10 survey areas exhibited statistically significant topographic change by erosion, deposition, or both during this time interval and that those changes could likely be linked to a variety of causes, including overland flow

Table 16. Summary of net topographic change between September 2007, April 2010, and September 2010.

[Survey area codes are National Park Service archeological site identifiers]

Survey area (monitoring period)	Area of erosion (m^2)	Area of deposition (m^2)	Total site area modeled with change (percent)	Average (max.) height of erosion (cm)	Average (max.) height of dep. (cm)	Approx. volume of erosion (–) (m^3)	Approx. volume of dep. (+) (m^3)
AZ:C:05:0031 (April 2010-Sept. 2010)	134.9	0	5.4	4 (30)	0 (0)	-5.7	0
AZ:C:13:0006 (Sept. 2007-April 2010)	27.0	8.8	2.8	15 (33)	9 (22)	-3.3	+0.8
AZ:C:13:0006 (April 2010- Sept. 2010)	2.2	0	0.2	6 (16)	0 (0)	-0.1	0
AZ:C:13:0336 (Sept. 2007-April 2010)	39.1	2.2	2.9	7 (27)	7 (15)	-3.6	+0.2
AZ:C:13:0336 (April 2010- Sept. 2010)	16.5	1.5	1.3	3 (9)	3 (5)	-0.6	+0.1
AZ:C:13:0099 (Sept. 2007-April 2010)	103.0	22.5	19.6	12 (63)	12 (59)	-17.3	+2.8
AZ:C:13:0099 (April 2010- Sept. 2010)	0.4	2.3	0.4	4 (6)	5 (9)	-0.02	+0.1
AZ:C:13:0099 playa (Sept. 2007-April 2010)	3.6	0.4	0.1	7 (13)	6 (7)	-0.2	+0.02
AZ:C:13:0099 playa (April 2010- Sept. 2010)	0.02	0	0.001	5 (6)	0 (0)	-0.001	0
AZ:C:13:0321 (April 2010-Sept. 2010)	13.9	0	10.0	4 (14)	0 (0)	-0.6	0
AZ:C:13:0348 and AZ:C:13:0346 (Sept. 2007-Sept. 2010)	85.3	21.2	3.5	9 (28)	7 (13)	-8.6	+1.3
AZ:B:10:0225 (Sept. 2007-Sept. 2010)	254.2	81.3	28.7	22 (160)	13 (55)	-120.3	+11.2
AZ:G:03:0072 US (Sept. 2007-Sept. 2010)	92.1	50.8	11.8	11 (52)	16 (60)	-13.8	+6.4
AZ:G:03:0072 DS (Sept. 2007-Sept. 2010)	0	0	0	0 (0)	0 (0)	0	0

gullying and aeolian sand transport. Further, taken as a whole for all sites monitored throughout the river corridor during this time period, the overall signal was related to erosion rather than deposition. These results reflect both the active geomorphologic environment in Grand Canyon and the potential for rapid archeological site change.

We also performed additional studies to test new lidar-based methods of tracking other indicators of archeological site change, such as structural element and artifact movement, change in cryptobiotic soil crust extent, and shifts in gully thalweg position. These results indicate that whereas most current terrestrial lidar instruments have some limitations with regard to measuring these site characteristics at subcentimeter accuracy and with laser amplitudes, newer technology may already be useful for addressing these limitations. The results lay out monitoring protocols using current instrumentation that can be adapted to other instrument platforms and in some cases, such as monitoring gully thalweg position, achieve a high degree of accuracy and usefulness for archeological site stability studies.

Whereas the topographic change results presented herein provide the highest level of change detection yet performed on entire archeological sites in Grand Canyon, additional work in combining these results with site-specific data on weather (for

example, Draut and others, 2009a,b; 2010b), geomorphology (for example, O'Brien and Pederson, 2009a,b), and hydrology and sandbar response (for example, Hazel and others, 2008, 2010) will provide a more thorough understanding of the causes of the documented topographic changes on these time scales. This information should provide land managers with an improved basis for making management decisions regarding archeological resources in Grand Canyon National Park.

Acknowledgments

Funding for this research was provided by the U.S. Geological Survey (USGS) Grand Canyon Monitoring and Research Center, in cooperation with the U.S. Bureau of Reclamation. Kristin Brown (USGS), Brian Fisher (Geodetic Analysis, LLC), and Keith Kohl (USGS) with Aaron Borling (USGS) provided field survey support for the September 2007, April 2010, and September 2010 data collection efforts, respectively, and their assistance is gratefully acknowledged. We thank Toby Minear (USGS) and Gary O'Brien (Utah State University) for providing detailed reviews that improved the quality of this report.

References

Anderson, K.C., and Neff, T., 2011, The influence of paleofloods on archaeological settlement patterns during A.D. 1050–1170 along the Colorado River in the Grand Canyon, Arizona, USA: Catena, v. 85, p. 168-186

Bellian, J.A., Kerans, C., and Jennette, D.C., 2005, Digital outcrop models—Applications of terrestrial scanning lidar technology in stratigraphic modeling: Journal of Sedimentary Research, v. 75, no. 2, p. 166–176.

Belnap, J., Kaltenecker, J.H., Rosentreter, R., Williams, J., Leonard, S., and Eldridge, D., 2001, Biological Soil Crusts: Ecology and Management, U.S. Dept. of Interior, Tech. Ref. 1730-2, 110 p., accessed September 30, 2011, at http://www.blm.gov/nstc/library/pdf/CrustManual.pdf.

Belnap, J., Phillips, S.L., Witwicki, D.L., and Miller, M.E., 2008, Visually assessing the level of development and soil surface stability of cyanobacterially dominated biological soil crusts: Journal of Arid Environments, v. 72, no.7, p. 1257–1264.

Boehler, W., Vicent, M.B., and Marbs, A., 2003, Investigating laser scanner accuracy: Presented at the XIX International Committee for Documentation of Cultural Heritage (CIPA) Symposium, Antalya, Turkey, 2003, 9 p., updated version (October 2003) accessed September 30, 2011, at, http://www.i3mainz.fh-mainz.de/publicat/cipa2003/laserscanner_accuracy.pdf.

Chen, J., Zhang, M.Y., Wang, L., Shimazaki, H., and Tamura, M., 2005, A new index for mapping lichen-dominated biological soil crusts in desert areas: Remote Sensing of Environment, v. 96, p. 165–175.

Collins, B.D., and Kayen, R., 2006, Applicability of terrestrial LIDAR scanning for scientific studies in Grand Canyon National Park, Arizona: U.S. Geological Survey Open-File Report 2006–1198, 27 p., available at http://pubs.usgs.gov/of/2006/1198/.

Collins, B.D., Brown, K.B., and Fairley, H.C., 2008, Evaluation of terrestrial LIDAR for monitoring geomorphic change at archeological sites in Grand Canyon National Park, Arizona: U.S. Geological Survey Open-File Report 2008–1384, 60 p., available at http://pubs.usgs.gov/of/2008/1384/.

Collins, B.D., Minasian, D., and Kayen, R., 2009, Topographic change detection at select archeological sites in Grand Canyon National Park, Arizona, 2006–2007: U.S. Geological Survey Scientific Investigations Report 2009–5116, 58 p., available at http://pubs.usgs.gov/sir/2009/5116/.

Draut, A.E., 2011, Vegetation and substrate properties of aeolian dune fields in the Colorado River corridor, Grand Canyon, Arizona: U.S. Geological Survey Open-File Report 2011–1195, 16 p., available at http://pubs.usgs.gov/of/2011/1195/.

Draut, A.E., and Rubin, D.M., 2008, The role of aeolian sediment in the preservation of archeological sites along the Colorado River corridor Grand Canyon National Park, Arizona: U.S. Geological Survey Professional Paper 1756, 71 p., available at http://pubs.usgs.gov/pp/1756.

Draut, A.E., Rubin, D.M., Dierker, J.L., Fairley, H.C., Griffiths, R.E., Hazel, J.E., Jr., Hunter, R.E., Kohl, K., Leap, L.M., Nials, F.L., Topping, D.J., and Yeatts, M., 2005, Sedimentology and stratigraphy of the Palisades, Lower Comanche, and Arroyo Grande areas of the Colorado River corridor, Grand Canyon, Arizona: U.S. Geological Survey Scientific Investigations Report 2005–5072, 68 p., available at http://pubs.usgs.gov/sir/2005/5072/.

Draut, A.E., Andrews, T., Fairley, H.C., and Brown, C.R., 2009a, 2007 weather and aeolian sand-transport data from the Colorado River corridor, Grand Canyon, Arizona: U.S. Geological Survey Open-File Report 2009–1098, 110 p., available at http://pubs.usgs.gov/of/2009/1098/.

Draut, A.E., Sondossi, H.A., Hazel, J.E., Jr., Andrews, T., Fairley, H.C., Brown, C.R., and Vanaman, K.M., 2009b, 2008 weather and aeolian sand-transport data from the Colorado River corridor, Grand Canyon, Arizona: U.S. Geological Survey Open-File Report 2009–1190, 98 p., available at http://pubs.usgs.gov/of/2009/1190/.

Draut, A.E., Hazel, J.E., Fairley, H.C., and Brown, C.R., 2010a, Aeolian reworking of sandbars from the March

2008 Glen Canyon Dam High-Flow Experiment in Grand Canyon, in Melis, T.S., Hamill, J.F., Bennett, G.E., Coggins, L.G., Jr., Grams, P.E., Kennedy, T.A., Kubly, D.M., and Ralston, B.E., eds., Proceedings of the Colorado River Basin Science and Resource Management Symposium, November 18–20, 2008, Scottsdale, Arizona: U.S. Geological Survey Scientific Investigations Report 2010–5135, p. 325–331, available at http://pubs.usgs.gov/sir/2010/5135/.

Draut, A.E., Sondossi, H.A., Dealy, T.P., Hazel, J.E., Jr., Fairley, H.C., and Brown, C.R., 2010b, 2009 weather and aeolian sand-transport data from the Colorado River corridor, Grand Canyon, Arizona: U.S. Geological Survey Open-File Report 2010–1166, 98 p., available at http://pubs.usgs.gov/of/2010/1166/.

Fairley, H.C., 2005, Cultural resources in the Colorado River corridor, in Gloss, S.P., Lovich, J.E., and Melis, T., eds., The state of the Colorado River ecosystem in Grand Canyon: U.S. Geological Survey Circular 1282, p. 177–192., available at http://pubs.usgs.gov/circ/1282/.

Fairley, H.C., Bungart, P.W., Coder, C.M., Huffman, J., Samples, T.L., and Balsom, J.R., 1994, The Grand Canyon river corridor survey project; archeological survey along the Colorado River between Glen Canyon Dam and Separation Canyon: Cooperative Agreement No. 9AA–40–07920, Grand Canyon National Park, Prepared in cooperation with the Bureau of Reclamation, Glen Canyon Environmental Studies, Flagstaff, Ariz.

Fairley, H.C., Collins, B.D., Draut A., Leap, L., and O'Brien, G., 2007, FY07–FY11 archeological site monitoring and research development project: Research proposal dated February 28, 2007, submitted to Grand Canyon National Park and National Park Service Research Permit Application System, March 5, 2007, copy on file at the U.S. Geological Survey, Grand Canyon Monitoring and Research Center, Flagstaff, Ariz., 49 p.

Gloss, S.P., Lovich, J.E., and Melis, T.S., eds., 2005, The state of the Colorado River ecosystem in Grand Canyon: U.S. Geological Survey Circular 1282, 220 p., available at http://pubs.usgs.gov/circ/1282/.

Grand Canyon Monitoring and Research Center, 2008, Survey control operations for the Colorado River Ecosystem: U.S. Geological Survey Grand Canyon Monitoring and Research Center, accessed August 11, 2008. at http://www.gcmrc.gov/about/programs/isp/dasa/survey/operations.aspx.

Hazel, J.E., Jr., Kaplinski, M, Parnell, R.A., and Fairley, H.C., 2008, Aggradation and degradation of the Palisades gully network, 1996 to 2005, with emphasis on the November 2004 high-flow experiment, Grand Canyon National Park, Arizona: U.S. Geological Survey Open-File Report, 2008–1264, 22 p., available at http://pubs.usgs.gov/ofr/2008/1264/.

Hazel, J.E., Jr., Grams, P.E., Schmidt, J.C., and Kaplinski, M., 2010, Sandbar response in Marble and Grand Canyons, Arizona, following the 2008 high-flow experiment on the Colorado River: U.S. Geological Survey Scientific Investigations Report 2010–5015, 52 p., available at http://pubs.usgs.gov/sir/2010/5015/.

Hereford, R., Fairley, H.C., Thompson, K.S., and Balsom, J.R., 1991, The effect of regulated flows on erosion of archaeological sites at four areas in eastern Grand Canyon National Park, Arizona—a preliminary analysis: U.S. Bureau of Reclamation, Glen Canyon Environmental Studies, Flagstaff, Ariz.

Hereford, R., Fairley, H.C., Thompson, K.S., and Balsom, J.R., 1993, Surficial geology, geomorphology and erosion of archaeological sites along the Colorado River, Eastern Grand Canyon, Grand Canyon National Park, Arizona: U.S. Geological Survey Open-File Report 93–517, 46 p.

Kaasalainen, S., Jaakkola, A., Kaasalainen, M., Krooks, A., and Kukko, A., 2011, Analysis of incidence angle and distance effects on terrestrial laser scanner intensity; search for correction methods: Remote Sensing, v. 3, p. 2207–2221.

Karnieli, A., Kokaly, R., West, N.E., and Clark, R.N., 2001, Remote sensing of biological soil crusts, in Belnap, J., and Lange, O.L., eds., Biological soil crusts; structure, function, and management: Berlin, Springer-Verlag, p. 431–455.

Kintigh, K., Altschul, J., Lipe, W., and Urquhart, N.S., 2007, Legacy monitoring data review panel report to the Grand Canyon Monitoring and Research Center: Report on file at the U.S. Geological Survey Grand Canyon Monitoring and Research Center, Flagstaff, Ariz., 63 p.

Kurz, T.H., Buckley, S.J., Howell, J.A., and Schneider, D., 2011, Integration of panoramic hyperspectral imaging with terrestrial lidar: The Photogrammetric Record, v. 26, no. 134, p. 212–228.

Leap, L.M., Andrews, N.B., and Kunde, J.L., 1996, 1996 summary report—monitoring of archeological sites along the Colorado River Corridor in Grand Canyon National Park: River Corridor Monitoring Project Report No. 37, 117 p., accessed August 1, 2008, at http://www.nps.gov/grca/historyculture/upload/FY1996.pdf.

Leap, L.M., Andrews, N.B., Hubbard, D.C., and Kunde, J.L., 1997, 1997 summary report— archeological site monitoring and management along the Colorado River Corridor in Grand Canyon National Park: River Corridor Monitoring Project Report No. 50, 103 p., accessed August 1, 2008, at http://www.nps.gov/grca/historyculture/upload/FY1997.pdf.

Leap, L.M., Kunde, J.L., Hubbard, D.C., Andrews, N.B., Downum, C.E., Miller, A.R., and Balsom, J.R., 2000, Grand Canyon monitoring project 1992–1999—synthesis and annual report for FY99: Grand Canyon National Park River Corridor Monitoring Project Report No. 66, Submitted to

Bureau of Reclamation, Upper Colorado Region, Salt Lake City, Utah, acquisition No. 99-AA-40-2340, 14 p., accessed August 1, 2008, at http://www.nps.gov/grca/historyculture/upload/FY1999.pdf.

Lichti, D.D., and Jamtsho, S., 2006, Angular resolution of terrestrial laser scanners: The Photogrammetric Record, v. 21, no. 114, p. 141–160.

Melis, T.S., ed., 2011, Effects of three high-flow experiments on the Colorado River ecosystem downstream from Glen Canyon Dam, Arizona: U.S. Geological Survey Circular 1366, 147 p., available at http://pubs.usgs.gov/circ/1366/.

O'Brien, G., and Pederson, J., 2009a, Geomorphic attributes of 232 cultural sites along the Colorado River in Grand Canyon National Park, Arizona: Report on file with the USGS Grand Canyon Monitoring and Research Center under cooperative agreement 04HQAG0122 with Utah State University, Utah, 201 p.

O'Brien, G. and Pederson, J., 2009b, Gully erosion processes and parameters at six cultural sites along the Colorado River in Grand Canyon National Park, Arizona: Report on file with the USGS Grand Canyon Monitoring and Research Center under cooperative agreement 04HQAG0122 with Utah State University, Utah, 140 p.

Olsen, M.J., Johnstone, E., Driscoll, N., Ashford, S.A., and Kuester, F., 2009, Terrestrial laser scanning of extended cliff sections in dynamic environments; parameter analysis: ASCE Journal of Surveying Engineering, v. 135, no. 4, p. 161–169.

Pederson, J.L., Petersen, P.A., MacFarlane, W.W., Gonzales, M.F., and Kohl, K., 2003, Mitigation, monitoring, and geomorphology related to gully erosion of cultural sites in Grand Canyon; Cooperative Agreement No. 01 WRAG0074 between Utah State University and U.S. Geological Survey, Grand Canyon: Grand Canyon Monitoring and Research Center, Flagstaff, Ariz., 250 p., accessed August 1, 2008, at http://www.gcmrc.gov/library/reports/cultural/Archaeology/Pederson2003.pdf.

Pederson, J.L., Petersen, P.A., and Dierker, J.L., 2006, Gullying and erosion control at archeological sites in Grand Canyon, Arizona: Earth Surface Processes and Landforms, v. 31, no. 4, p. 507-525.

Thompson, K.S., and Potochnik, A.R., 2000, Development of a geomorphic model to predict erosion of pre-dam Colorado River terraces containing archeological resources: SWCA Environmental Consultants Cultural Resources Report 99–257, US Geological Survey, Grand Canyon Monitoring and Research Center, Flagstaff, Ariz.

Tongway, D.J., and Smith, E.L., 1989, Soil surface features as indicators of rangeland site productivity: Australian Rangeland Journal, v. 11, no. 1, p. 15–20.

Topping, D.J., Schmidt, J.C., and Vierra, L.E., Jr., 2003, Computation and analysis of the instantaneous-discharge record for the Colorado River at Lees Ferry, Arizona—May 8, 1921, through September 30, 2000: U.S. Geological Survey Professional Paper 1677, 118 p., available at http://pubs.usgs.gov/pp/pp1677/.

Tressler, C., 2011, From hillslopes to canyons; studies of erosion at differing time and spatial scales within the Colorado River drainage: Logan, Utah, Utah State University, All Graduate Theses and Dissertations, Paper 1109, 99 p., accessed May 9, 2012, at http://digitalcommons.usu.edu/etd/1109.

Tressler, C., and Pederson, J.L., 2010, Testing terrestrial lidar for tracking surface-particle creep at a cultural site in Grand Canyon National Park, Arizona: Utah State University internal report to USGS Grand Canyon Monitoring and Research Center, Cooperative Agreement 04HQAG0122, 29 p.

U.S. Geological Survey, 2008, Grand Canyon Monitoring and Research Center: Internet map server, accessed July 26, 2012, at http://www.gcmrc.gov/gis/silvermap1.aspx/.

Yeatts, M., 1996, High elevation sand deposition and retention from the 1996 spike flow; an assessment for cultural resources stabilization, in Balsom, J.R., and Larralde, S., eds., Mitigation and monitoring of cultural resources in response to the experimental habitat building flow in Glen and Grand Canyons, Spring 1996: Final report dated December 31, 1996, submitted to Grand Canyon Monitoring and Research Center, copy on file at the U.S. Geological Survey, Grand Canyon Monitoring and Research Center, Flagstaff, Ariz., 335 p.

Produced in the Menlo Park Publishing Service Center, California
Manuscript approved for publication July 20, 2012
Text edited by Peter H. Stauffer
Layout and design by Judy Weathers